ISSN 1000-9620

海洋通报

Marine Science Bulletin

NATIONAL MARINE DATD AND
INFORMATION SERVICE OF CHINA

2011
Volume 13
Number 2

MARINE SCIENCE BULLETIN

Vol. 13 No. 2 Oct. 2011

CONTENTS

Response of environmental sensitive grain size group in Core FJ04 from mud area in the north of East China Sea to East Asian winter monsoon evolvement ..... SUN Xiao-yan et al. (01)

The Kuroshio front to the east of Taiwan: seasonal feature, variability and mechanism .....WANG Qi et al. (13)

Sea-level change and forecast in the future — climate of the past, today and future .....YUE Jun et al. (33)

A review on quantitative analysis of suspended sediment concentrations ..... KUANG Liang et al. (51)

Integrated assessment of sea water quality based on BP artificial neural network .....LI Xue et al. (62)

Investigation of fecal coliform and typical enteric virus in representative beaches of China ..... FAN Jing-feng et al. (72)

Organization and storage model of marine information and its application in the "China Digital Ocean" ..... LIU Jin et al. (83)

LIBRARY
Pacific Islands Fi... ...ce Center
NOA...
Honolulu, Hawai'i

Response of environmental sensitive grain size group in Core FJ04 from mud area in the north of East China Sea to East Asian winter monsoon evolvement

LIBRARY
MAR 05 2012
National Oceanic & Atmospheric Administration
U.S. Dept. of Commerce

SUN Xiao-yan[1], LI Xi-bin[2, 3], YUE Xiao-feng[1], MEN Xiang[1]

1. National Marine Data and Information Service, Tianjin 300171, *China;*

2. Tianjin Marine Environmental Monitoring Central Station, State Oceanic Association (SOA), Tianjin 300451, *China;*

3. Tianjin Marine Environmental Monitoring and Forecasting Center, Tianjin 300451, *China;*

Abstract: AMS^{14}C dating and grain-size analysis for Core FJ04, located at mud area in the North of East China Sea provide us a high-resolution grain-size distribution curve varying with depth and time. This paper got environmental sensitive grain-size group by using standard deviation method, and proved that the selected sensitive grain-size group is an important proxy which can be used to reconstruct intensity of East Asian Winter Monsoon (EAWM). Then we got reconstruction of EAWM evolvement since 3 ka B.P., which revealed two main phases: (1) 3 - 1.15ka B.P., relative weak EAWM with middle frequency fluctuation; (2) 1.15 - 0ka B.P., really strong EAWM with high frequency fluctuation. And 1.15 ka B.P. is a distinct turning point. During the whole period, 11 intense events of EAWM were recorded and correlated well with other climate records, but the response extent was different, which showed consistency of climate change and particularity of region response.

Keywords: shelf of East China Sea, mud area, sensitive grain size group, East Asian Winter Monsoon

In recent years, scientists gradually recognized that short period and abrupt events during Holocene affected activities and development of humankind deeply. Searching for high-resolution proxies became much more urgent [1, 2].East Asian Monsoon which was the active factor of East Asian Winter-Summer Monsoon system influenced climate of Chinese Mainland greatly. For a long time, grain size and susceptibility of the Chinese loess have been regarded as proxies of EAWM and East Asian Summer Monsoon (EASM) respectively. However, it is difficult to use the losses deposit to study high-resolution climate changes in historical records documented by human being, on centennial or even

Received on Aug. 11, 2011

Corresponding author: sxy.ily@163.com

shorter scale, due to the restriction of sedimentation rate. Thus, ice cores, peat, pollen, lacustrine sediments and stalagmite were also used as high-resolution proxies of EAM. Continental shelf of East China Sea was an area where EAWM dominated. Searching for a high resolution proxy to reveal climate change from mud area of continental shelf of East China Sea is of significance.

Along with appearance of laser instrument, progress of sampling technology and dating method, less sample required and high resolution could reach. As a result, palaeoenvironment research by using granularity of sediments has developed a lot. Sensitive grain-size groups separated from multi-leptokurtosis frequency distribution curve to discuss sedimentology significance began to be used in palaeoenvironment research. Sun et al.[3], Xiao et al. [2, 4, 5, 6], Xiang et al.[7, 8] and Wan et al.[9] had got sensitive grain-size groups to record evolvement of EAM from sediments of Okinawa Trough, East China Sea, and South China Sea separately by using granularity-standard deviation method.

In this paper, by using AMS^{14}C dating and grain-size analysis of core FJ04, we attempt to find a high-resolution proxy from sediments to record environmental evolvement, and discuss evolvement of EAWM.

1 Sampling and testing

1.1 Sampling

The sediments analyzed in this study is from core FJ04, which was collected by using gravity sampling pipe during summer cruise of Dongfanghong No.2 of Ocean university of China for National Keystone Basic Research Program "Marine Physical environmental change and climate response in the continental shelf of East China Sea" in June 2006. The sample was encapsulated immediately after recovery in order to confirm the surface sediment. FJ04 (Fig. 1, located 31.68°N, 125.81°E), water depth is 67 m, the length of the core is 167 cm. It was sectioned into 2 cm slices in lab, we got 83 subsamples and all of them were done grain size analysis.

1.2 Chronology

The chronology of core FJ04 was performed at Guangzhou Geochemistry Institute of the Chinese Academy of Sciences and National Key Lab of Nuclear Physics and Technique, Peking University. The material used for chronology was the benthonic foraminifera A. compressiuscula with the diameter larger than 63 μm. The three uncorrected ^{14}C ages were converted to the calendar ages using the international universal

software Calib 5.02[10]. The age model was constructed by linear interpolation between different AMS^{14}C dates, and then the deposition rate and sample resolution were calculated (Tab. 1). Tab. 1 shows that the deposition rate varied significantly. The deposition rate during 1 - 1.54 cal. ka BP was much faster than in the early and later stages. The highest sample resolution reaches 8.7 a/cm.

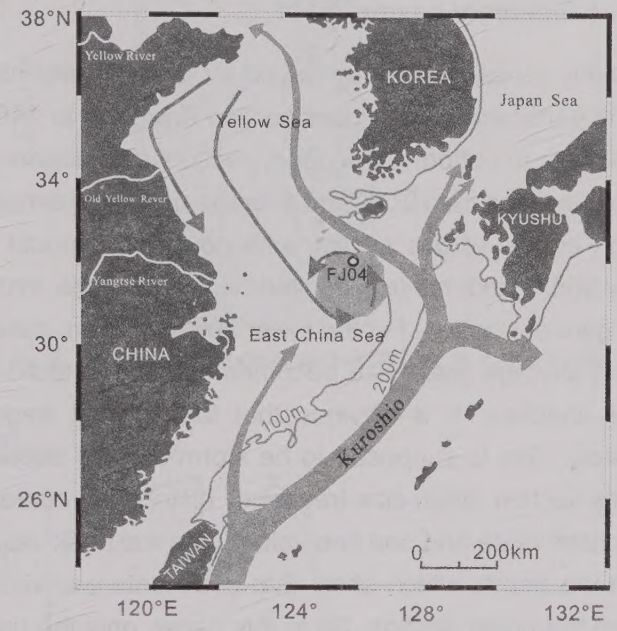

Fig.1 Location of core FJ04 and main currents of modern surface circulation of studied area

Tab. 1 AMS^{14}C age and sample resolution in Core FJ04

Depth / cm	AMS^{14}C age / a B. P.	Calendar age / cal. a B. P.	Deposition rate / cm/ka	Resolution / a/cm
38-40	1 279 ± 32	997	39.1	51.2
100-102	1 857 ± 34	1 540	114.2	17.5
153-155	3 261 ± 32	3 242	37.75	53.0

1.3 Grain size analysis

Grain size analysis was performed by using Malvern 2 000 laser instrument at the Key Lab of Submarine Geosciences and Prospecting Techniques of Ministry of Education in Ocean university of China. The measurement range of the instrument is 0.02 - 2 000 μm, the grain size resolution is 0.01Φ, and the repeated measurement error is lower than 3%. Samples were preprocessed with excess H_2O_2 for 24 h to remove organism. Hydrochloric acid was not used to release carbonate, because one of the main sediment sources in the study area was from the Yellow River which contained a lot of granule carbonate grain. The

biogenesis component (mainly >63 *μm* foraminifera shell) in the sediment was low with a mean content of less than 0.3% in the top 150 cm of the core.

2 Result

2.1 Lithology and sedimentary environment

Core FJ04 is mainly composed of gray clayed silt, and partially interrupted by thin fine sand. The sediment is generally fine in upper section (from top to 146 cm) and coarse in lower section (from 146 cm to bottom). The upper section is homogeneous clayed silt, with coarse population (>63 μm) less than 0.3% and average grain size almost no change (Fig. 2). Frequency distribution curves of this section with obvious unimodal are basically alike, which show relatively stable sedimentary environment and single material source, and is believed to be stable gyre deposition. For the lower 20 cm section, sand content increases, silt content decreased average grain size becomes coarser, selection becomes worsen, dark-colored mineral enriches, It is obvious that larger shell fragments present and accumulate disorderedly. This is supposed to be storm-derived deposit or other disaster event deposit. For this section, grain-size frequency distribution curves changed with two obvious peak (one coarse value and one fine value), and the peak value of coarse particle increases along with the depth, which show that sedimentary environment of the lower section is distinct from the upper section. So in this paper, only the upper 146 cm section was discussed as follows.

2.2 Sensitive grain size group separation

By caculating the standard deviation of each grain size grade, we defined four grain-size values, about 0.98 μm, 5.7 μm, 23 μm and 88 μm (Fig. 4), which may be sensitive to the sedimentary environment. However, for grain size (>63 μm) was mainly biogenic depoit and its content was less than <0.3%, so only grain size (>63 μm) was considered. We devided three grain-size groups, 11 - 63 μm, 2 – 11 μm and <2 μm and calculated the content and average grain size for each group (Fig. 5). Almostly no change of content for grain size group <2 μm in our studied depth range, so grain size group <2 μm was not sensitive grain size group to environment. Percentage of grain size group 2 - 11 μm and 11 - 63 μm changed a lot along the depth, but average grain size group of 2 - 11 μm showed no change, which indicate that content of grain size group 2 - 11μm changed as a result of variety of content grain size group 11 - 63 μm. Therefore, grain size group 11 - 63 μm was the sensitive grain size group to environment in core FJ04, this sensitive grain size group was very close to Xiang [7] obtained from Core B2 which is near to our study area.

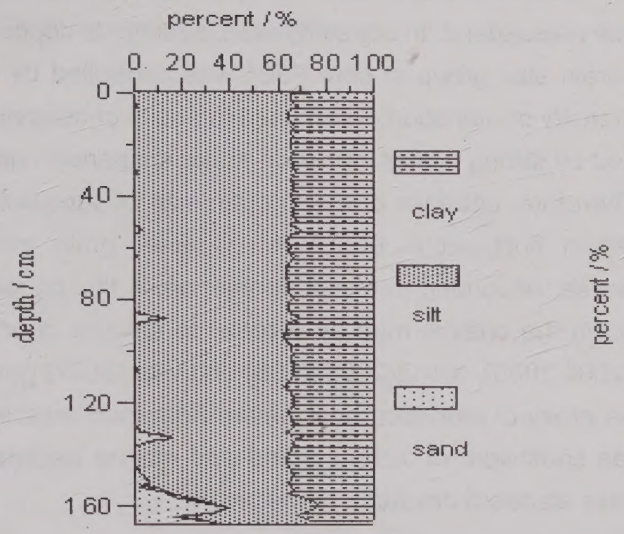

Fig. 2 Lithologic characteristics of core FJ04

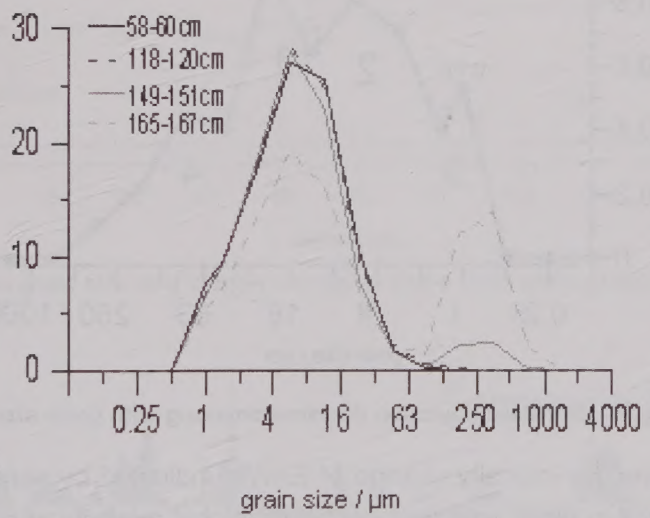

Fig. 3 Grain size frequency distribution of core FJ04

3 Discussions

Core FJ04 located at mud area in the north of continental shelf of East China Sea, the so called "North mud area of ECS", which is mainly derived from suspended sediments from Yellow River [13-15] and is transported southward by Yellow Sea Coastal Current [18]. Suspended sediments in continental shelf of Yellow Sea and East China Sea have an obvious characteristic of "store in summer and transport in winter". Suspended matter in

water body in winter is multiple of that in summer as winter storm cause sediments of Subei old Yellow River estuary resuspend. In our study area, sediments deposit mostly in winter [17]. Variety of sensitive grain size group in core FJ04 was controlled by Yellow Sea Coastal Current. In winter, intensity of monsoon determined intensity of coastal current, Yellow Sea coastal current droved by strong winter monsoon make suspended grain became coarser to our study area. Therefore, changes of mean grain size of sensitive grain size group in core FJ04 could reflect fluctuations of EAWM. Coarser grain indicate strong winter monsoon, and vice versa. According to this phenomenon, in this paper we use the vertical grain-size distribution in the coastal mud as a proxy to discuss changes of the Chinese paleo-climate. Xiao(2004,2005), Xiang(2005,2006) and Wan(2007) got sensitive grain size groups to be used as proxy of monsoon evolvement from mud area in inner shelf of East China Sea, mud area southwest of Jizhou Island and marine sediments in South China Sea by using grain-size standard deviation respectively.

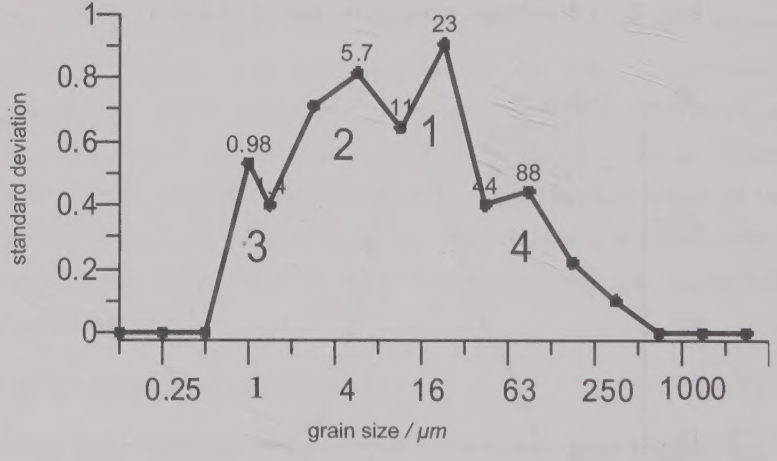

Fig. 4 Standard deviation distribution along with grain size

In order to compare intensity change of EAWM indicated by sensitive grain size in core FJ04 with record in other area and search for global relativity of climate change, we collected oxygen isotope data from Hongyuan peat [19], Jinchuan peat [20], Dunde ice core [21] and Greenland ice core [22] respectively, we also gathered air temperature data for the last 5 ka from Zhu [23]. By calculating mean grain size of sensitive grain size group (11 - 63 *μm*) in core FJ04, we got intensity of EAWM evolvement could be splitted into two phases: (1) 3 - 1.15 ka B.P. rather weak intensity od ESWM with middle extent fluctuation, among this period there are a few winter monsoon intensified events; (2) 1.15 - 0 ka B.P. very strong EAWM with high frequency fluctuation. 1.15 ka B.P. was a turning point. The general trend of climate change revealed in core FJ04 resembled record in Hongyuan peat, Jinchuan peat, Dunde ice core and Greenland ice core. But the turning point event deflect

among those records. Further more, changing of mean grain size of sensitive grain size recorded 11 intensified winter monsoon events.

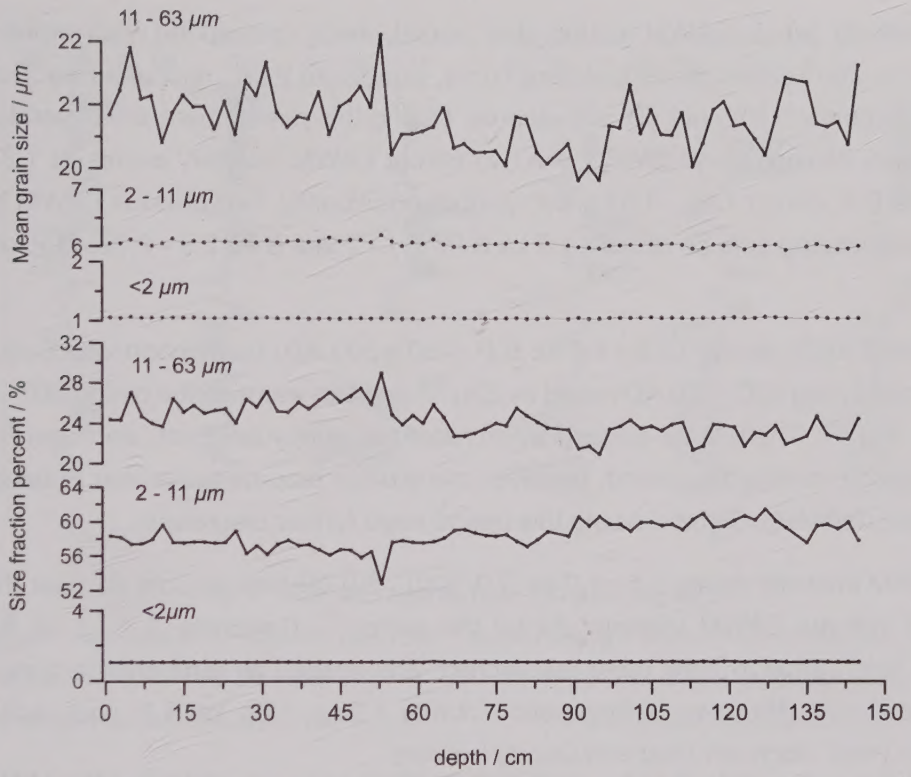

Fig. 5 Mean grain size and content variety of three main grain group of core FJ04

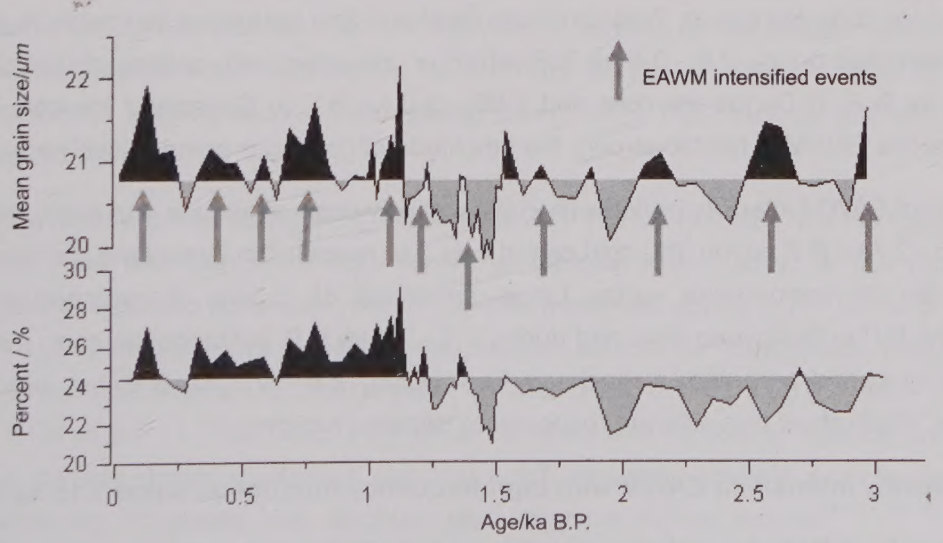

Fig. 6 Mean grain size and content variety of sensitive grain size group (11 - 63 *μm*) of core FJ04

3.1 Relatively weak EAWM with high frequency fluctuation during 3 - 1.15 ka B.P. period

Relatively weak EAWM during this period,which correspond with warm period indicated by Zhu kezhen air temperature curve, Hongyuan Peat, Jinchuan Peat,Dunde ice core and Greenland ice core climate records. During this period there are several obvious phases, very obvious weak EAWM with two abrupt EAWM intensify events at 1.2 ka B.P. and 1.4 ka B.P. during 1.15 - 1.5 ka B.P. period. Additionally, four obvious EAWM intensify periods exist during periods of 1.5 - 1.9 ka B.P., 2.1 - 2.2ka B.P., 2.5 - 2.7ka B.P. and 2.9 - 3.0 ka B.P..

Weak EAWM during 1.15 - 1.5 ka B.P. (450 - 800 AD) correspond with Suitang first warm period during 570 - 770 AD raised by Zhu [23] and first warm period during 500 - 800 AD raised by Wu [24]. There is no Suitang warm record in Hongyuan Peat, Jinchuan Peat and Dunde ice core during this period, however many other records prove that Suitang Warm period exist definitely. Climate during this period need further discussion.

EAWM intensify during 1.5 - 1.9 ka B.P. (450 - 50) AD period, Core B2 near the study area also indicate EAWM intensify during this period [7]. Generally, 2 - 1.5 ka B.P. was regarded cold period in most other researches, Zhu kezhen air temperature curve reveal cold period exist. However, Warm period during 1.53 - 1.68 ka B.P. was recorded in Hongyuan Peat, Jinchuan Peat and Dunde ice core.

EAWM intensified during 2.1 - 2.2 ka B.P. which corresponded with cooling period in Greenland ice core, Hongyuan Peat, Jinchuan Peat and Zhu kezhen air temperature curve. EAWM intensified during 2.9 - 3.0 ka B.P. which is coincident with cooling period during 3.0 - 3.1 ka B.P. in Dunde ice core and 2.95 - 3.0 ka B.P in Greenland ice core. And intensity of the EAWM is not too strong, the amplitude of cooling is comparatively small.

Distinct EAWM intensify period with comparatively large amplitude and long duration during 2.5 - 2.7 ka B.P period, this cold period was also recorded in Greenland ice core and Zhu kezhen air temperature curve. Large amplitude of cooling is recorded during 2.9 - 2.7 ka B.P in Hongyuan Peat and during 2.8 - 2.7 ka B.P. in Dunde ice core, there is also cooling period recorded in Jinchuan Peat during 2.9 - 2.7 ka B.P. but with less amplitude, which show that different response to climate changing.

3.2 Relatively intensified EAWM with high frequency fluctuation since 1.15 ka B.P.

Generally, EAWM intensified during this period which corresponds to cold period in Zhu kezhen air temperature curve and oxygen isotope record of Greenland ice core. And it

reveal four obvious EAWM intensified periods 1.15 - 0.95 ka B.P., 0.85 - 0.65 ka B.P., 0.5 - 0.3 ka B.P., 0.25 - 0.03 ka B.P. and three transitory weaken periods 0.95 - 0.85 ka B.P., 0.65 - 0.5 ka B.P. and 0.3 - 0.25 ka B.P.

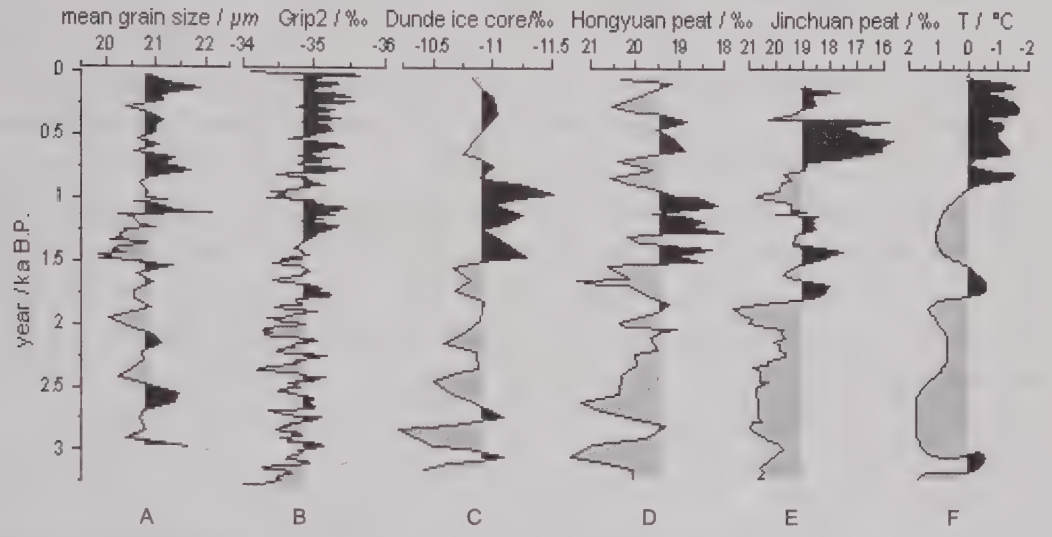

Fig. 7 Climate records from different regions

A: average grain-size curve for 11 - 63 μm of Core FJ04 B: GRIP2 oxygen isotope curve of Greenland ice core [22]

C: oxygen isotope curve of Dunde ice core D: oxygen isotope curve of Hongyuan Peat [19]

E: oxygen isotope curve of Jinchuan Peat [20] F: Zhu kezhen air temperature curve [23]

EAWM intensified during 1.15 - 0.95 ka B.P (800 – 1 000 AD)which coincident with cold period during 800-950 AD in Suitang Warm period raised by Wu[24]. Hongyuan Peat, Jinchuan Peat, Greenland ice core and Dunde ice core all reveal distinct cooling period. Afterwards, EAWM weakened during 0.95 - 0.85 ka B.P. (1 000 - 1 100 AD) which corresponds to Suitang second warm period during 950 - 1 050 AD, but this warm period only last 100 years.

EAWM intensified during 0.85 - 0.65 ka B.P.(1 100 - 1 300 AD), but Hongyuan Peat, Jinchuan Peat and Dunde ice core record all indicate warm period at this time which coincident with middle ages warm period. EAWM weakened during 0.65 - 0.5 ka B.P.(1 300 - 1 450 AD). Dunde ice core reveal that temperature ascend constantly since 1 300 AD and with the maximum value at 1 400 AD. EAWM intensified during 0.3 - 0.5 ka B.P (1 450 - 1 650 AD), 0.25 - 0.03 ka B.P (1 700 - 1 920 AD) which correlate with traditional “little ice age”. “Little ice age” climate shows an obvious globality which recorded widely in Such as Greenland ice, Dunde ice, Hongyuan peat, Jinchuan peat and other climate records[19-21, 24-25].

4 Conclusion

The authors get environmental sensitive grain size group in core FJ04 by using grain size standard deviation method, which proves the selected sensitive grain size group is an important proxy. The mean grain size of this sensitive group can be used to reconstruct the Asian w inter monsoon intensity. The reconstruction of the East Asian winter monsoon evolvement since 3 ka B.P. reveals two main phases: (1) 3 - 1.1 5 ka B.P., with relative weak intensity and medium frequency fluctuation. (2) 1.15 - 0 ka B.P., with really strong and high frequency fluctuation. 1.1 5 ka B.P. is a distinct point. During the whole period. 11 obvious winter monsoon buildup events were recorded and correlated well with other climate records, but showed different extent response which proves the consistency of climate change.

Reference

[1] WANG Pin-xian, JIAN Zhi-min. Searching high resolution paleoenvironmental records: A review [J]. Quaternary Sciences, 1999, 19 (1):1 - 17.

[2] XIAO Shang-bin, ZHANG Jing-sui, CHREN Mu-hong. Exploring High-Resolution Records of the Holocene East Asian Monsoon from Mud Sediments on Shelves of China Marginal Seas [J]. Journal of China Three Gorges University (Natural Sciences), 2007(8), 29(4):343 - 347.

[3] SUN You-bin, GAO Shu, Li Jun. A primary study on Environmental sensitive grain size on terrigenous sediment in marginal sea [J]. Chinese Science Bulletin, 2003, 48(1):83-87.

[4] XIAO Shang-bin, LI An-chun, JIANG Fu-qing. Sediment record and climate significance of recent 2 ka mud on the inner shelf of the East China Sea [J]. Chinese Science Bulletin, 2004, 49(21): 2 233 - 2 238.

[5] XIAO Shang-bin, LI An-chun. A Study on Environmentally Sensitive Grain-size Population in Inner Shelf of the East China Sea [J]. Acta Sedimentologica Sinica, 2005(3), 23(1):122 - 128.

[6] XIAO Shang-bin, LI An-chun, CHEN Mu-hong. Recent 8 ka Mud Records of the East Asian Winter Monsoon from the Inner Shelf of the East China Sea [J]. Earth Science-Journal of China University of Geosciences, 2005(9), 30(5):573 - 581.

[7] XIANG Rong, YANG Zuo-sheng, Y. Saito. East Asia Winter Monsoon change of recent 2 300 a recorded by environmental sensitive grain-size population change in the Mud Area Southwest off Cheju Island, ECS [J]. Science in China (Series D), 2006, 36(7):654 - 662.

[8] XIANG Rong, YANG Zuo-sheng, GUO Zhi-gang. Paleoenvironmental Implications of Grain-Size Component Variations in the Mud Area Southwest off Cheju Island, ECS [J]. Earth Science-Journal of China University of Geosciences, 2005, 30(5):582 - 588.

[9] WAN Shi-ming, LI An-chun, XU Fang-jian. East Asia Winter Monsoon change of recent 20Ma from grain size analysis of ODP1146 site from north of South China Sea [J]. Science in China (Series D), 2007, 37(6):761 - 770.

[10] Stuiver M, Reimer P J, Bard E, et al. INTCAL 98 radiocarbon age calibration, 24000-0 cal BP [J]. Radiocarbon, 1998, 40: 1 041 - 1 083.

[11] SUN Dong-huai, AN Zhi-sheng, SU Rui-xia. Mathematical approach to sedimentary component partitioning of polymodal sediments and its applications [J]. Progress in Natural Science, 2001, 11(3): 269 - 276.

[12] Prins M A, Postma G, Cleveringa J, et al. Controls on terrigenous sediment supply to the Arabian Sea during the late Quaternary: the Makran continental slope [J]. Marine Geology, 169(3-4): 351 - 371.

[13] YANG Zuo-sheng, GUO Zhi-gang, WANG Zhao-xiang. Corresponding relation and affection between suspended body and water mass of Yellow sea, East China Sea and adjacent sea area [J]. Journal of Ocean University of Qingdao, 1991, 25(3):55 - 69.

[14] YANG Zuo-sheng, GUO Zhi-gang, WANG Zhao-xiang, et al. Basic pattern of transport of suspended matter from the Yellow Sea and East China Sea to the eastern deep seas [J]. Acta Oenological Sinica, 1992, 14(2):81 - 90.

[15] Milliman J D, Beardsley R C, Yang Z S, et al. Modern Huanghe drived on the Outer Shelf of the East China Sea: identification and potential transport mechan ism [J]. Continental Shelf Research, 1985, 4:175 - 188.

[16] SUN Xiao-gong, FANG Ming, HUANG Wei. Spatial and temporal variations in suspended particulate matter transport on the yellow and East China Sea shelf [J]. Oceanology and Limnology, 2000, 31(6):581 - 587.

[17] GUO Zhi-gang, YANG Zuo-sheng, LEI Kun. Seasonal variation of the Sedimentary danamic processes for the mud area in the north East China Sea [J]. Journal of Ocean University of Qingdao, 1999(7), 29(3):507 - 513.

[18] GUO Zhi-gang, YANG Zuo-sheng, WANG Zhao-xiang. Influence of water masses on the distribution of sea-floor sediments in the Huanghai Sea and the East China Sea [J]. Journal of Ocean University of Qingdao, 1995, 25(1): 75 - 83.

[19] XU Hai, HONG Ye-tang, LIN Qing-hua, et al. Temperature change over the past 6 000a from cellulose oxygen isotope of Hongyuan peat [J]. Chinese Science Bulletin, 2002, 47(15):1 181 - 1 186.

[20] HONG Ye-tang, JIANG Hong-bo, TAO Fa-xiang, et al. Temperature record of Jinchuan peat δ18O over the last 5 000 a [J]. Science in China (Series D), 1997, 27(6) :525 - 530.

[21] YAO Tan-dong, Thompson L G. Temperature variation over the past 5 000 a from the record of Dunde ice-core [J]. Science in China (Series D), 1992(10):1 089 - 1 093.

[22] Stuiver M, P M Grootes, T F Braziunas. The GISP2 ^{18}O climate record of the past 16 500 years and the role of the sun, ocean and volcanoes [J]. Quaternary Research, 44:341 - 354.

[23] ZHU Ke-zhen. Primary study on climatic change over the past 5 000 a [J]. Science in China (Series A), 1973(2):168 - 189.

[24] WU Hong-qi, Dang An-rong. Fluctuation of Climatic Change in Temperature of Tang Dynasty [J]. Quaternary Research, 1998 (1): 31 - 38.

[25] Tan M, Liu T, Hou J, et al. Cyclic rapid warming on centennial-scale revealed by a 2 650 year stalagmite record of warm season temperature [J]. Geophys. Res. Lett., 2003, 30(12): 1 617 - 1 620.

[26] WANG Shao-wu. Research on the Little Ice Age Climate [J]. Quaternary Research, 1995, (3): 202 - 212.

中国东海北部泥质区敏感粒度组分对东亚季风演变的响应

孙晓燕[1]，李希彬[2,3]，岳晓峰[1]，门 翔[1]

（1. 国家海洋信息中心，天津 300171；2. 国家海洋局天津海洋环境监测中心站，天津 300451；
3. 天津市海洋环境监测预报中心，天津 300451）

摘 要：本文运用粒级-标准偏差方法对 FJ04 孔146 cm以上部分进行敏感粒度组分分析与提取，证明选取的敏感粒度组分是本区重要的环境替代性指标，其平均粒径的变化可以用来指示东亚季风的强弱。获得了东海北部泥质区3 ka以来东亚冬季风强度的演化过程，结果表明东亚季风经历了两个主要的演变阶段：①3 - 1.15 ka B.P.为东亚冬季风较弱，中等程度波动阶段，期间也存在几次冬季风加强期；②1.15 ka B.P.为东亚冬季风强盛、高频率波动阶段。1.15 ka B.P.是一个明显的转折点。此外，3 ka 敏感粒度组分平均粒级的变化还记录了11次冬季风增强事件，与全球其他地区的气候记录具有极好的对应关系，但在不同的地区的响应程度不同，说明气候变化存在全球一致性和区域响应的特殊性。

关键词：东海陆架；泥质区；敏感粒度组分；东亚冬季风

The Kuroshio front to the east of Taiwan: seasonal feature, variability and mechanism

WANG Qi[1], LI Wei[1, 2*], MA Ji-rui[1, 2], HAN Gui-jun[1, 2], ZHANG Xue-feng[1, 2], WANG Xi-dong[1, 2]

1. *National Marine Data and Information Service, State Oceanic Administration, Tianjin* 300171, *China*

2. *Key Laboratory of Marine Environmental Information Technology, State Oceanic Administration Tianjin* 300171, *China*

Abstract: Oceanic front, especially Kuroshio front, is an important phenomenon that is of great significance for scientific research, national economy and military uses. However, Kuroshio front to the east of Taiwan (KFETW in brief) was rare investigated. In this study, reanalysis method is used to study the KFETW's temporal and spatial variability and frontogenesis mechanism. It is found that although surface thermal front to the east of Taiwan is not obvious, there is an all-year strong Kuroshio thermal front called KFETW under the surface. The KFETW is connected to the south section of Kuroshio front in the East China Sea (KFECS in brief) and distributes along the east coastline of Taiwan. The KFETW has multi-scale variation feature. It has significant seasonal signal, and its intensity and width reach their maximum in summer. By using the reanalysis results obtained from this study, frontogenesis and changing mechanisms of the KFETW are discussed. It is found that both the Kuroshio and up-welling to the east of Taiwan can affect this front, and the up-welling may be the predominant factor in KFETW's frontogenesis and maintenance mechanism.

Keywords: Kuroshio front; the east of Taiwan; reanalysis; seasonal feature; frontogenesis

1 Introduction

Since 1960s, a lot of studies about Kuroshio to the east of Taiwan and adjacent areas have been carried out by oceanographers in National Taiwan University. Based on the hydrographic observations around Taiwan from July 1962 to January 1963, the oceanic environment around Taiwan was studied by Chu (1963) which indicated that the isotherms along the east coast of Taiwan have the warp-up trend and this phenomenon could be ascribed to cold water due to up-welling induced by topography.

Received on Dec. 24, 2010

*Corresponding author: liwei@mail.nmdis.gov.cn

The Cooperative Study of the Kuroshio current and adjacent region (CSK) was executed during 1965 to 1977. From 1965 to 1969, R/V YANG MING was engaged in CSK, and in 1968, R/V CHIU LIEN devoted itself to research work (Guan, 1983). In the North Pacific Experiment (NORPAX), six cruises were implemented during the 1974-1975 by the R/V CHIU LIEN for hydrographic measurements, and geostrophic transport of the Kuroshio has been calculated. Based on the hydrographic data collected by the above six cruises of R/V CHIU LIEN, Chu (1976) made the section graphs of temperature, salinity and geostrophic current between Taiwan and Ishigakijima. These section observations suggest that the subsurface isotherms to the east of Taiwan have the trend of warping up shoreward. The general description about CSK can be referred to Guan (1983) which reviews primary study on Kuroshio to the east of Taiwan and in East China Sea made by Chinese and Japanese oceanographers since CSK.

In recent two decades, a lot of research works on oceanic features of Kuroshio near Taiwan were carried out. For example, in Kuroshio Edge Exchange Processes (KEEP), Kuroshio front and eddy to the northeast of Taiwan (Lin et al., 1992), Kuroshio countercurrent (Chuang et al., 1993) , water exchange (Chern et al., 1990), up-welling (Liu et al., 1992) and so on have been studied. An interesting feature of current velocity northeast of Taiwan is cold-water upwelling, which has been studied by Liu et al. (1992), Tang et al. (2000) and Wu et al. (2008) successively. Jing and Li (2003) studied a large quasi-stationary cold-core, cyclonic eddy southeast off Taiwan. Sun (1987) demonstrated the seasonal variation of the surface axial of Kuroshio. By using observations from the World Ocean Circulation Experiment (WOCE) PCM-1 moored current meter array in the east Taiwan channel, Kuroshio to the east of Taiwan was systematically studied (Johns et al., 2001; Lee et al., 2001; Zhang et al., 2001). Some new research results about Kuroshio to the east of Taiwan have been obtained by using shipboard ADCP measurement (Liang et al., 2003) and numerical model (Hsin et al., 2008). In the above literatures, studies about Kuroshio front mainly focused on the Kuroshio front to the northeast and southeast of Taiwan, while Kuroshio front to the east of Taiwan (KFETW in brief) was rare investigated.

In general, unlike the research (Tang, 1992; Tang, et al., 1992) on Kuroshio front in the East China Sea (KFECS in brief) which has employed criterion of thermal front, extracting oceanic front information and systematically studying temporal and spatial variation and its mechanism, the research on the KFETW is rarely involved, although this front is of great significance for national economy and military uses. Therefore, it is necessary to carry out further research on the KFETW in practice.

In this paper, reanalysis method is used to study seasonal feature, variability and mechanism of the KFETW. The reanalysis procedure and reanalysis results are described

in the following section. Section 3 gives the spatial distribution and temporal variation of the KFETW by using the reanalysis obtained from this study. The frontogenesis and changing mechanisms of the KFETW are discussed in section 4. Conclusions will be given in section 5.

2 Reanalysis

There is no long-time temperature observation section to permit us to analyze the spatial and temporal variation of the KFETW. Fortunately, reanalysis that makes use of observation and background information as well as physics constraint can provide us the possibility of analyzing the KFETW dynamically. In this section, a reanalysis product is provided.

2.1 Model configuration

In this study the Princeton Ocean Model with generalized coordinate system (POMgcs in brief) (Mellor et al., 2002; Ezer and Mellor, 2004) serves as the dynamic model in reanalysis. The source code of POMgcs can be downloaded from the website (http://www.aos.princeton.edu).

The study area extends from 10°S to 52°N in latitude and from 99°E to 150°E in longitude. The model grid spacing is varied from 1/2° to 1/8°. In POMgcs, the z-level or the original σ-level of POM or the hybrid vertical grid of both can be chosen. Due to the huge range and the complicated bathymetry of the study area, the hybrid coordinate of POMgcs is in use following the study of Mellor et al. (2002). The σ-level vertical grid is used in area with local depth less than 200m. In area with local depth greater than 200 m, the σ-level vertical grid is used when level depth is greater than certain proportion of the local depth and the z-level standard vertical grid is used in other level. In order to simulate satisfactorily the upper mixed layer and thermocline, most of the vertical levels are set to z-level at the upper ocean, while only a few vertical levels near seafloor are set to terrain-following σ-level to represent the seafloor preferably to avoid the stair-step effect. Coarse vertical level near seafloor can make the hydrostatic consistency criteria satisfied. There are 35 vertical levels with the maximum depth of 5 035 m.

Monthly-mean temperature and salinity (T-S) fields in January of the Estimating the Circulation and Climate of the Ocean (ECCO), World Ocean Atlas 2005 (WOA05) and NMDIS are combined to form the first-guess fields by using the multi-grid data assimilation scheme (Li et al., 2008). The corresponding sea surface height (SSH) is adopted from ECCO and the corresponding velocity field is set to zero.

In order to obtain a steady state based on the above first-guess fields, the model should spin up for 40 years. In this spin-up procedure, the open boundary conditions for SSH, T-S and velocity are provided by Simple Ocean Data Assimilation (SODA) multi-year monthly-averaged product. The meteorological driving force fields, such as wind, air temperature and cloud, use the multi-year monthly-averaged results from National Centers of Environmental Prediction (NCEP) reanalysis. After 40-year model run a steady state is obtained. Then T-S observations from 1979 to 1985 are assimilated into POMgcs for another 6-year run. The obtained results then serve as the initial fields for this reanalysis.

This reanalysis spans 20 years from January 1986 to December 2005. Then T-S observations from 1986 to 2005 are assimilated into POMgcs to generate reanalysis products. In this reanalysis procedure, SODA monthly-mean product of each year serves as the open boundary condition for SSH, T-S and velocity. Wind field between January 1st, 1986 and June 30th, 1999 is the NCEP reanalysis wind field with temporal resolution 6-hour and horizontal resolution 1.875° × 1.875°. And from 1st July 1999 to December 31st, 2005, the wind field is changed to the Quick Scatterometer (QuikSCAT) wind field with horizontal resolution 0.25° × 0.25°. Other meteorological driving force fields, such as air temperature and cloud, use the NCEP reanalysis results.

2.2 Data and quality control procedure

The oceanic observations assimilated into this reanalysis system include: T-S observations of Nanson, CTD, all kinds of BT and Argo profiles, multi-satellite altimeter sea surface height anomaly (SSHa) and satellite remote sensing sea surface temperature (SST).

The quality control for the observed level data includes checks for position/date/time, depth duplication, depth inversion, range, excessive gradient, and density, etc. Prior to the next step in the quality control procedure, the data are interpolated from observed levels onto standard depth levels. Then further quality control is performed on these standard depth level data. The further quality control includes climatologically standard error checks, that is, picking up the profiles beyond the standard error to make man-machine check, and density stability check for the standard level data.

The quality control procedures on the Argo float data are basically listed as follows: remove duplicate cycle, position on land test, impossible speed test, constant value checks for pressure, temperature and salinity, global range test, regional range test, remove duplicate pressure and pressure inversion test, spike test, gradient test for salinity and temperature, density stability test, etc. Besides, the calibration method developed by Wong, Johnson and Owens (2003), hereinafter WJO in brief, is employed to calibrate the sensor

drift of salinity measurements from the Argo data with regional T-S relationships, by using the spatial and temporal nearby historical hydrographic data.

The multi-satellite altimeter SSHa data are obtained from the altimeter data user service website in France (http://www.jason.oceanobs.com). These data are developed by merging SSHa data of TOPEX/POSEIDON (T/P), Jason-1, ERS-2 and Envisat with the multi-year mean surface level deducted. The 7-day averaged grid SSHa dataset from 1994 to 2005 is then developed by interpolating the above merged SSHa data to 0.25°×0.25° grid.

The satellite remote sensing SST data are from Reynolds SST datasets (Reynolds et al., 2007) (ftp://eclipse.ncdc.noaa.gov/pub/OI-daily/NetCDF/). These products have been developed using optimum interpolation to merge Advanced Very High Resolution Radiometer (AVHRR) infrared satellite SST data and in situ data from ships buoys, and furthermore merge Advanced Microwave Scanning Radiometer (AMSR) when AMSR became available in June 2002. These products include a large-scale adjustment of satellite biases with respect to the in situ data. The horizontal resolution is 0.25°×0.25° and the temporal resolution is one day.

2.3 Oceanic data assimilation scheme

In order to extract long and short wavelength information in turn quickly from observations system and provide objective and accurate analysis, the multi-grid 3-dimensional variational (3D-Var) data assimilation scheme is used in this reanalysis to assimilate T-S profiles and satellite remote sensing SST. The basic idea of this data assimilation scheme can be referred to Li et al. (2008) and Li et al. (2010).

In order to guarantee the consistence of T-S in the data assimilation procedure, the salinity adjustment scheme of Troccoli et al. (2002) is used. When assimilating the satellite altimeter SSHa, according to the study of Zhu and Yan (2006), this study converts satellite altimeter SSHa into T-S "pseudo observation" based on traditional 3D-Var in which the vertical correlation of temperature background error is taken into account. And some modifications are made. The non-linear model T-S relationship is treated as strong constraint in cost function in this procedure, which makes the cost function only be a function of temperature. Salinity is directly derived from temperature based on model T-S relationship. Therefore, the model T-S relationship can be conserved during assimilating SSHa data. Then the T-S "pseudo observation" derived from satellite altimeter SSHa can be assimilated into model by using the above multi-grid 3D-Var data assimilation scheme to adjust temperature and salinity.

2.4 Reanalysis results

Detailed validation/verification of this reanalysis result will not be discussed in this paper since it is beyond the scope of this study. Here only one temperature section comparison on April 9th, 1992 is given in Fig. 1, where temperature structure of this section is satisfactorily reanalyzed, and especially northward warm tongue of Kuroshio is very clear. The trend of warping up shoreward is also obvious in this reanalysis result, which is also consistent with the observation very well. Reanalysis can provide us the possibility of analyzing the KFETW dynamically because it can combine observation and background information as well as physical constraint. Therefore, the reanalysis results will be used in next section to study the KFETW.

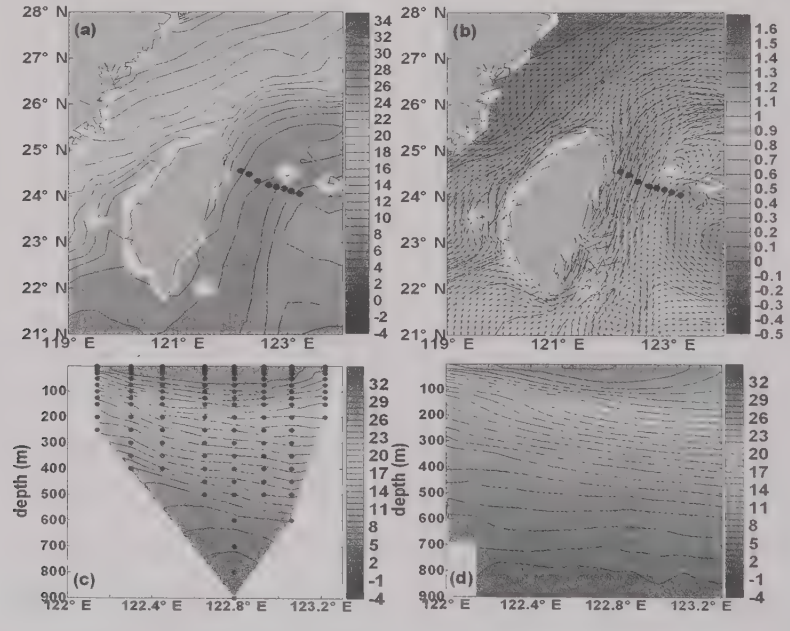

Fig. 1 Temperature section comparisons on April 9th 1992

(a) sea surface temperature (Unit: ℃) in this reanalysis; (b) sea surface height (Unit: m) in this reanalysis, with arrow representing surface velocity in this reanalysis and black points representing location of observations; (c) temperature section (Unit: ℃) made by using observations with black points representing location of observations; (d) temperature section in this reanalysis (Unit: ℃).

3 Spatial distribution and temporal variation of KFETW

3.1 Spatial distribution of KFETW

Different criterions to judge oceanic front may be employed by different

oceanographers for different purposes. In this paper, the criterion $|\nabla T| \geq 0.1\,^{\circ}C / nmile$ (that is $|\nabla T| \geq 0.054\,^{\circ}C / km$) used by Tang et al. (1992) is applied to serve as the thermal front criterion for the KFETW.

After calculating the horizontal temperature gradient of each level from the daily reanalysis results of this study, intensity and width information of oceanic thermal front are extracted based on the strong criterion of thermal front $|\nabla T| \geq 0.054^{\circ}C / km$. Climatological statistics on these intensity and width information in area from 117°E to 130°E in longitude and from 19°N to 33°N in latitude indicate that the surface KFECS is evident in spring, autumn and winter, and the intensity and width of the KFECS reach their maximum in winter, while almost no surface KFECS is found in summer; as for subsurface intensity of front in winter is equivalent to that in summer. All of these results agree with the previous study results of Tang et al. (1992). However, almost no surface thermal front can be found to the east of Taiwan for all seasons, while in subsurface the KFETW is evident (Fig. 2). This front is connected to the south section of the KFECS and distributes along the east coastline of Taiwan.

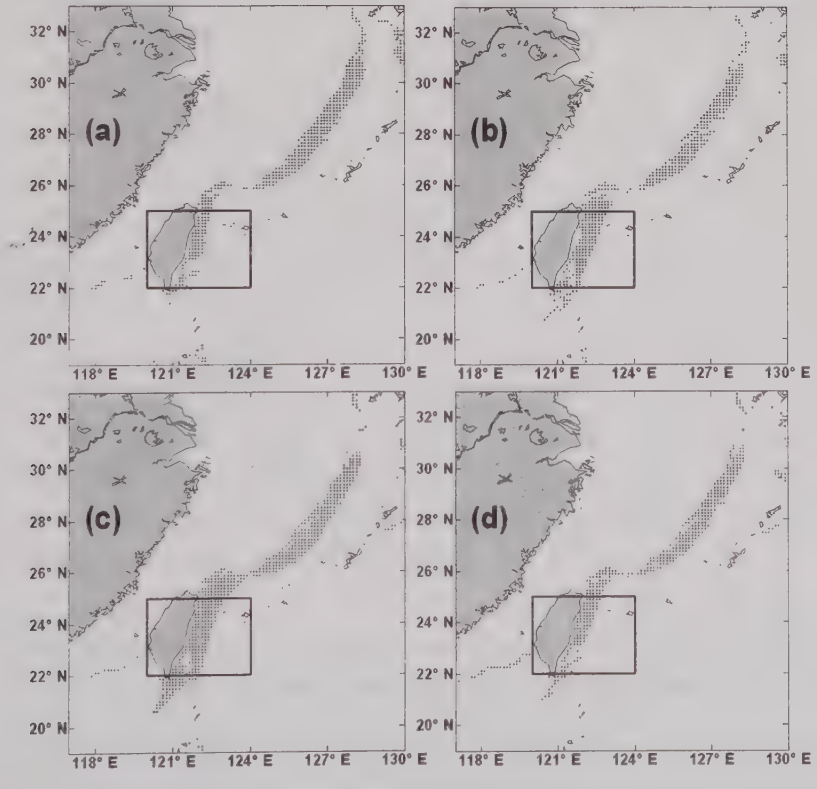

Fig. 2 Multi-year average distribution of thermal front at 150 m level in January

(a), April (b), July (c) and October (d) calculated from the reanalysis result in this paper, with black rectangular representing the study area.

Multi-year average characteristics of this KFETW are calculated from the reanalysis results. It is found that the KFETW can exist between 20 m and 350 m and there is all-year front between 150 m and 350 m. Thickness of this front varies from 200 m to 330 m. Horizontal position of this front tends to move eastward with depth increasing. The variation amplitude of the north end of this front is larger than that of the south end, which may be related to the Kuroshio seasonal variation near northeast of Taiwan (Sun, 1987). With depth increasing, both intensity and width of the KFETW has the tendency of decrease following increase.

3.2 Temporal variation of KFETW

Applying the maximum entropy spectral analysis and prominence check to the above mentioned daily intensity and width information of the KFETW, it is found that the KFETW not only has the significant annual cycle, but also exhibits the significant multi-scale variation cycle, like 2.5-year, 1.7-year, 248-day, 188-day, 124-day, 93-day and 58-day which are shown in Fig. 3. The prominent inter-annual variation of the KFETW may be related to the inter-annual variation of the Kuroshio. This section will focus on seasonal variations of this front.

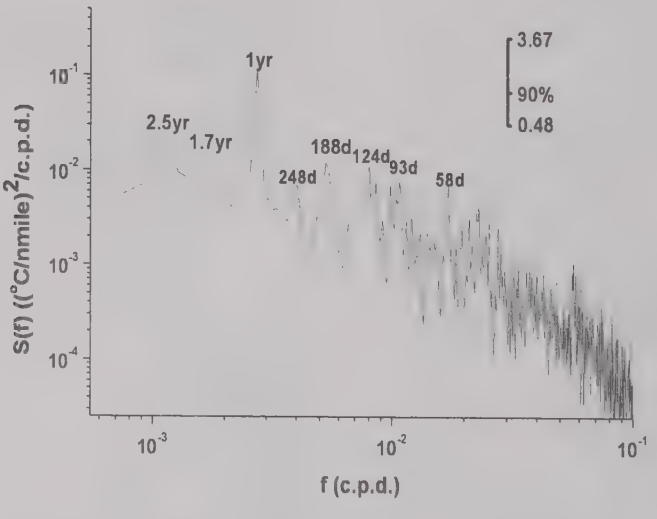

Fig. 3 Maximum entropy spectral analysis of KFETW intensity of 150 m calculated from the reanalysis results in this paper.

After making multi-year monthly average on the above daily intensity and width information, it is found that above 75 m or below 200 m, seasonal signal is not evident while the seasonal signal is obvious between these two levels. Fig. 4 shows the seasonal feature of intensity and width of this front between 100 m and 200 m, and it can be seen

that both intensity and width reach their maximum in summer, which is consistent with the result from observations analysis and numerical simulations in this study. The thickness of this front also has seasonal signal and reaches its maximum during May to July. From Tab. 2 of Tang (1992), it can be seen that the intensity of south session of the KFECS gets its maximum in summer. Since the north end of this KFETW joints with the south session of the KFECS, these two fronts may have some similar features.

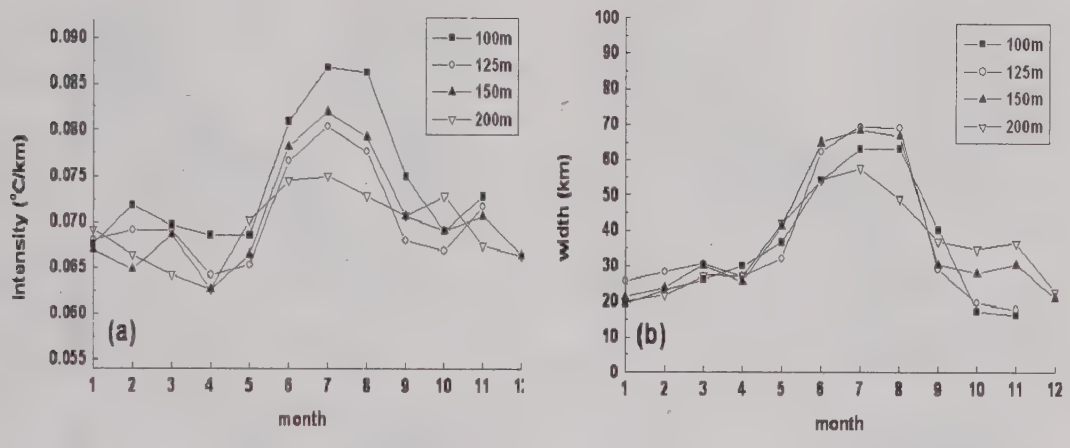

Fig. 4 Seasonal variation of intensity (a) and width (b) of KFETW between 100 m and 200 m calculated from the reanalysis results in this paper

4 Frontogenesis and changing mechanisms of KFETW based on reanalysis results

Frontogenesis and changing mechanisms of KFETW will be discussed in this section. Actually, there are many possible frontogenesis mechanisms for the KFETW, for example, sea surface wind, sea surface heat flux, Kuroshio flux and its axis, up-welling and oceanic eddy and so on. In this paper, only impacts of Kuroshio flux, its axis and up-welling on the KFETW are discussed based on reanalysis results of this study.

4.1 Up-welling

Up-welling can result in frontogenesis. Furthermore, lots of studies about the relationship between Kuroshio front and up-welling indicate that up-welling exists in Kuroshio front zone in East China Sea (Wan et al., 1994), and below 100m level, the main frontogenesis mechanism of the KFECS is Kuroshio water's up-welling not only in summer but also in winter (Tang et al., 1992). Vertical velocity at 100m level and in section 24°N (121°E~131.5°E) east of Taiwan derived from the reanalysis result of this study by using

continuity equation are shown in Fig. 5. Up-welling zone and down-welling zone distributed near the shelf-slope area, and along Kuroshio up-welling zones mainly locate to the left side of the KFECS while down-welling zones locate at both sides. However, as for the KEFTW up-welling zones mainly locate at the left side of this front while down-welling zones locate at the right side. All these distribution patterns of up-welling and down-welling are consistent with the previous study (Wan et al., 1994).

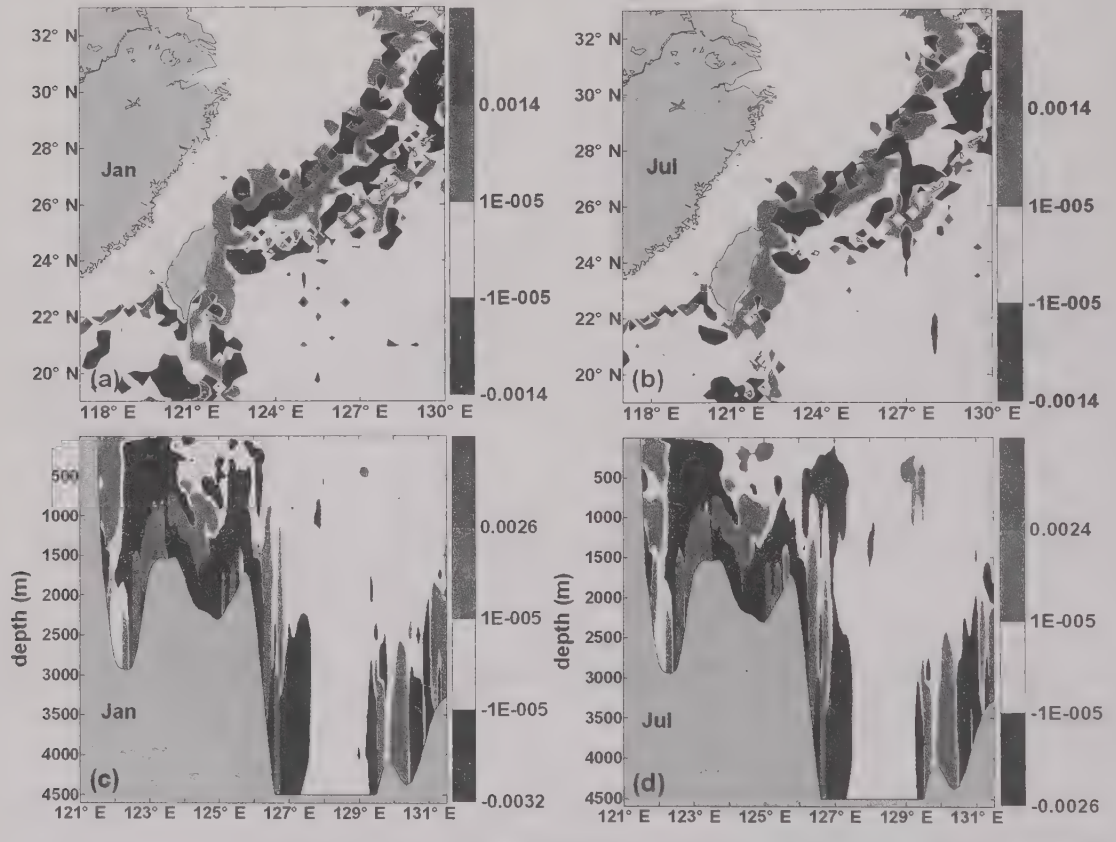

Fig. 5 Vertical velocity in 100 m level (top) and in section 24°N (121°E - 131.5°E) to the east of Taiwan (bottom) in January (left) and July (right) derived from the reanalysis result of this study. (Unit: m/s).

Considering temperature tracer equation $\frac{\partial T}{\partial t} + w\frac{\partial T}{\partial z} + other_term = 0$, it can be obtained that

$$\frac{\partial}{\partial t}\left(\frac{\partial T}{\partial x}\right) = -\frac{\partial w}{\partial x}\frac{\partial T}{\partial z} - w\frac{\partial}{\partial z}\left(\frac{\partial T}{\partial x}\right) - \frac{\partial}{\partial x}(other_term) \quad (1)$$

if $\frac{\partial T}{\partial z} \geq 0$ and $\frac{\partial w}{\partial x} \leq 0$, that is, up-welling velocity onshore is greater than that of offshore,

the contribution of the first term on the right side of equation (1) to the horizontal temperature gradient is not negative which may intensify thermal front. For the KFETW, up-welling zones locate at onshore cold water side while down-welling zones locate at offshore warm water side, which may make the condition $\frac{\partial w}{\partial x} \leq 0$ easily satisfied. And considering temperature always decreases with depth increasing, condition $\frac{\partial T}{\partial z} \geq 0$ is also satisfied. All of these two conditions may intensify the KFETW, so up-welling may be a significant frontogenesis and maintenance mechanism of the KFETW. Fig. 6 shows cross spectrum between up-welling velocity at 150 m level to the east of Taiwan and intensity of the KFETW at the same level calculated from reanalysis results in this study. Among correlation coefficients at periods above 30-day, those of 341-day, 72-day, 58-day and 55-day may exceed 0.5, which indicates that at these periods up-welling velocity and intensity of the KFETW have significant correlations. Based on the reanalysis results in this study temporal variation of up-welling on the left side and down-welling on the right side of Kuroshio to the east of Taiwan (22°N - 25°N, 121°E - 124°E) is shown in Fig. 7. And it is found that the difference between up-welling on the cold water side and down-welling on the warm water side of Kuroshio can reach its maximum in July, which suggests that maximum of the KFETW intensity may appear in summer.

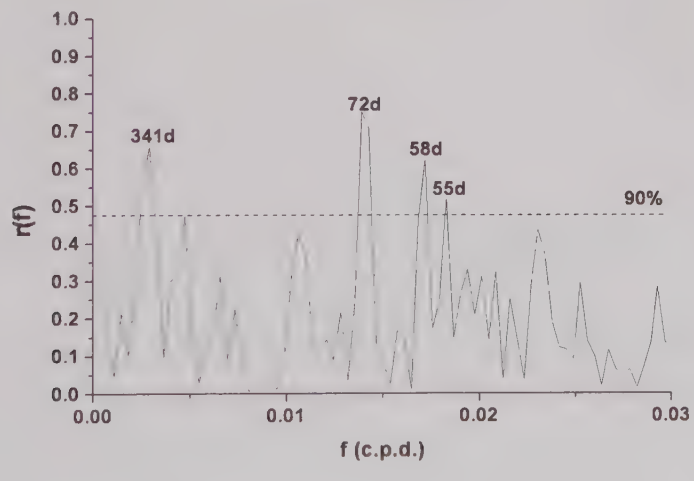

Fig. 6 Cross spectrum between up-welling velocity at 150 m level to the east of Taiwan and intensity of KFETW at the same level calculated from reanalysis results in this study

4.2 Kuroshio flux and its axis

The KFETW is a thermal front between Kuroshio warm water and cold water near Taiwan east coast, so Kuroshio warm water may affect this front considerably. Fig. 8 shows

cross spectrum between Kuroshio flux to the east of Taiwan and intensity of the KFETW at 150 m level calculated from reanalysis results in this study. Among correlation coefficients at periods above 30-day, those of 341-day, 109-day, 88-day, 55-day, 50-day, 46-day, 43-day and 41-day may exceed 0.5, which indicates that at these periods Kuroshio flux and intensity of the KFETW have significant correlations. Further study (not shown here) indicates that strong correlation also exists between zonal location of Kuroshio axis and that of the KFETW of corresponding level. And correlation between the zonal location of Kuroshio axis and that of the north end (25°N) of the KFETW is stronger than that between the zonal location of Kuroshio axis and that of the south end (23.5°N) of the KFETW. From winter to summer, the Kuroshio flux to the east of Taiwan increases, and by warming the upper water temperature to the east of Taiwan the Kuroshio warm advection can enlarge the horizontal temperature gradient between both sides of the Kuroshio axis and may intensify and broaden the KFETW. Meanwhile, with Kuroshio axis moving eastward, the position of the KFETW also moves eastward. On the contrary, from summer to winter, with Kuroshio axis moving westward, the intensity and width of the KFETW decrease and the position of this front moves westward.

4.3 Comparison between the contributions of Kuroshio advection and up-welling

From above discussion, Kuroshio and up-welling all have significant impact on the seasonal variation of the KFETW, so it is worth to study which factor is more important. Since the KFETW relates closely to the warping up trend of isotherm onshore with cold water to the west side and warm water to the east side, one can choose two points (point 1 and point 2 in Fig. 9) from both sides respectively to analyze temporal evolution of temperature value. Temporal evolution of temperature value of the point on cold water side represents the contribution of up-welling to horizontal temperature gradient and that on warm water side represents the contribution of Kuroshio warm advection to horizontal temperature gradient. Since there is all-year strong KFETW between 150 m and 350 m, only temporal evolution of temperature value between these two levels is discussed. Fig. 10 shows the seasonal variation of temperature value of point 1 on cold water side (121.625 °E, 23.500 °N) and that of point 2 on warm water side (122.375 °E, 23.250 °N) at 200 m level in the reanalysis results of this study. Statistics show that amplitude of seasonal variation on cold water side is 2.67 times larger than that on warm water side, from which it can be presumed that contribution of up-welling to the KFETW may be larger than that of Kuroshio warm advection.

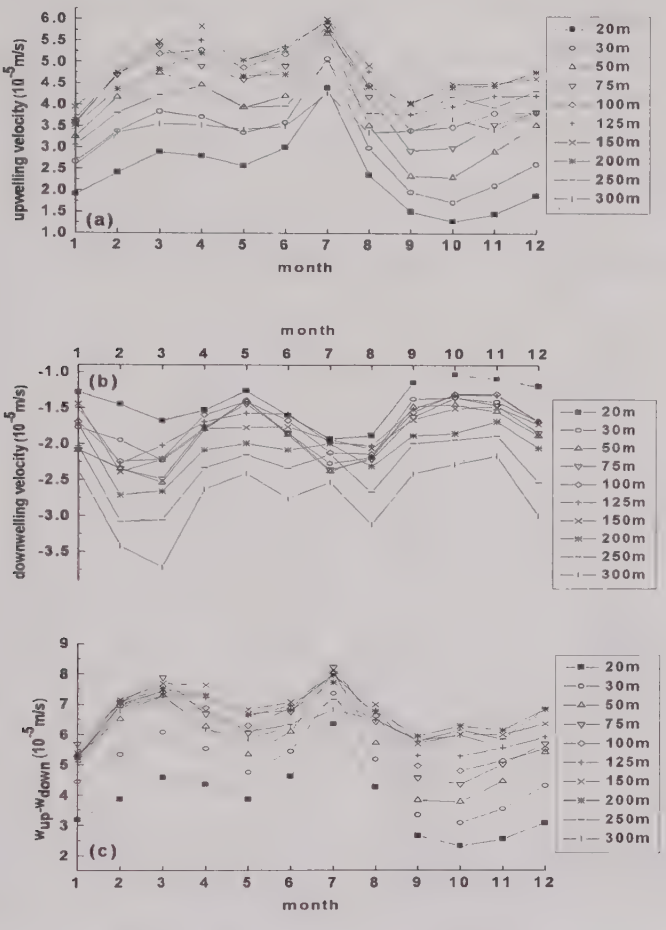

Fig. 7 Temporal variation of up-welling to the left side and down-welling to the right side of Kuroshio of each level to the east of Taiwan (22°N - 25°N, 121°E - 124°E) derived from the reanalysis results of this study

(a) up-welling; (b) down-welling; (c) up-welling menus down-welling

Furthermore, diagnostic method is used to make a careful evaluation of these two kinds of contribution. The diagnostic equation is as follows,

$$\frac{\partial T}{\partial t}+U\frac{\partial T}{\partial x}+V\frac{\partial T}{\partial y}+W\frac{\partial T}{\partial z}=\frac{\partial}{\partial x}\left(A_H\frac{\partial T}{\partial x}\right)+\frac{\partial}{\partial y}\left(A_H\frac{\partial T}{\partial y}\right)+\frac{\partial}{\partial z}\left(K_H\frac{\partial T}{\partial z}\right)-\frac{\partial R}{\partial z} \tag{2}$$

Then contributions of up-welling term $-W\frac{\partial T}{\partial z}$ and Kuroshio warm advection term $-U\frac{\partial T}{\partial x}-V\frac{\partial T}{\partial y}$ to temporal variation of temperature at both points are estimated on Arakawa C grid. For simplicity, other terms, such as diffusivity term and heat-flux term, are not

discussed in this paper. Fig. 11a shows the contributions of warm advection and up-welling to the temperature of each point of Fig. 9. And it is found that on cold water side, the contribution of up-welling term is as 6.4 times as that of Kuroshio warm advection, while on warm water side the contribution of up-welling term is as 0.68 times as that of Kuroshio warm advection. Contribution of up-welling to the temperature difference between these two points triples that of Kuroshio warm advection (Fig. 11b). Therefore, a preliminary conclusion can be drawn that up-welling may be the predominant factor in the frontogenesis and maintenance mechanism of the KFETW.

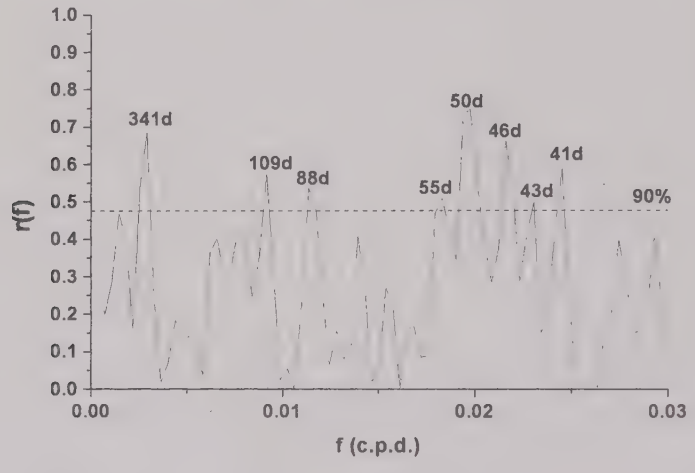

Fig. 8 Cross spectrum between Kuroshio flux to the east of Taiwan and intensity of KFETW at 150 m level calculated from reanalysis results in this study

Fig. 9 Comparison between contribution of Kuroshio warm advection and that of up-welling to temperature difference. Black solid lines are isotherm lines with point 1 locating to the left and point 2 locating to the right

From the above discussion about the impacts of the Kuroshio warm advection and up-welling on the KFETW, frontogenesis mechanism of this front can be summarized as follows: The Kuroshio to the east of Taiwan carries vast warm and saline water, and the Kuroshio warm advection raises the upper water temperature to the east of Taiwan. At the same time, the up-welling is strong due to water depth varying sharply in the coast to the east of Taiwan, and the elevating cold water convenes with the Kuroshio warm water, forming stronger horizontal temperature gradient, thereafter, the KFETW is created in the offshore area to the east of Taiwan. The cross spectral analysis indicates that the stronger the up-welling and the Kuroshio flux are, the stronger the intensity of the KFETW is. Because the up-welling and the Kuroshio flux reach the maximum in summer, the KFETW caused by their cooperation in this area is the strongest in summer.

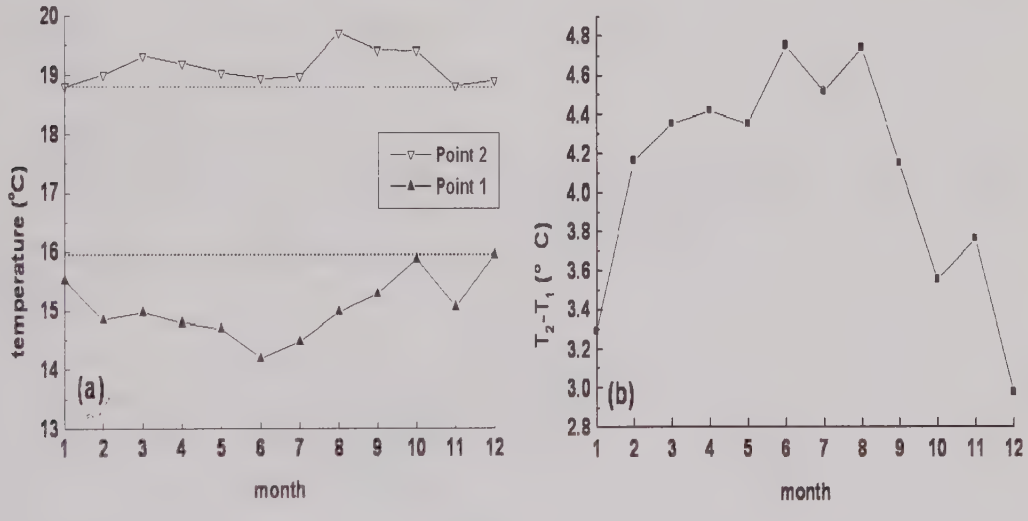

Fig. 10 (a) seasonal variation of temperature value of point 1 on cold water side and that of point 2 on warm water side, shown in Fig. 9, at 200 m level in reanalysis results of this study; (b) seasonal variation of temperature difference between point 2 and point 1

Monthly variation of vertical velocity to the east of Taiwan derived from the reanalysis result in this study is shown in Fig. 12. It can be seen that vertical velocity reaches its maximum at about 200 m level and almost decreases gradually to zero from 200 m to surface which results in that surface horizontal temperature gradient can not satisfy the criterion of thermal front. Therefore, given that up-welling may be the predominant factor in the frontogenesis, the KFETW can only exist in subsurface while there is almost no thermal front on the surface to the east of Taiwan.

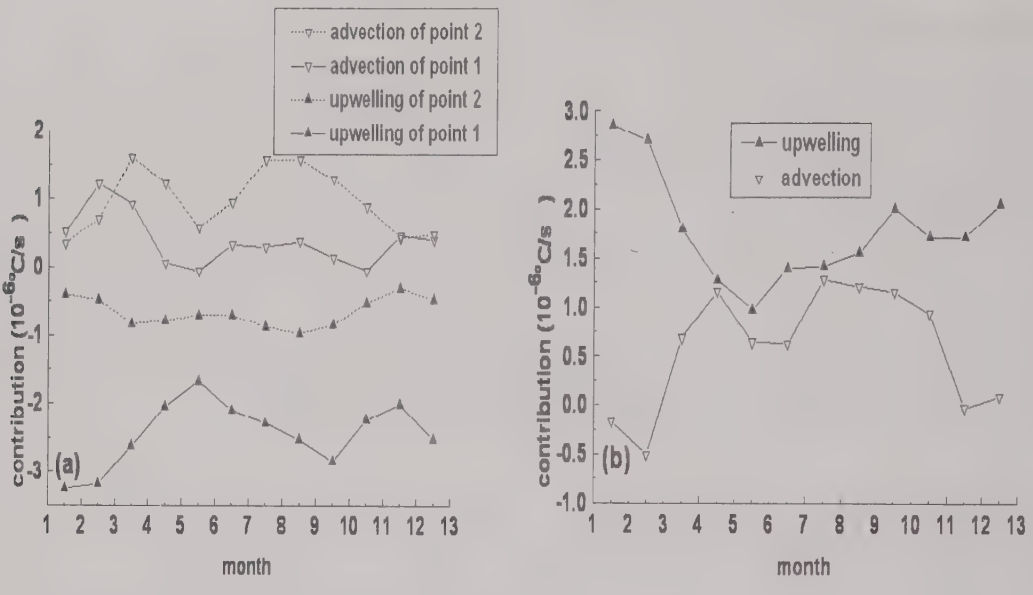

Fig. 11 (a) contributions of warm advection and up-welling to the temperature of each point of Fig. 9; (b) contributions of warm advection and up-welling to the temperature difference of these two points.

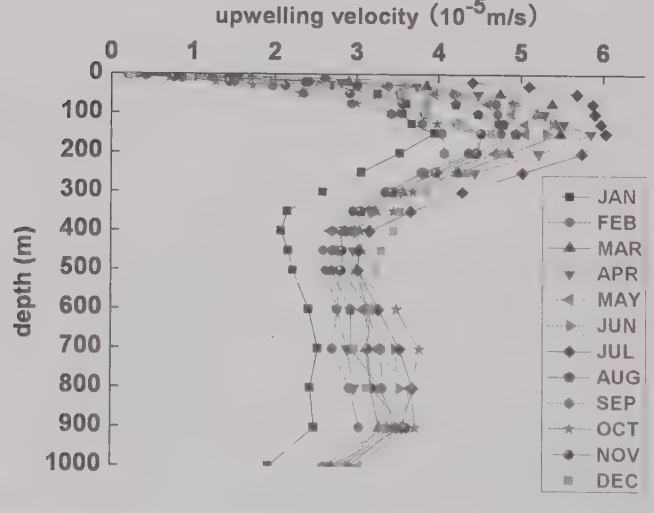

Fig. 12 Monthly average vertical velocity to the east of Taiwan versus depth derived from the reanalysis result in this study

It is worth to note that variation of the thickness of the KFETW is different from that of the KFECS. Tang (1992) indicated that the thickness of the KFECS in summer is thinner than that in winter. But as mentioned above, the thickness of the KFETW in summer is

obviously thicker than that in winter. The difference between these two jointed fronts may be caused by their different frontogenesis mechanism. Seasonal stratification of shelf water has significant impact on the structure of the KFECS, mechanism of which has been discussed by Tang (1992), whereas the KFETW is mainly generated by the confluence of cold water up-welled to the east of Taiwan and Kuroshio warm water. Because the up-welling velocity in summer is stronger than that in winter to the east of Taiwan, the thickness of the KFETW in summer is thicker than that in winter.

5 Conclusion

In this paper, reanalysis was used to study seasonal feature, variability and mechanism of the KFETW. Conclusions have been drawn as follows:

Although the surface thermal front to the east of Taiwan is not obvious, there is an all-year strong Kuroshio thermal front under the surface, called the KFETW. The KFETW can exist between 20 m and 350 m and there is all-year front between 150 m and 350 m. Thickness of this front varies from 200 m to 330 m. Horizontal position of this front has the trend of moving eastward with depth increasing. The variation amplitude of the north end of this front is larger than that of the south end. With depth increasing, both intensity and width of the KFETW has the tendency of decrease following the increase.

This thermal front not only has the significant annual cycle, but also has the significant multi-timescale variation cycle. For seasonal signal, both intensity and width reach their maximum in summer. The thickness of this front also has seasonal signal and reaches its maximum during May to July.

Both the Kuroshio warm advection and up-welling can affect the KFETW, and the stronger the up-welling and the Kuroshio flux are, the stronger the intensity of the Kuroshio thermal front is. Because the up-welling and the Kuroshio flux are strongest in summer, the KFETW is the strongest in summer. Diagnostic analysis suggests that the contribution of the up-welling to this thermal front is three times than that of the Kuroshio warm advection, that is to say, the up-welling is the main mechanism for the frontogenesis and maintenance of the KFETW. The up-welling velocity reaches its maximum at 200 m level and from this level to surface almost reduces to zero. Therefore, the surface thermal front to the east of Taiwan is not obvious while the subsurface frontal intensity is strong.

Acknowledgments

This study was jointly supported by grants of the National Basic Research Program of

China (No. 2007CB816001), the National Natural Science Foundation of China (No. 41030854, 40906016 and 40906015).

Reference

[1] Chen D X. Marine Atlas of Bohai Bay, Yellow Sea and East China Sea (Hydrology) [M]. Beijing: China Ocean Press, 1993: 423 - 426.

[2] Chern C S, Wang J, Wang D P. The exchange of Kuroshio and East China Sea Shelf water [J]. Journal of Geophysical Research, 1990, 95: 16 017 - 16 023.

[3] Chu T Y. The Oceanography of the Surrounding Waters of Taiwan. Report of the Institute of Fishery Biology of Ministry of Economic Affairs and National Taiwan University [R]. 1963, 1(4): 29 - 37.

[4] Chu T Y. Study of the Kuroshio current between Taiwan and Ishigaki-jima [J]. Acta Oceanographica Taiwanica, 1976, 6: 1 - 24.

[5] Chuang W S, Li H W, Tang T Y, et al. Observations of the Countercurrent on the Inshore side of the Kuroshio Northeast of Taiwan [J]. Journal of Oceanography, 1993, 49: 581 - 592.

[6] Ezer T, Mellor G L. A generalized coordinate ocean model and a comparison of the bottom boundary layer dynamics in terrain-following and in z-level grids [J]. Ocean Modelling, 2004, 6: 379 - 403.

[7] Guan B X. Principal Development and Status for Investigation and Research of Kuroshio to the East of Taiwan and in the East China Sea [J]. Acta Oceanologica Sinica, 1983, 5(2) : 133 - 146.

[8] Hsin Y C, Wu C R, Shaw P T. Spatial and temporal variations of the Kuroshio east of Taiwan, 1982-2005: A numerical study [J]. Journal of Geophysical Research, 2008, 113: C04002.

[9] Jing C S, Li L. An initial note on quasi-stationary, cold-core Lanyu eddies southeast off Taiwan Island [J]. Chinese Science Bulletin, 2003, 48(19) : 2 101 - 2 107.

[10] Johns W E, Lee T N, Zhang D X, et al. The Kuroshio East of Taiwan: Moored Transport Observations from the WOCE PCM-1 Array [J]. Journal of Physical Oceanography, 2001, 31: 1 031 - 1 053.

[11] Lee T N, Johns W E, Liu C T, et al. Mean transport and seasonal cycle of the Kuroshio east of Taiwan with comparison to the Florida Current [J]. Journal of Geophysical Research, 2001, 106(C10): 22 143 - 22 158.

[12] Li W, Xie Y F, Deng S M, et al. Application of the Multigrid Method to the Two-Dimensional Doppler Radar Radial Velocity Data Assimilation [J]. Journal of Atmospheric and Oceanic Technology, 2010, 27(2): 319 - 332.

[13] Li W, Xie Y F, He Z J, et al. Application of the Multi-grid Data Assimilation Scheme to the China Seas' Temperature Forecast [J]. Journal of Atmospheric and Oceanic Technology, 2008, 25(11): 2 106 - 2 116.

[14] Liang W D, Tang T Y, Yang Y J, et al. Upper-ocean currents around Taiwan [J]. Deep-Sea

Research II, 2003, 50: 1 085 - 1 105.

[15] Lin C Y, Shyu C Z, Shih W H. The Kuroshio Fronts and Cold Eddies off Northeastern Taiwan Observed by NOAA-AVHRR Imageries [J]. Terrestrial, Atmospheric and Oceanic Sciences, 1992, 3: 225 - 242.

[16] Liu K K, Gong G C, Lin S, et al. The Year-Round Upwelling at the Shelf Break Near the Northern Tip of Taiwan as Evidenced by Chemical Hydrography [J]. Terrestrial, Atmospheric and Oceanic Sciences, 1992, 3: 243 - 276.

[17] Mellor G L, Hakkinen S, Ezer T, et al. A Generalization of a Sigma Coordinate Ocean Model and an Intercomparison of Model Vertical Grids. Ocean Forecasting: Conceptual Basis and Applications. Berlin: N. Pinard, J. Woods (Eds.), 2002, Springer 55 - 72.

[18] Reynolds R W, Smith T M, Liu C, et al. Daily high-resolution blended analyses for sea surface temperature [J]. J. Clim., 2007, 20(22) : 5 473 - 5 496.

[19] Sun X. Analysis of the surface path of the Kuroshio in the East China Sea. In: Sun, X. (Ed.), Essays on the Inverstigation of Kuroshio. Beijing: Ocean Press. 1987, 1 - 14

[20] Tang T Y, Tai J H, Yang Y J. The flow pattern north of Taiwan and the migration of the Kuroshio [J]. Continental Shelf Research, 2000, 20: 349 - 371.

[21] Tang Y X. On Regional Difference of the Kuroshio front in the East China Sea [J]. Journal of Oceanography of Huanghai & Bohai Seas, 1992, 10: 1 - 9.

[22] Tang Y X, Zheng Y F, Yasuaki N. A Preliminary Study on the Three Dimensional Structures of the Kuroshio Front in the East China Sea [M]. Proceedings of China-Japan Joint Symposium of the Cooperative Research on the Kuroshio (4). Beijing: China Ocean Press, 1992, 33 - 42.

[23] Troccoli A, Balmaseda M A, Segschneider J, et al. Salinity adjustments in the presence of temperature data assimilation [J]. Monthly Weather Review, 2002, 130: 89 - 102.

[24] Wan B J, Guo B H, Tang Y X. Current Structure Along Cross-Kuroshio Front Section in the East China Sea [J]. Oceanologia et Limnologia Sinica, 1994, 25(6): 652 - 658.

[25] Wong A, Gregory P S, Johnson C, et al. Delayed-Mode Calibration of Autonomous CTD Profiling Float Salinity Data by $\theta - S$ Climatology [J]. Journal of Atmospheric and Oceanic Technology, 2003, 20: 308 - 318.

[26] Wu C R, Lu H F, Chao S Y. A numerical study on the formation of upwelling off northeast Taiwan [J]. Journal of Geophysical Research, 2008, 113, C08025.

[27] Zhang D X, Lee T N, Johns W E, et al. The Kuroshio East of Taiwan: Modes of Variability and Relationship to Interior Ocean Mesoscale Eddies [J]. Journal of Physical Oceanography, 2001, 31: 1 054 - 1 074.

[28] Zhu J, Yan C X. Nonlinear balance constraints in 3DVAR data assimilation [J]. Science in China (D), 2006, 49: 331 - 336.

台湾以东黑潮锋时空分布及形成机制研究

王 琦[1]，李 威[1,2]，马继瑞[1,2]，韩桂军[1,2]，张学峰[1,2]，王喜东[1,2]

（1. 国家海洋信息中心，天津 300171；2. 国家海洋局海洋环境信息保障技术重点实验室，天津 300171）

摘 要：海洋锋是重要的海洋现象，具有重要的研究意义。尽管台湾以东与黑潮之间表层无明显的锋区，但在水下却常年存在较强的海洋锋，这一现象的研究至今尚少见，本研究采用再分析手段，系统分析了温度锋时空变化规律及其形成变化机制。

关键词：黑潮锋；台湾以东；再分析；时空分布；形成机制

Sea level change and forecast in the future — climate of the past, today and the future

YUE Jun[1, 2, 3], DONG Yue[4], CHEN Man-chun[5], HAN Fang[1, 3], DUAN Huan-chun[1, 3], WANG Guo-ming[2]

1. *Tianjin Huabei Geology Depertment of prospecting Institute of Geology, Tianjin* 300181, *China;*
2. *Tianjin Institute of Geology and Mineral Resources Ministry of Land and Resources, Tianjin* 300170, *China;*
3. *Geological Research Institute of North China Geological Exploration Bureau, Tianjin* 300170, *China;*
4. *Universty of Texas at Utsxa San Antonio, Texas* 78249-1644, *USA;*
5. *National Marine Data and Information Service, Tianjin* 300171, *Chin;*

Abstract: The sea-level change is resulted from superposition of sun, moon and other planeries, and earth itself, biological process, atmosphere and oceanography, as well as artificial actions. As a result, the sea level change is really a sensitive integral variation value of many variations, or a combined function of coupling effects of various big systems. Therefore the above mentioned superposed action of different systems and the coupling effect of sun earth and biological aspects may be called as sun earth biological coupling effect system. Based on this hypothesis, the corresponding sun dynamic, air dynamic, water dynamic and earth dynamic conceptional models are established in order to research the multiple coupling effects and feedback machanism between these big systems.

In order to determine the relations, effectness and coherent relation of different variations, the quantity, analysis is conducted through collective variation and stage division. The quantity analysis indicates that the earths spindle rotation speed is the dynamic mechanism controlling the sea level change of fluctuation. The change rate of sea level in the world is +1.32 ± 0.22 mm/a, while the sea level change rate in China is only+1.39 ± 0.26 mm/a in average. If take the CO_2 content as the climate marker, eight cold stages (periods) are grouped out since two hundreds years AC. The extreme cold of the eighth cold stage started approximately at 1850 years AC. and if the stage from the extreme cold to extreme warm is determined as long as 200 years, the present ongoing warm stage will end at about 2050 years, there after the temperature will begin to tower. If the stage between cold and warm extremes lasts for 250 years, then the temperature will become lower at about 2100 year. Until to that time, the sea-level is estimated to raise +7 - +11 ± 3.5 cm again, and there after, the sea level will begin the

Received on Apr. 14, 2010

Corresponding author: yuejun79@gmail.com

new lowering trend. In the same time, the climate will enter into next new cold stage, subsequently.

Keywords: Sun earth biological coupling effect system, sea-level change mechanism, change rate of the sea-level, climate cold stage, forecast of the sea-level, changes in the future

The sea-level change is accounted as the index of climate change. And it has similar trend with climate change, that has certain universal significance in the world and natural regulation. The sea level change is also regarded as superposed results of sun, luna and other plenary, celestial bodies and earth action, biological process, atmosphere and oceanography, as well as some man made factors. So that, the sea level change is a sensitive integral variation value among many variations, or an assemble function of several big systems and their coupling effect. For this reason, from the cosmos entirety point of view, the author considered the superpose and coupling effect of above mentioned systems as sun earth biological coupling effect system (Fig. 1).

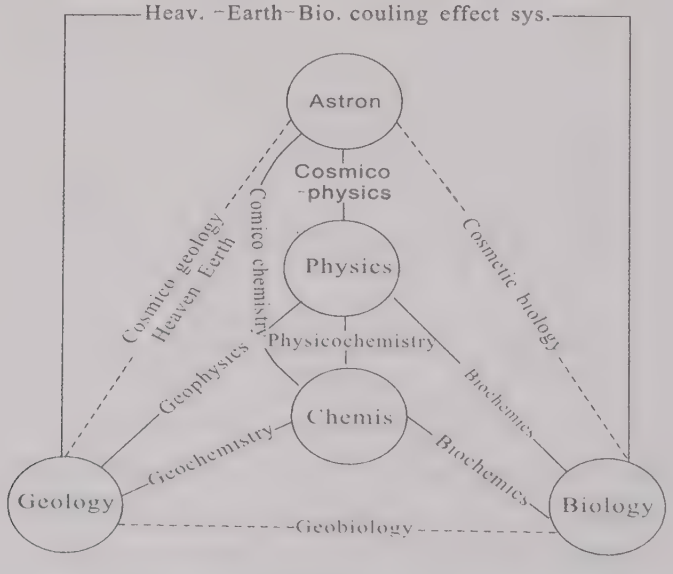

Fig. 1 Construction of sun earth Biological system

Heav.-Heaven, Bio.-Biological, sys.-systems, Astron. -Astronomy, chemis. –chemistry

In the sun earth biological coupling effect system, the sun and earth as a united entirety are comprehensively multihorizontal and multidisciplinary studied in order to establish corresponding evolutional pattern [1-7]. Based on the collective variation of data available, the author analyzed the relation [8-10], effectiveness and relevant relation between each variation quantitively, subsequently the sea-level change in the future is

forecasted (Fig. 2).

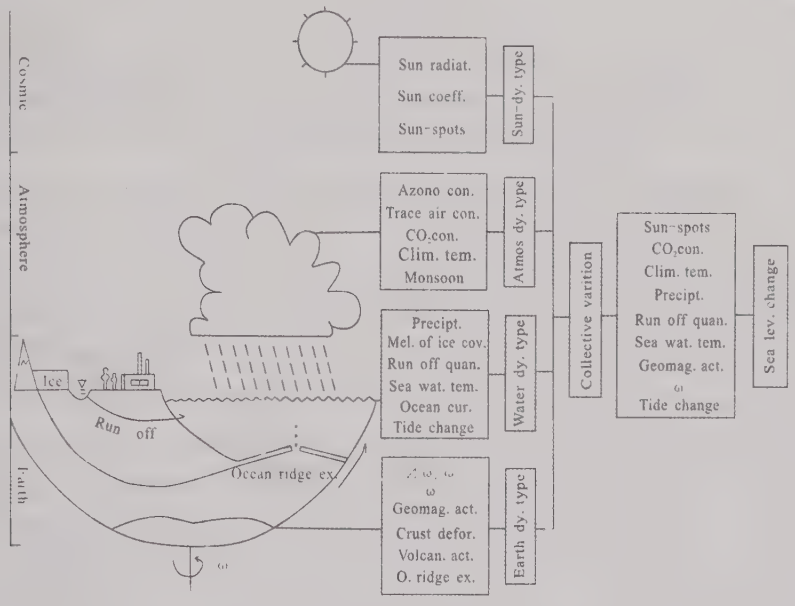

Fig. 2 Analysis pattern of sun earth biological coupling effect system, sea level change mechanism and their forecast

($\Delta\omega/\omega_0$-The relative variation value of Earth spindle rotation rate, ω-Earth spindle rotation speed O. - ocean, ex. - expansion, radit. - radiation, coe. - coefficient, con.-content, clim.- Climate, tem. - temperature, precipit. - precipitation, mel. - melting, cov. - cover, quan. - quantity, wat. - water, cur. - current, Geomag. - Geomagnetic, defor. - deformation, volcan. - volcanic, act. - activity, dy. - dynamic, lev. - level).

1 The coupling effects of some big systems on the sea-level change

The sea-level change has multiple superposed coupling effect of natural facts, such as cosmic and Earth, the earth and atmosphere, the earth and oceans the atmosphere and ocean, as well as other big systems, that they are constantly mutually relating and transforming mutually constraining and coupling, there present not only chain reacting, but also contain multiple types of coupling effect. For example, the sun dynamic effect, in which the sun is the dynamic and energy resources pushing the earth, atmosphere and oceanic circulation, as well as the photosynthesis of biological there. It must say that, the sun is the essential for the oceanic tide and the earth. The sun is also the important sources of earth's light energy and heat energy. The sea-level both absorbs light energy and reflect light energy. The sun's coefficient and sun's radiation value, as well as relative sun sports. Sun represents the main index of sun's activity, that directly or indirectly control

the sea-level change. The main energy of air dynamic effect and atmosphere system comes from sun. The sun's radiation and air atmosphere depend not only on the main air elements, but also depend on the concentration's change of trace elements (H_2O, CO_2, O_3) and other scarce elements. The sun system exerts vast effect on the earth's atmosphere zone, though the atmosphere absorb only small section of sun's radiation, but the atmosphere transform its own small part of dynamic power to the sea surface, in such a way, it draws the oceanic circulation in great scale, so it spurs the circulation and change of CO_2 gas, occurred by natural phenomenan with considerable dynamic power, which exerts profound effect on the sea-level change. Simultaneously the gravitational power of tide power of celestial body conducted its action through atmosphere circulation. Its horizontal and vertical distribution controls the precipitation, cold and warm climate change, subsequently cause the sea-level fluctuation. The hydrodynamic effect, the world's ocean surface change and dynamic transformation are influenced by sun celestial drawing water power, and the atmosphere system. The sea water exchange with atmosphere zone through evaporation, precipitation and coagulation such as tide, ice stream, ice cover melting, river runoff, oceanic current in the oceanic current in the oceans and salt content of sea water, are the dynamic power, affecting the sea-level action. Owing to the rotation of the earth, the vertical component varies between south and north direction force the ocean current change to assymetrically between east and west direction. But the east-west orientation of oceanic current is generally abstracted, while the south-north direction of the current is more active, while the warm current in the equator will move to both boles, while the bole coldcurrent moves to equator. The circulation of cold current and warm current leads the expention and contraction of ocean entity. It exerts the effect on the sea-level change, which is much bigger than that caused by general ocean current. The earth dynamic effect and the regular change caused by sun radiation, may be related with the oribit factors all the big celetials, especially the effect of (Jupiter and Saturn) power causing periodically perturbation, that attract the inclination of earth self-spindle axle and the eccentric rate of earth's orbit around the sun and months tides, leading the earth s spindle ocean rotation causing the permanently rotation along the normal orbit plain procession. The earth self-rotation speed caused from this precession is dynamic machanism of sea-level change. The earth is a dynamic entity. The sea water covers the earth surface. The change of earth sphere directly reflects the sea-level. The crust deformation (land surface subsidence) plate movement, volcanic activity in the sea base and oceanic ridge expention, all these factors change the ocean basin volume, that may be resulted in the fluctuation of the gravitational field of the earth, magnetic activity, earth bole migration and the inter quality distribution of earth, as well as celestial move, all of these factors exert action on the sea-level, that spurs the adjustment and reaction of the sea-level.

2 The machenism analysis of sea-level change

The effect factors exerting sea-level change are numerous. In the nature, the sea-level change is mainly caused by the coupling effect results of several big systems. The sea-level change in different duration of scale shows certain regular characters.

2.1 The relations between sea-level and the primary data of relevant factors

The authors separately analyzed the curve character of sea-level of primary data in different time series of relevant factors, and calculated the relevant relations of parallel of superposed relations. The parallel and superpose relations between sea-level and different factors.

We calculate the Brest sea-level data in long duration of time period (1820 -1981) and the relation of sea-level with different factors and the relevant relation between different factors (Fig. 3). From Fig. 3, we can see the coexist and superposition relation between sea-level and different factors.

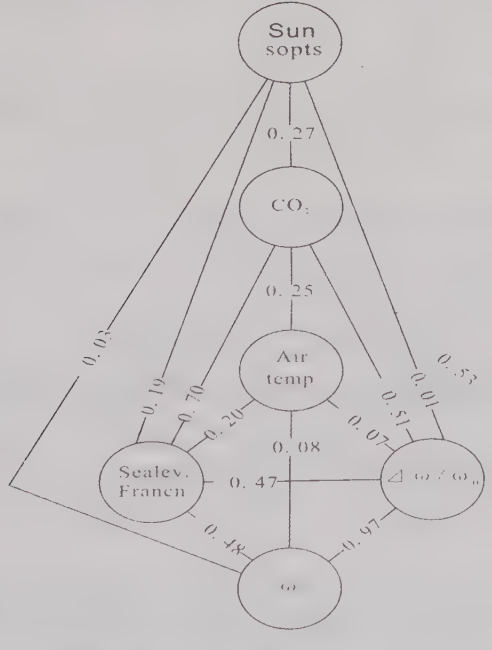

Fig. 3 Coexist and superpose relation between sea level and original data of different factors

The relation between sea level and earth spindle rotation speed (ω) and the relative change value of earth spindle rotation angle speed ($\Delta\omega/\omega_0$) shows negative relation (0.48 - 0.47), but the relevant coefficient become more obviously. While it shows positive relevant relation with climate temperature. As to the CO_2 content and sun sports relative

value, the relative coefficient is bigger (0.70). But the earth spindle rotation speed and the earth spindle angle rotation's speed change show negative relevant relation with other factors, such as sea-level, air temperature, CO_2 content and sun sports relative value, and have close relations with CO_2 content (0.53 - 0.51) and the relation between them ($\omega,\Delta\omega/\omega_0$) is more close, and the correlation coefficient is 0.97. This indicates the relation between the CO_2 content change with the natural factors, the above mentioned analysis is almost coincident or consistent.

2.2 Relation between sea-level and stage character of relevant factors

The sea-level change processes according to natural regulation and it may be divided into raising stages and lowering stages, that means as generally speaking the periodical fluctuation. However, the periodic concept has different standard scales and it is difficult to acknowledge it united. So that, in this paper, we apply the "Stage"'s change to analyze the different factor's trend. Though relative mathematic model, the random stage series division is applied, in this way, the artificially imagined stage series division is excluded that makes character analysis of the stage change becomes more reasonable and the stage division's method, steps and principal are described as follow:

The method and steps of stage division:

The optimum division is applied in this paper as stage division approach [7, 11 - 14]. The steps applied are as follow:

The first step: through the mathematic pattern (coherent relation group analysis) selection of relevant factors, relating with sea level (for example, astronomy, meteorogic, oceanography and earth factors). Second step: the relevant data collected from the international and selected China sea-level monitor stations are optimum divided and calculated. The third step: the subdivided groups are statistically calculated in figures and tables in vertical ocean statistics the division group's probability for each monitor stations from year to year, while in the horizontal ocean the stage trend characteristics are analyzed.

The general principle for determination of "stages". The stage described in this paper has some uncertainties because the time series of stages last for different duration. So that the time scale of stages should be determined by the statistic trend of practical data. It is carried out according to following principles.

(1) Taking into consideration the stability of every horizontal division boundary of different factors, and multiple groups of vertical accumulated division sorts.

(2) Consider action of the closeness of horizontal stage time intervals.

(3) The similarity of corresponding boundaries in horizontal ocean.

(4) Evaluate and analyze the effectiveness of gained results (correlate with other results) and feasility of the program (e.g the coincidence of the gained stage with the theoretical period or the natural rule).

Based on the above mentioned stage division principles, the author obtained the sea-level in different stage series with stage trend characters of different factors, that provided the strong base for further analysis of sea level change mechanism.

2.3 R type group analysis of sea-level with different factors

In order to analyze the variation relations between sea-level and factors, the author based on the stage division principle conducts the stage division of Brest's sea-level (1807-1981), the relative value of Sun's sports(1678-1988), CO_2 content (1676-1990), air temperature (England,1687-1976) and earth spindle rotation speed (1623, 1685-1990). The average value of 6 stages calculated according to the principles are analyzed by R type of group analysis (see Fig. 4).

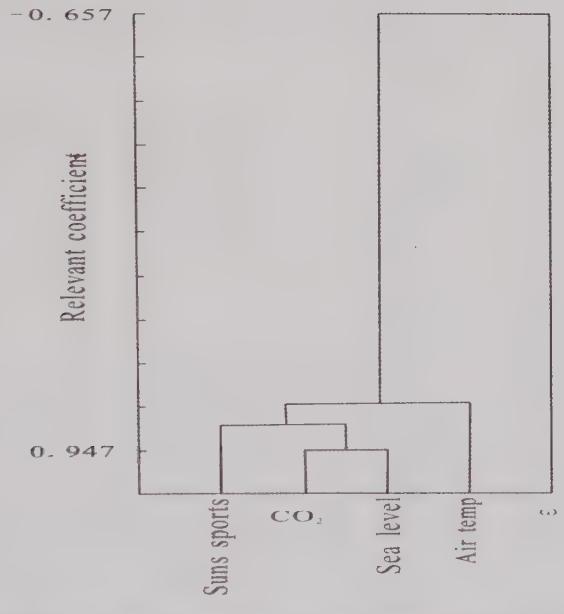

Fig. 4 R type group analysis of average value of sea-level and various factors

One can see from Fig. 4, that the sea-level firstly aggregates with CO_2 content and aggregates with the relative value of sun sports, and the next is the air temperature, and all these factors show the positive relation with sea-level, and the relevant coefficient is relative high. But the spindle relation of the earth as an isolate factor shows negative relation with the relative value of sun sports, CO_2 content, air atmosphere and sea-level

and the negative coefficient is relatively big too, namely the relative coefficient is accounted to 0.657. In this way, it shows that the earth spindle rotation speed, as the main mechanism controlling the sea level change, is basically coincided with the above mentioned theoretical analysis, and close to the results of calculated analysis, showed in Fig. 3.

3 The speed rate's analysis of sea-level change

The speed rate (in mm/a) of sea-level change indicates the fluctuation trend of sea level. The sea level change rate shows in raising (+) and falling (-). But the general trend of the sea-level change in the world shows consistant raising at present.

3.1 The sea-level change in the world

The world's sea level change is a global wide. Six sea-level monitor stations in the whole world are selected in this paper, namely the data form Sydney, Australia, Seattle, America, San Francisco, America, Brest, France, Marseile, France and Bombai, India. Based on the above mentioned stage division principle, the author analyzed the sea-level change data from the above mentioned six sea-level monitor stations. About 30 years sea-level change periodicity are obtained (see Tab. 1)

Tab. 1 shows the change rate of Sydney sea-level is + 0.51 mm/a, that in Seattle is +1.99 mm/a, that in San Francisco is +2.02 mm/a, the sea-level change in Brest is +1.53 mm/a, in Marseile +1.13 mm/a, in Bombai +0.73 mm/a. The general sea-level fluctuation rate is +1.3 2 ± 0.22 mm/a.

3.2 The sea-level change in China

China has very long sea coastal zone, that shows difference in region [14], the groupnese of the sea-level data and the periodic change of sea-level [15].

The annual average of sea-level fluctuation rate change in the world, recorded in manual monitor stations shows minimum change in mm/a. But the average sea-level in different stages shows different diversity (from m level to cm level). If compare the average sea-level of a day with that of month, or compare month's to year's and one year's to multiple year's, it certainly could not obtain the precise value of sea level. However, this is just mistaken method easy to be taken. The inconsistent conclusion in the sea-level study, is mainly because of the stage diversity applied for sea level change, except the complex objective factors of sea level change, or incorrect sea level data cited [16]. Owing to most of sea level monitor stations in China, are set up in relative short time, it is difficult to divide long stage of sea level change. So that the stage division in this paper is obtained mostly

through statistics. Among them, the 9-10 year stage shows more clearly during the monitor period. If combine two such stages into one relative long stage, that means 19 year stage, is basically coincided with the theoretical periodic change. It shows that the stage division applied in this paper is reasonable. But owing to short monitor time period of the data, it is difficult to apply common theoretical period (19 Year stage) as a sea level change stage. In this way, the ten year and half period is applied in the paper. The sea level data from 9 sea-level monitor stations along coastal zone of China are applied in this paper (see Tab. 2). From Tab. 2, it can be seen that, the sea level fluctuation rate in Huludao is +0.25mm/a; -1.31mm/a in Qinhuangdao; +3.54 mm/a in Tanggu; +3.04 mm/a in Yangjiaogou; +0.36mm/a in Yantai; -1.46 mm/a in Wusong; +3.54 mm/a in Xamen; +3.66 mm/a in Haikou; +0.86 mm/a in Beihai. Through calculation, that excep the lowering of sea-level in Qinhangdao, all the sea-level in all other station shows raising trend, at +1.39 ± 0.26 mm/a rate in average.

Tab. 1 Sea-level change in the world in the stage of 30 years

Region	Station	Relative sea level	Monitor date	stage	Average value of sea-level	Difference Value / mm	Annual raise(+)falling(-) rate / mm/a
Australia	Sydney (1897-2007)	6974	1897-1922	26	6961	-28.2	+0.51
			1923-1949	27	6932.8		
			1950-1978	29	6992.5	+59.7	
			1979-2007	29	7004.4	+11.9	
America	Seattle (1899-2007)	7047	1899-1924	26	6968.1	+31.7	+1.99
			1925-1949	25	6999.8		
			1950-1978	29	7072.8	+73.0	
			1979-2007	29	7132.9	+60.1	
	San Francisco (1898-2007)	6992	1898-1924	27	6910.6	+46.4	+2.02
			1925-1950	26	6957.0		
			1951-1979	29	7014.6	+57.6	
			1980-2007	28	7078.1	+63.5	
France	Brest (1807-2006)	6986	1895-1923	29	6963.7	+49.7	+1.53
			1924-1950	27	7013.4		
			1951-1979	29	7039.6	+26.2	
			1980-2006	27	7090.9	+51.3	
	Marseile (1885-2006)	6929	1893-1921	29	6873.6	+32.9	+1.13
			1922-1949	28	6906.5		
			1950-1978	29	6967.4	+60.9	
			1979-2006	28	6969.8		
India	Bombay (1878-1993)	7026	1892-1921	30	6986.4	+49.5	+0.73
			1922-1949	28	7035.9		
			1950-1978	29	7050.4	+14.5	
			1979-1993	(15)	7038.7	-11.7	
The sea- level data analysis for 6 monitor stations in the world							+1.32 ± 0.22

3.3 Different approaches for calculation of sea-level fluctuation rate

The research approach for sea-level change and calculation method for sea-level fluctuation rate has been a major research project for relevant scholars and researchers. From Tab. 3 you can see that the sea level fluctuation's rate in the world calculated by different approaches are basically similar each to other and varies in the range from 0.5 to 1.4 mm/a, but mostly in about 1 mm/a; the sea level change rate along the coastal zone in China calculated by chinese experts is mostly in 0.7 mm/a. From this we recognized that there exist difference not only in geographic sea sectors, but also present in different time stages. However, the author concluded that the world's sea-level change trend in the future will be less than 1 mm/a, based on the analysis of data available at present.

Tab. 2 The sea level in China in stage of 30 years

Region	Station	Relative sea level	Monitor date	stage	Everge value of sea level	Difference Value / mm	Annual raise(+)falling(-) rate / mm/a
China	Huludao (1954-2008)	1630	1954-1980	27	1626	+7	+0.25
			1981-2008	28	1633		
	Qinhuangdao (1944-2008)	888	1950-1979	30	907	-38	-1.31
			1980-2008	29	869		
	Tanggu (1915-2008)	1544	1922-1949	28	1423	+48	+3.54
			1950-1979	30	1571		
			1980-2008	29	1632	+61	
	Yangjiaogou (1951-2008)	3110	1951-1977	27	3074	+76	+3.04
			1978-2002	25	3150		
	Yantai (1953-2008)	2151	1953-1980	28	2146	+10	+0.36
			1981-2008	28	2156		
	Wusong (1944-2003)	2096	1949-1977	29	2114	-38	-1.46
			1978-2003	26	2076		
	Xamen (1954-2008)	3561	1954-1980	27	3510	+99	+3.54
			1981-2008	28	3609		
	Haikou (1952-2008)	1535	1952-1979	28	1481	+106	+3.66
			1980-2008	29	1587		
	Beihai (1954-2008)	2568	1954-1980	27	2556	+24	+0.86
			1981-2008	28	2580		
	Sea level date analysis from 9 monitor stations along coastal zone						+1.39 ± 0.26

4 The predict sea-level change in the future

The sea-level change closely relates with climate change. So that, if we want to predict the sea-level change trend in the future, we should research into the present climate change and climate evolution in detail.

4.1 The similar trend between sea-level change and climate change

The sea-level change shows close relation (Fig. 3) and similar trend with the climate change. When the sea-level rise, the climate temperature rise, and when the sea-level

lowers, the climate temperature subsequently lowers too. But at present the relevant both domestic and foreign scholars focus on the effect of CO_2 content on climate and sea-level, and regard it as a major indicator to research. However, the author and relevant scholar recognize that the CO_2 content change occurs as a natural phenomenan and that reflects the circulation action as well as the indicator of climate change [21]. So that the climate change do not resulted from the artificial increase or decrease of CO_2 in the atmosphere. In the warming climate stage, the increase of CO_2 content caused by the artificial factors may promote the climate to be warmer, but in the cold stage, such action could do nothing to affect the climate. The data available indicates that the content of CO_2 consistently increase occurs only in the last few decades. But such increase of CO_2 content superposes on or coupling with the ongoing warming weather temperature raise, caused by natural factor [22, 23].

Tab. 3 Sea level change rate in the world calculated by different methods [7]

Region	Authors	Relation sea Level Change / mm/a	The applied methods
world	B Gutenberg (1941)	1.1±0.8	Multiple sea-level data
	E Lisitzin (1958)	1.12±0.36	Analysis of 6 sea-level monitor stations
	H Fairbridge (1961)	1.12	Sea-level data analysis
	V L Gorntz (1982)	1.2	Analysis of regional sea-level
	Fang Qiaoying et al. (1985)	0.50-1.40	Analysis of special regional sea-level
	Vivien Gornitz[17] (1987)	1.2±0.3	Arithmetic average method of sea-level
	Huang Liren et al.[18] (1993)	1.2-1.4	Analysis of equilibrium and benchmark
	Unal, Ghi (1995)	1.62±0.38	Analysis of data of the sea-level
	This test	1.32±0.22	stage division
China	Zheng Wenzhen (1991)	1.40	Comparison method of moving average
	Zhao Mingcai[19] (1997)	1.30±0.36	Comparison method of moving average
	Wu Zhongding [20] (2003)	1.05-1.55	Analysis of data of the sea-level
	This test	1.39±0.26	stage division

4.2 Analysis of eight cold sages since 200 years AD

Based on the curve of CO_2 content, compiled by Mörner N A [23] the author calculates the corresponding data and then optimumly divides the CO_2 content (Tab. 4). The consistant and stable boundaries are taken as the stage boundaries, at the same time we calculate the average value in corresponding stages. Based on these accounts, a CO_2 content stage curve was drawn, which may be regarded as climate evolution curve (Europe). Then compared it with China's climate change curve, established by Zhu Kezhen [24 - 27], the famous China's meteorologist. As a result, eight cold stages (cold stages) are divided (Fig. 5) since 200 AD. From Tab. 4, you can see that the cold stage may last for 100 years or more or less, that is basically coincided with the results obtained by Flohn. But the interval (warm stage) between cold extremes are probably for 200 - 250 years, but mostly last for 200 years. Now the change characters of cold stages are analyzed as follow.

The first cold stage started from 269 a to 370 a AD. The stage lasts for 102 years. From the curve behavior in Fig. 5, one can see that it principally coincides with the temperature curve, established by Zhu kezhen approximately similar to the first cold stage divided by Chen Jiaqi [28]. In the first cold stage, the cold reached the extreme peak in the first half of fourth century AD (I 366 AD), while Bohai Gulf (Changli Yingkou) was frozen for 3 years successfully and the temperature at that time was 2 °C - 4 °C lower than present.

Tab. 4 Analysis of eight cold stages since 200 AD

Cold Stage	Stages / age Optimum division of CO_2 content	Yearnum. in each stages	the year difference in cold stages	Zhu Kezhen[24]] (1979)	Chen Jiaqi [28] (1992)
I	269 - 370 (4, 6, 7 - 20) (14 - 20)	102	212	(Middle-end of 3th C) From half of 4th C	End of 4thC
II	461 - 581 (8 - 20) (4, 11 - 20)	121	221	Infirred cold in first half of 6th century	
III	690 - 801 (4, 6 - 9, 16 - 20) (4 - 20)	112	237	Cold in beginning of 7th C warm from middle of 7th C	
IV	915 - 1 037 (6 - 10) (4 - 20)	123	243	no record	begin of 10th
V	1 157 - 1 279 (18 - 20) (7, 14 - 20)	123	201	12th century	Late of 12th
VI	1 377 - 1 479 (12-20) (13-20)	103	198	15th century	end of 15th
VII	1 579 - 1 676 (6-20) (3, 5 - 7, 15 -20)	98	225	17th century	17th century
VIII	1 799 - 1 900 (5 - 9, 13 - 20) (7 - 20)	102		19th century	19th century

The second cold stage began from 461 AD ended at 581 AD, that last for 121 years. The data available stated that an ice room was built at Fuzhou mountain near Nanjing and analyzed the occurance and source of ice in the locality, which indicate the possibility of cold climate at that time. It also confirmed the years average temperature at that time was 1 °C lower than present, but in winter by 2 °C colder than present. At first half of sixth century, the climate in Henan region and Shandong region was colder than the present. The Huaihe River was ice up in 516 year AD. The above mentioned description is

coincided with the CO_2 lower value, that means the second cold stage. For these reason, the mentioned stage was inferred as the II Cold stage.

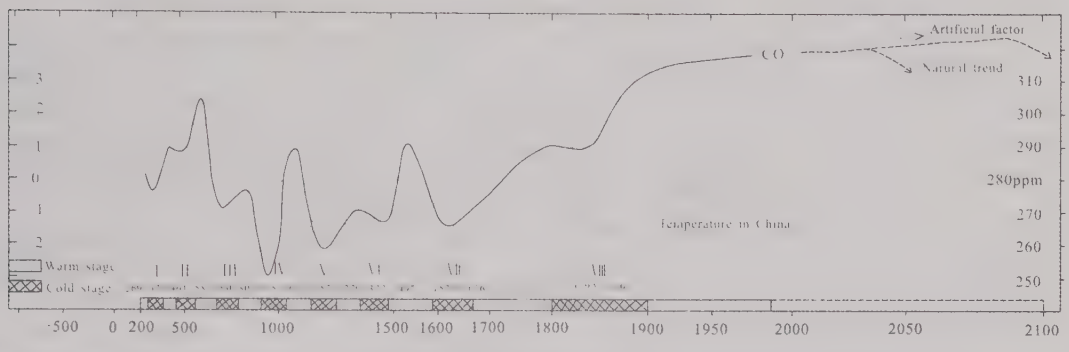

Fig. 5 Climate(temperature) evolution in China in last 5 thousands years(……)and compared it with Europe and climate forecast in the future (The climate curve is based on Zhu Kezhen)

The power series is applied in the horizontal time scale, so that the scale reduces from right left.

The III cold stage lasting from 690 to 801 AD., accounted for 112 years. The data available indicates the climate in China became warmer since middle age of 7th century. Based on these the climate in China was cold at the beginning of 7th century at least. Thus it is coincided with the CO_2 content lower stage, which is termed as the third cold stage (Fig. 5). Based on the above mentioned analysis, the author inferred that the climate deteriorate at that time.

The IV cold stage lasted from 915 to 1037 AD accounting for 123 years, when China was in serious war status at that time. No data available. However this cold stage is basically coincided with the analysis conducted by chen Jiaqi. At the same time J Gribbin and H H Lamb indicated that the 10th and 11th centuries China was in cold stage [29] (Tab. 4).

The V cold stage lasting from 1157 to 1279 lasts for 123 years. There are many historical records for the mentioned cold stage. The South canal, Suzhou city was often ice up before and after 1155 year in winter. The Huaihe River was frozen in 1186 and 1219, and snow often precipitated in Hangzhou, Zhejiang (Hangzhou) during spring festival in 1260, and in April at that time the climate was 1 °C - 2 °C lower than present. The cold climate then spread to whale South China and south west China. For example, in 1178, before or after the Lizhi streets, which may tolerant to 4 °C temperature were freezed to death in Guangdong, Guangxi, South part of Fujian provinces and South segment of Sichuan province. The mentioned cold stage is principally coincided with the analysis result of Zhu Kezhen and Chen Jiaqi.

The VI cold stage from 1377 to 1479 lasted for 103 years. H Flohn indicated 1429 -

1465 interval was serious climate deteriorating period in Middle Europe, for example in Germany and Austria area [30]. H.H.Lamb infered that the famine occurred in England in 1430 years was caused by cold climate [31].

Simultaneously, owing to severe winter in 1430, when the minimum temperature lowered to 20 °C - 25 °C the grape trees which widely spread in the southern England and in some regions of Germany were seriously damaged, and caused to stop plant grape. At the same time the Taihu Lake and Hanshui River in China were ice up in two times (respectively in 1454, 1416, 1416, 1449). At the same time, Huaihe River was iced up in 1454. The research results of Zhu Kezhen also indicated that the cold stage occurred at the mentioned time in China.

The 7th cold stage from 1575 - 1676 lasted for 98 years. If the cold stage is divided by a century, than the 17th century is the most cold century, in which there were 14 serious cold winters. The cold climate in 1626 - 1650, the climate deteriorated in Zoufang Lake, Japan, but the same cold climate started in China only in 1651 to 1675. The historic data recorded both orange and mandarin orange spread in Jiangxi were completely damaged by cold current two times occurring in 1654 and 1676, respectively. During the same time in Taihu Lake, the water freezed twice; while in Dongting Lake, the water freezed for three times, but in Hanshui and Huaihe Rivers, the water freezed for five times. In Poyang Lake the water freezed once in 1670. John Eddy stated the cold climate, occurred before or later 1645 was just coincided with the durable stage of lower value of sun's activity measured by sun's sports[32]. The cold climate occurred in this stage in China was probably synchronous with that in Russia, Germany, and England in Europe.

The Ⅷ cold stage, from 1799 to 1900 Lasted for 102 years. During this cold stage the most cold climate occurred in the first half of 19th century. In times river at London city the water was completely freezed for several times around 1810. In England the cold climate started from 1815. During the same time the water in Taihu Lake and Poyang Lake freezed for three times, and six times in Hanshui River; water in Dongting Lake freezed in 1877. While in Huaihe River, water freezed in 1845. There were 10 severe cold winters in 19th century. This cold stage is basically coincided with temperature curve, established by Zhu Kezhen, and close to description of Chen Jiaqi.

4.3 Trend analysis of sea-level change in the future

At first, regarding to sea-level change caused mainly by natural factors or by artificial factors, the author based the analysis of great amount of data available, concludes that the sea-level change mainly depends on natural factors. From Fig. 5, we see that the 8th cold climate stage started from 1856 AD, according to the above mentioned cold warm extreme

value of the stage if it lasts for 200 years, then the present developing warm stage will end at 2050, and then will start the lower temperature. By calculating, we find that the cold warm extreme interval lasts for 250 years, and then the temperature will be lower since 2100. Before that time, the present sea-level will raise for +7 - +11 ± 3.5 cm [33, 34]. Since then the sea-level will trend to lowering. In the same time the climate will enter into next new cold stage [35, 36]. However, there are some uncertainties in the future trend of the sea level change, that turn into heat point or focus point of international research [37 - 40]. The relevant information are often published in papers and magazines, since the sea-level change closely related with the national economy and the people's livelihood, with industrial development distribution in the coastal cities, as well as the live environment of mankind in the future. It could not neglect the fact that the earth is now in the warm climate stage and the next cold climate stage will come at about 2 050 - 2 100, in the future, the sea-level will start to lower. However, before that time, the sea-level will consistantly rise in considerable scale level (mm/a), that may cause erosion in some section of coastal zone, that may bring some damages in the future.

Acknowledgement

This research was supported by the National Natural Foundation of China (40940025), National Science Foundation of Tianjin (07ZCGYSF02400, 09JCYBJC07400), Program of China "973" (2007CB411807), Open Fund of the Key Lab of Global Change and Marine-Atmospheric Chemistry, SOA (GCMAC0806) and National Natural Science Foundation (41006002).

Reference

[1] LI S G. Astronomy, geology and ancient documents [M]. Beijing: Science Press. 1972, 3 - 115.

[2] QIAN Xue-sheng. Comprehensive Study of The Mutualrelations Among Cosmos, Earth and Life [M]. Beijing: China Science and Technology Press,1989, 1 - 5.

[3] Herman J R, Goldberg R A. Sun, Weather and Climate. Scientific and Technical Information NASA 1978.

[4] XU Dao-yi. Comprehensive Study of The Mutualrelations Among Cosmos, Earth and Life [M]. Beijing: China Science and Technology Press, 1989, 433 - 437.

[5] Malone T H. Global Change [M]. Beijing: Earthquake Press. 1990.

[6] Milankovitch M. Mathematische Klimalehre und astronomische Theorie der Klimaschwankungen. Handbuch der Klimatologie (Koppen W and Geiger R, eds.), Gebr. Borntraeger, Berlin, 1930, (Ⅰ)Part A: 1 - 76.

[7] Li Fenglin, Yuejun ,Li Jianfen, et al. Present Marine Erosions on The coast of Bohai Sea. Collective [M]. Tianjin: Tianjin Science and Technology Press, 1996, 137 - 164.

[8] Kellogg W W, Schneider S H. Climate stabilization: for better or for worse [J]? Science, 1974, 186 - 1 163.

[9] Friedman H. The Change in the World: some Intersect Study Problem between Sun and Earth [M]. Beijing: Earthquake Press, 1990, 164 - 167.

[10] Morner N A. Earth Rheologe, Isostasy and Eustasy [M]. University of California, 1980, 535 - 553.

[11] Yue Jun, Jiang Mingmei. The division and correlation of Nihewen Beds by multiple elements statistics and analysis [J]. Oceanographic Geology and Quaternary, 1986, 6(2): 81 - 94.

[12] Yue Jun, Jiang Mingmei. Stratigraphic Division and correlation of Nihewan Beds by multivariate statistic analysis [J]. Chiness Journal of geochmistry, 1992, 11(3): 261 - 276.

[13] Yue Jun, Wen Qizhong. The Analysis Pattern for Palaeoenvironmental Evolution of Nihewan Beds [J]. Acta Geologic Sinica, 1990, 64(3): 248 - 256.

[14] Yue Jun, Wen Qizhong. Analytical model for the Palaeoenvironmental Evolution of the Nihewan Beds [J]. Acta Geologica Sinica, 1991, 4(1): 77 - 86.

[15] Cabanes C, Cazenave A, Provost C L. Sea level rise during past 40 years determined form satellite and in situ observations [J]. Science, 2001, 294: 840 - 842.

[16] Wang Zhihao. The Sea Level in 20 Century: The Sea Level Change in China [M]. Beijing: Oceanography Press. 1986, 237 - 245.

[17] Vivien Gornitz. Sea-Level Fluctuation and Coastal Evolution [M]. 1987, 3 - 16.

[18] HUANG li-ren, MA Qing. Global change of the sea-level in recent decades [J]. Acta Oceanologica Sinica, 1993, 15(6): 76 - 82.

[19] Zhao Mingcai, He jiazhong. The Prediction of the Sea Level Rise Along China and its Effect on the Coast. See:The Impacts of Sea Level Rise on the Major Vulnerable Areas of the China's Coastal Zone and Relevant Strategies [M]. Du Bilan Chairman. BeiJing: China Ocean Press, 1997, 37 - 42.

[20] Wu Zhong-ding, Li Zhan-qiao, Zhao Ming-cai. The Process and Prediction of SeaLevel Change of China Offshore Waters in 50 Years [J]. Hydrogeaphic surveying and charting. 2003, 23(2):17 - 19.

[21] Rohert Cook. Major Biogeochemical Cycles and Anthropogenic Changes [J]. Episodes, 1984, 7(2): 3 - 7.

[22] Sherwood B, Idso. The CO_2 - Climate Controversy [J]. Boreas, 1984, 13(2): 93 - 94.

[23] Morner N A. Terrestrial variations within given energy, mass and momentum Budgets; paleoclimate, sea Level, paleomagnetism, differential rotation and geodynamics [M]. 1988, (260): 455 - 478.

[24] Zhu Kezhen. The Primery Study on Climate Change Since Recent 5 Thousand Years in China [M]. BeiJing: Science Press. 1979, 475 - 489.

[25] Zhang Jijia, Ge Ling. Basics of mid and long-term weather forecast [M]. Beijing: Meteorological Press. 1981, 287 - 317.

[26] Ren zhenqiu. Discussion of China Climate Anomaly and Its cause of formation in recent 5000

years [J]. Agricultural Archaeology, 1986, 1: 298 - 303.

[27] Zhang De-er. A Compendium of Chinese Meteorological Records of the Last 3000 year [M]. Nanjing: Phoenix Press, 2004, 258 - 3 666.

[28] Chen Jiaqi, Pan Liangbao. The Primery Study on Historic Climate Change in Lower Streams of Changjiang River and Huaihe River. The Research Development on China's Climate and Sea Level Change(Ⅱ) [M]. Beijing: Oceanography Press, 1992, 39 - 40.

[29] Gribbin J, Lamb H H. The Climate Change in Historic Period [M]. Transtated by Fu zhongbin, Li jingjun, Wu xiangding, et al. Beijing: Oceanography Press, 1991, 68 - 81.

[30] Flohn H. Klimaschnitte in Mittel Euuropa seit 1000; Bluthgen J. 1964. Allgemeine Geographie, 1959, 447, Berlin.

[31] Lamb H H. Biological Significance of Climate Changes in Britain [M]. Academia Press, 1965, 3 - 33.

[32] Du Bilan, Liu Fakong, Zhang Jinwen. The Sea Level Rise Threatening China's Coastal Vulnerable Zone and it's Prediction. See:The Impacts of Sea Level Rise on the Major Vulnerable Areas of the China's Coastal Zone and Relevant Strategies [M]. Du Bilan Chairman, BeiJing: China Ocean Press, 1997, 1 - 9.

[33] Chen J L, Wilson C R, Chambers D P, et al. Seasonal global water mass budget and mean sea level variations [J]. Geophysical Research Letters,1998, 25(19): 3 555 - 3 558.

[34] Church J, Gregory J M, Huybrechts P, et al. Changes in sea level [C]. Climate Change 2001:The Scientific Basis, Contribution of Working Group I to the Third Assessment Report of the Intergovernmental Panel on Climate Change. New York: Cambridge University Press, 2001: 639 - 693.

[35] Lila Efha. The ice age will come sonner [M]. Geographic Knowledge. Beijing: Sciences Press, 1992, (4): 22.

[36] Thomas M K. Changes in the Climate of Ontario [M]. In Changes in the Fauna of Ontario. University of Toronto Press, 1957.

[37] Houghton J, Global Warming [M]. Authorized translation from the English language edition published by Lion Publishing plc, 1994.

[38] Qin Dahe, Ding Yihui, Su Jilan, et al. Assessment of Climate and Environment Changes in China (I): Climate and environment changes in China and their projection [J]. Advancss in climate change, 2005, 1(1): 4 - 8.

[39] Chen yiyu, Ding Yongjian, She Zhixiang, et al. Assessment of Climate and Environment Changes in China (II): Measures to adapt and mitigate the effects of climate and enviromment changs [J]. Advances in climate change, 2005, 1(2): 51 - 57.

[40] International development trend and foreground analysis [EB/OL]. 2005-12-22.

海平面变化与未来预测
—— 气候的过去、现在和未来

岳军[1,2,3]，DONG yue[4]，陈满春[5]，韩 芳[1,3]，段焕春[1,3]，王国明[2]

（1. 天津市海洋地质勘查中心，天津 300170；2. 国土资源部天津地质矿产研究所，天津 300170；
3. 天津华北地质勘查局地质研究所，天津 300170；4. University of Texas at San Antonio, Texas 78249-1644, USA；
5. 国家海洋信息中心，天津 300171）

摘 要：海平面变化是由于太阳、月球等几大行星的天体作用、地球本身作用、生物作用、大气作用和海洋作用及人为因素等叠加作用的结果。所以，海平面变化是许多变数中一个敏感的积分变量，或是各大领域系统耦合效应的一个组合函数。为此，可将上述各个方面的叠加作用和耦合影响称为“天地生耦合效应系统”。并据此建立了相应的日动型、气动型、水动型和地动型等概念模型，旨在研究几大作用之间的多重耦合效应和反馈机制。通过集合变量，采用了时段划分的方法进行定量分析，以确定各变量之间的联系性、有效性和相关性，初步获得地球自转速度是控制海平面变化的动力机制；世界海平面速率为+1.32 ± 0.22 mm/a，中国海平面速率为+1.39 ± 0.26mm/a。以CO_2含量为气候指标，划分出了公元200年以来的八个冷段（冷期）。第Ⅷ冷段极大值大约出现在公元1850年前后，若按冷暖极值距200年计算，则由目前正在发展的暖期，将在公元2050年前后结束，而后开始降温；若按冷暖极值距250年间隔计算，将在公元2100年前后开始降温，彼时，世界海平面将上升+7 ～ 11 ± 3.5 cm左右（在气候暖期的过程中），且其后海平面将呈下降趋势，与此同时，气候将进入下一个新的冷期（亦即第Ⅸ冷段）。

关键词：天地生耦合效应系统；海平面变化机制；海面升降速率；气候冷期；未来预测

A review on quantitative analysis of suspended sediment concentrations

KUANG Liang[1], YU Hua-ming[2*], DING Yang[2], LI Xi-bin[3], KUANG Hua[4]

1. Department of Maritime System, Stevens Institute of Technology, Hoboken, NJ 07030, USA;

2. College of Physical and Environmental Oceanography, Ocean University of China, Qingdao 266003 Shandong Province, China;

3. Tianjin Marine Environmental Monitoring Central Station, Tianjin 300451, China;

4. Heyuang Polytech College, Heyuan 571000, Guangdong Province, China

Abstract: Information on the concentration of suspended sediments in coastal waters is necessary for the understanding and management of the coastal environment. Traditionally, suspended sediment concentration (SSC) has been measured by time-consuming and costly boat surveys which allow the accurate measurement of SSC for single points in space and time. In order to obtain the instantaneous measurement of SSC, a variety of remote sensing method has been adopted. Remote sensing from airborne and spaceborne sensors has been proven to be a useful adjunct to such surveys as it provides an instantaneous and synoptic view of sediments that would otherwise be unavailable. Dominique Durand and Jerome Bijaoui in 2000 presented a feasible study on optical remote sensing of shallow-water environmental parameters. Yogesh C. Agrawal and H. C. Pottsmith in 2001 tried to use Laser Diffraction Sensors to measure Concentration and Size Distribution of Suspended Sediment. Francisco Pedocchi and Marcelo H. Garcia in 2006 made an evaluation of the LISST-ST instrument for suspended particle size distribution and settling velocity measurements. H.K.Ha and W-Y.Hsu in 2009 tried to measure suspended cohesive sediment concentration using ADV backscatter strength. Shuisen Chen, Ligang Fang in 2009 managed to use remote sensing of turbidity in seawater intrusion reaches of Pearl River Estuary.

In this article, the brief review of most of the technologies or methods used to observe the suspended sediment concentration is executed. As the most powerful technology in the remote sensing, acoustic backscatter device is discussed in detail. A comparison between those traditional and modern technologies is made to clarify its future application and development.

Received on March 14, 2011

*Corresponding author: hmyu@ouc.edu.cn

Keywords: suspended Sediment Concentration, optical backscatter sensor, acoustic backscatter sensor

Introduction

Sediment transport has been a great interest to scientists and engineers working in water quality, geology, and hydraulics for a long time due to the complex of hydrodynamics, sediment dynamics, water-sediment interaction and the lack of precise measurement. Understanding the mechanism of sediment transport can benefit human beings in various aspects, from keeping dam damaged due to sediment accumulation, making navigation channel smooth, keeping track of contaminant constrained in sediment particles and protecting beach from being eroded. Thus, it's of great importance and significance to improve our understanding of sediment transport and its dynamics.

In order to fully understand its processes and dynamics, it's essential and valuable for us to seek a reliable and accurate method of measuring sediment concentration, particle size and other related properties. Over the past decades, interest in sediment movement has focused on the detailed effects of turbulent currents, wave action, and their combined effect on the transport of sedimentary materials [1]. The measurement of suspended sediment concentration in the ocean has always been a difficult task and no single device or technique seems adequate for all requirements [2].

To measure the suspended load transport, a wide range of instruments is available from simple mechanical samplers to sophisticated optical and acoustical (electronic) sensors, including electromagnetic current meters (ECM), Laser Doppler Anemometry (LDA), Laser In Situ Scattering Transmissometry (LISST), airborne and spaceborne sensors, Miniature Optical Backscatter (MOB) and Acoustic Backscatter Sensors (ABS). Most instruments are used as point-integrating instruments which mean the measurement of the relevant parameters in a specific point above the bed as a function of time [2]. Some instruments are used as depth-integrating samplers, which mean continuous sampling over the water depth by lowering and raising the instrument at a constant transit rate time [2]. With all the current developed devices, the sediment particle size, settling speed, suspended sediment concentration can all be investigated easily and less-costly.

1 Review on measuring instruments for sediment transport

1.1 Pump sampler

The water-sediment sample is pumped through a filter (see Fig. 1) which separates all particles larger than the mesh size of the applied filter material. To separate the sand fraction, nylon filter material with a mesh size of 50 um can be used. The water volume is recorded by means of a (simple) volume meter. After taking a sample, the filter system is opened and the filter material with the sand catch is removed and returned to the laboratory for drying, weighing and size analysis. During removal of the filter, the pumping is continued using a bypass system. The filtration method cannot be used in a silt environment with silt concentrations larger than about 50 mg/l because of rapid filter blocking by the fine silt particles [3].

The sand concentrations are determined as:

$$c = G / V$$

in which: G= dry mass of the sediment (mg), V= volume of the water sample (l).

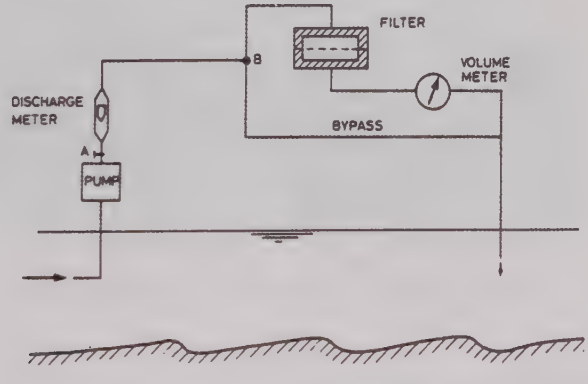

Fig. 1 Sketch of pump sampler

1.2 Spaceborne SPM measurement

The first person who did their work in analyzing SPM concentration with satellite data is Kritikos in 1974. Then in 1978 Holyer advanced the application by discussing progress toward universal multispectral suspended sediment algorithm. In the Coastal Zone Color Scanner era (1978 - 1986), coastal waters were observed as "Turbid" areas with high particulate concentrations [4]. At that time, qualifying suspended sediment matter (SPM) concentration has been a challenge in coastal waters. However, the pronounced color

signature from sediments gave us a clue on potential capability to qualify SPM concentration with improved ocean radiance sensors. The advances in the theoretical analysis of particle scattering and absorption and the enhancement of the spaceborne ocean sensors have made the quantitative analysis of SPM available. Recently, many works have been done to obtain the global suspended sediment concentration by spaceborne ocean sensors. Landsat, SPOT, the Advanced Very High Resolution Radiometer (AVHRR), the Sea-viewing Wide Field-of-view sensor and MODIS have all provided data (See Fig. 2)that have been used for accurate SPM estimation in specific applications and settings[4]. In the late 1990s and the first years of the 21st century, China, India, Korea also launched satellites with ocean color sensors capable of providing data for SPM determination. The next generation of spaceborne ocean color sensors, currently under development, includes hyperspectral instruments with high spatial resolution (Orbview-4, NEMO/COIS). With the current plethora of sensors and the advanced capability of computers, the ability to accurately determine SPM concentration should be enabled [4].

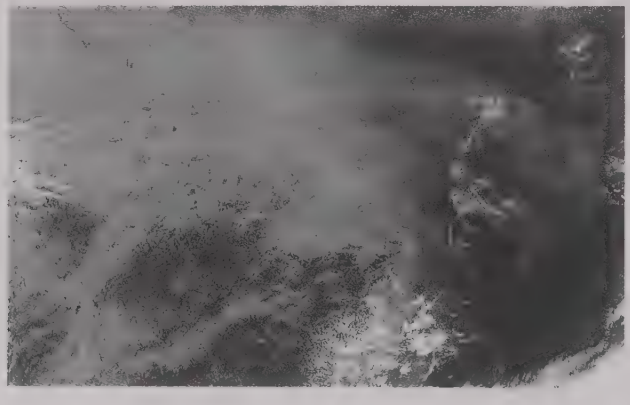

Fig. 2 SeaWiFS image of sediments in the East China Sea [4]

1.3 Optical and acoustical instruments

1.3.1 General Principles

Optical and acoustical sampling methods have the ability for the continuous and contactless (non-intrusive) measurement of sediment concentration. This is the most important advantage compared with the traditional mechanical sampling methods, like pump sampler. Although optical and acoustical waves are different, the instruments developed for sampling or measuring the suspended sediment concentration are similar and based on the same physical principles: transmission, scattering, transmission-scattering.

Optical backscatter sensor is an optical sensor for measuring turbidity and solids

concentrations by detecting infra-red light or laser light scattered from suspended particles (See Fig. 3). The radiation scattered from the object of interest is recorded and analyzed to obtain the concentration. The sensor utilized is sensitive the particle size, water property and other factors. Downing J P. Sternberg is the first group to formally utilize the optical sensor to study the suspended sediment processes in 1981. Rijn et al. made a lot contribution to this field later. Agrawal Y C. and Pottsmith H C, in 2000 raised the idea of using LISST-ST for measuring sediment settling velocity and suspended concentration and put it to application.

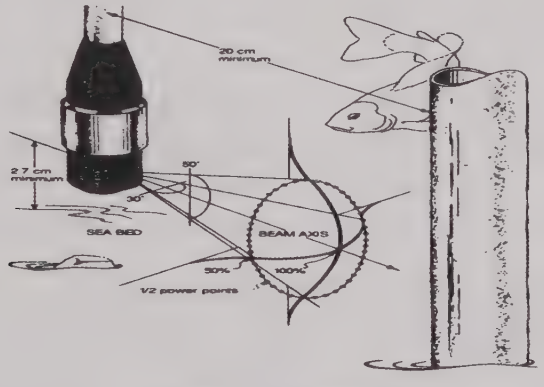

Fig. 3 OBS sensor

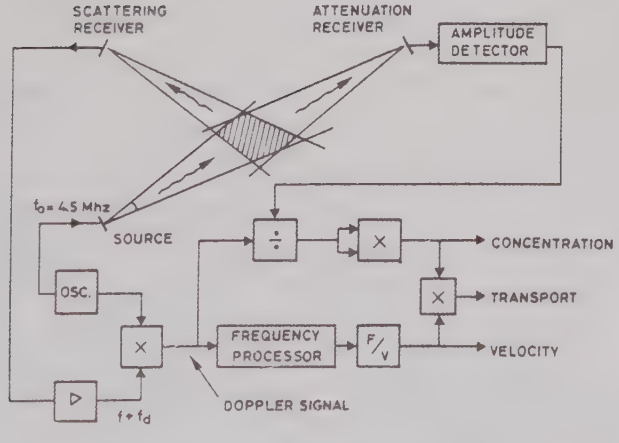

Fig. 4 ABS measuring system

The difference between acoustic backscatter sensor and optical backscatter sensor is the usage of ultrasound waves. In 1978, Jansen R H J who worked in Delft Hydraulic Company became the first scientist to raise the concept of using ultrasonic scattering to obtain the in-situ sediment concentration. However, Hay in 1983 was the first person for lying out and published the theoretical work for reversing the acoustic pressure to sediment concentration. And Young et al. was the first people to bring their application of acoustic

measurements of suspended to public. Then Thorne and Hanes expanded the theoretical background of the acoustic in detail in 1992. In the last decade, many complicated and reliable acoustic instruments have been developed, like the Acoustic Sand Transport Meter (ASTM) in 1994, UHCM, ADV in 2005.

1.3.2 Performance of OBS and ABS

The performance of the OBS-sensor is claimed to be superior to most other in-situ turbidity sensors, because of small size and sample volume, linear response and wide dynamic range, insensitive to bubbles and phytoplankton, ambient light rejection and low temperature coefficient and low cost.

The most severity of OBS is its high attenuation in water, and more than 98% diminished after traveling for only 0.2 m. The OBS sensors are about the same size as the length of gradients in the sand concentration being measured. This will cause hydrodynamic noise in the output signal because of turbulent flow around the sensor.

For OBS, the wave length and particle size must be of the same order of magnitude in order to get an optimal sampling resolution. Therefore, the optimal method is most suitable for silt particles (> 50 um) for Infra-red light, 5 - 500 um for LISST-ST (Laser). The upper concentration limit for optical sampler is about 500 mg/l due to insufficient light penetration of the optical sensor in condition with high concentration 1.

Compared with OBS, the ABS has more advantages. The potential of acoustics to provide the required parameters for assessing and developing sediment transport formulae is significantly greater, although most studies gain by a synergy of optics, acoustics and conventional instrumentations. Unlike OBS's rapid attenuation in water, the acoustic wave can travel longer and has a full spectral of measuring velocity, SPM concentration, and particle size at the same time. For ABS, the acoustic method is most suitable for sand particles (>50 um), and the upper concentration limit is 10 000 mg/l, however, the relationship between acoustic response and concentration becomes non-linear when its greater than 500 mg/L and does not work well for non-cohesive sediment due to it is sensitive to particle size, which has the same problem as the OBS.

2 Application of acoustic backscattering sensor (ABS)

Given the above mentioned advantages of acoustic backscattering sensor (ABS), an example [5] of its application in real marine environment will be presented here. The ABS has a wide range of application and can be adapted for different functionalities including the measuring currents (ADCP), sediment particle size and sediment concentration (ADV)

and used for different environments, like estuary, river, Open Ocean, wave environment and so on. There have been some researchers put ABS into different marine environments, including Vincent and Green, 1990; Hanes, 1991; Thorne 1993; Hay and Sheng, 1992; Osbourne and Vincent, 1996; Thorne and Hardcastle, 1997, Williams, et al., 2000; Hill D C, 2003; H K Ha 2009. The application of ABS in the tidal estuary is also reported by Thorne and Hardcastle in 1997.

In this example, the basic principle and procedure will be presented. For detailed theory description, information can be found in Peter D. Thorne's paper in 1990 and 2001. The acoustic sensors used in this application work exactly the same way as the aforementioned backscattering sensors including optical and acoustic ones. One thing should be noted for acoustic sensor is that the near range for acoustic should be treated with caution due to its complexity and big errors. From Fig. 5, we can see that the sound pulse will be scattered back from the objects it encountered, and the acoustic column is divided into near field and far filed. After the receiver sensor which is mounted at the same location with transceiver, its acoustic pressure is recorded, digitalized and analyzed. However, the recorded data is pressure filed instead of sediment concentration or sediment particle size. What the researchers developed is an algorithm which can be used to transform the pressure inversely into sediment concentration, based on empirical experiment, calibration and digital data analysis. And the particle size distribution can also be deduced through Multifrequency ABS sensors. The detailed algorithm can also be found in Peter D. Thorne's paper in 2000.

The experiment setup can be found in Fig. 6. In this application, the instruments used consist of seven acoustic backscattering sensors, ABCDE. The frequency of sensor ABCDE is between 0.5-5MHz. The sensor works better for concentration below 500 mg/l and particle size above 63 micro meters. The sediment properties will only be determined precisely by combining all those sensors. The Sensor A for sediment concentration works well for static water, but not for marine environment with currents changing frequently due to wave and wind effects. However, with the CDVP (B), the effects of the currents can be quantitatively determined. The bed ripple profiler can be operated in low grazing angles towards the bed and the RMSE is as low as 0.008 m. The sensors BDE are used to determine the bed morphology variation and can be coupled with sensors AB to derive the more accurate particle sizes.

The temporal suspended sediment concentration (SSC) profiles (Fig.7) are presented and comparison between ABS observed particle size, SSC and pump sampled are also showed (Fig. 7). From the Fig. 8, we can find that the application results is good and can be used to measure the sediment properties reliable and precisely enough.

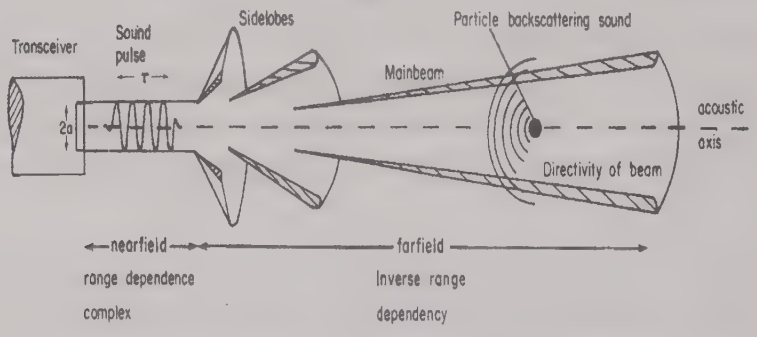

Fig. 5 The schematic illustration of how acoustic backscattering works

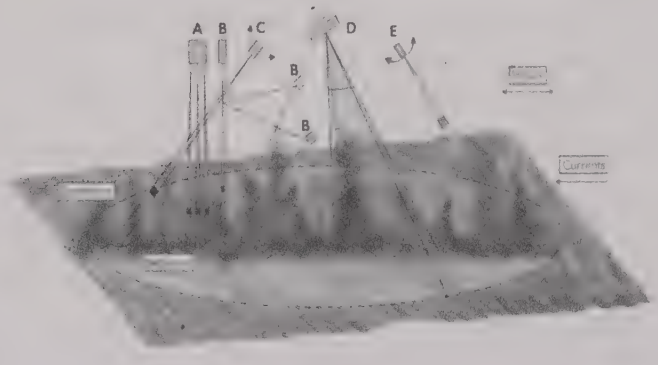

Fig. 6 Experiment setup

A: Multifrequency Acoustic Backscattering for measuring suspended sediment particle size and concentration profiles. B: Coherent Doppler Velocity Profiler for measuring three orthogonal components of flow velocity. C: Bed Ripple Profiler for measuring the bed morphology along a transect. D: High Resolution Sector Scanner for imaging the local bed features. E: Backscatter Scanning System for measuring the relationship between morphology and suspended sediments.

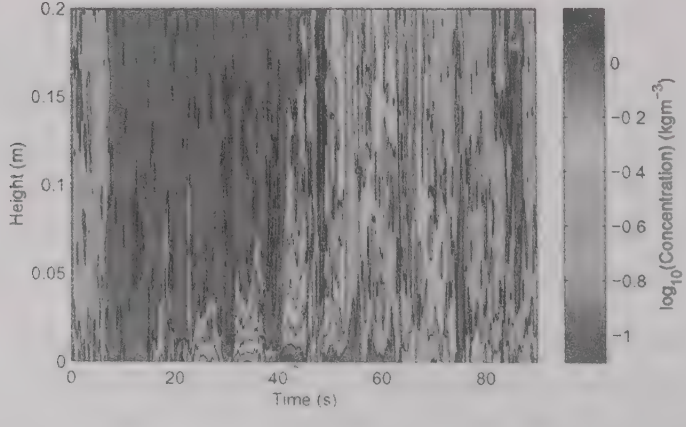

Fig. 7 An example of temporal suspended sediment concentration (SSC) profile

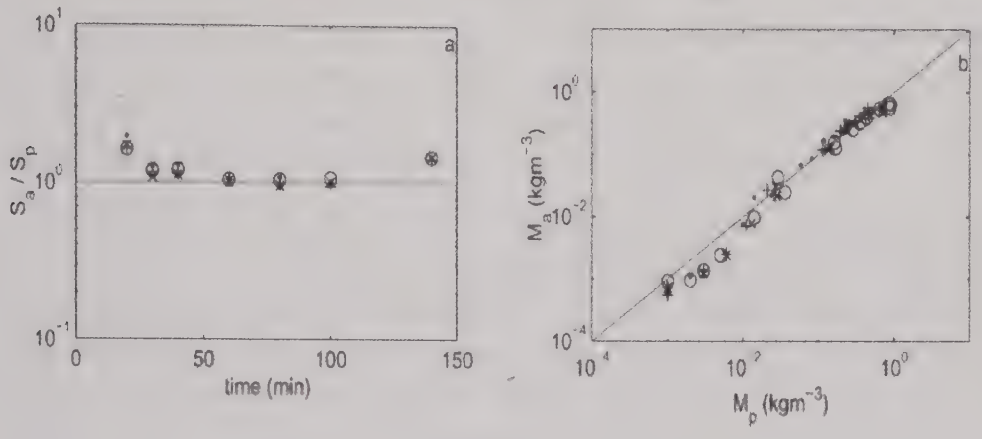

Fig. 8 Comparison of particle size and SSC between acoustic observed and pump sampled

From the simple review of this application, the usage of acoustic backscattering sensors is reliable to measure the suspended sediment concentration, particle size distribution and leads to further understanding of small-scale sediment processes. But there are limitations and shortcomings for each of the sensors (ABCDE). For example, the morphology profiler only operate along a single transect and transects should be orthogonal for a two-dimensional ripple field to reduce its errors. And it's also limited by its lower grazing angle. For flow sensors, the size of the particle will affect its measurement and the maximum range-velocity ambiguity equation also imposes system limitations. For sediment concentration, it's working successfully for homogeneous non-cohesive sediments. But the complexity of marine environment is not fully understood, such as the biological effects, interaction between non-cohesive and cohesive particles. Besides, the restrain imposed by the relationship between acoustic wave frequency and attenuation is a tradeoff for transverse and lateral resolution. The higher frequency will have better resolution but higher attenuation. And the algorithm mentioned before has significant influence on results too. Overall, it can be used for sediment study in marine environments.

3 Future development

As discussed above, all the instruments developed have their advantages and disadvantages. For the samplers, it is good for point measurement but is not good for getting spatial and temporal data. But it's necessary for calibration for remote sensors. Satellite can be very useful for obtaining synoptic picture large-scale SSC distribution, especially for estuary and high SSC water bodies However; it's very hard to validate its performance and accuracy due to its large scale and can't be used for small-scale studies,

like turbulent effects. Optical Backscatter Sensor is easy to operate, but limited for its fast attenuation when it's traveling deeper and not working well for high concentration (500 mg/L). But it is working better for silt/ cohesive sediment compared with ABS. Acoustic Backscattering Sensor has its unique verdicts: wide range of application (velocity, SSC, SPM), non-intrusive in deep water measurement, higher concentration waters and so on.

Since different instrument have their own virtues and advantages, it's very reasonable for us to combine various sensors and make each sensor as complimentary for the other. Like in this application example, even though only ABS is used, different physical principles of acoustic waves are adapted to develop different sensors and put together for better performance. For ABS system, better mathematical and theoretical algorithm for inverse problem should be developed in future and other factors that influence ABS performance, like bubble, biological, particle accumulation, should be further studied and incorporated into the algorithm. Besides, numerical modeling for sediment can also be used to calibrate sensors.

4 Summary

In this article, various remote sensing methods are reviewed and their advantages and disadvantages are discussed. From the previous discussion, we can find that neither of those methods is perfect, but they can work well as their design purposes. For instance, the spaceborne SPM can be used for obtaining synoptic picture of global or large scale sediment distribution, LISST or ADS and other OBS can be used as a quantitatively way for investigating suspended sediment concentration (SSC), while the traditional time consuming pump sampler can be used for validation. All those instruments have their specific advantages and should be applied the same time to get better resolution and more accurate results.

Acknowledgement

This research is supported by the National Marine Renewable Energy Program (No. GHME2011ZC03, GHME2010ZC08, GHME 2010ZC11 and GHME2010ZC01) and Study of the Key Technology of the Forecast of Global Ocean Circulation and Sea Ice (2011BAC03B02).

References

[1] Thorne P D, Vincent C E, Hardcastle P J, et al. Measuring suspended sediment concentrations using acoustic backscatter devices [J]. Marine Geology, 1991, 98 (1): 7 - 16.

[2] Thorne P D, Hardcastle P J, Soulsby R L. Analysis of acoustic measurements of suspended sediments [J]. Journal of Geophysical Research (Oceans), 1993, 98 (C1): 899 - 910.

[3] Rijn L C. Manual sediment transport measurements. Delft: The Netherlands: Delft Hydraulics Laboratory, 1986.

[4] Halifax. 8th International Conference on Remote Sensing for Marine and Coastal Environments. NS, Canada, May 17-19, 2005.

[5] Thorne P D, Hanes D M. A review of acoustic measurement of small-scale sediment processes [J]. Continental Shelf Research, 2002, 22 (4): 603 - 632.

关于定量监测悬浮泥沙浓度方法的回顾和展望

匡 良[1]，于华明[2]，丁 扬[2]，李希彬[3]，匡 华[4]

（1. 斯蒂文斯理工学院，新泽西 07030 美国；2. 中国海洋大学海洋环境学院，山东 青岛 266003；
3. 国家海洋局天津海洋环境监测中心站，天津 300451； 4.河源职业技术学院，广东 河源 571000）

摘 要：获取近岸水体中悬浮物浓度及相关信息对于理解和管理海洋环境相当重要。历史上对于悬浮物浓度的监测往往通过费时费力的出海观测，而这种观测具有很大的局限性，每次观测只能获取一个站位的信息。为了更快更有效的获得即时悬浮物浓度相关信息，很多新的监测手段及相关科技被开发及应用。各种机载，卫星载遥感设备被用于获得及时，全面的沉积物信息。Dominique Durand，Jerome Bijaoui 在 2000 年刊发了关于光学传感设备可以有效应用于浅海海洋环境中以获取各种环境参数。Yogesh C，Agrawal H C，Pottsmith 等人于 2001 年尝试用激光传感设备获取水体悬浮沉积物浓度及相关粒径分布信息。Francisco Pedocchi，Marcelo H，Garcia 于 2006 年分析了关于用 Laser In-Situ Scattering and Transmissometry (LISST-ST)监测悬浮物颗粒粒径及沉降速度的可靠性。H K Ha，Hsu W Y 在 2009 年尝试了用声学多普勒测速仪(ADV)监测可凝性沉积物浓度。Chen Shuisen，Fang Ligang 在 2009 年成功应用海水浊度遥感信息研究沉积物侵入黄河口影响范围。在文章中回顾了近些年大部分关于水体（海口，近岸等）沉积物浓度监测相关科技及方法。同时展现了一个 ABS 的具体应用实例，通过实例分析更好的了解各种监测方法的优略。详细分析了作为最近国际上应用做广泛的声学多普勒测速仪(ADV)的其优势，应用范围等相关信息。对比了传统的分析方法和近代分析方法，以此呈现未来海洋悬浮物浓度监测科技的发展趋势。

关键词：悬浮物监测；悬浮物速度分析；光学探测器；声学探测器

Integrated assessment of sea water quality based on BP artificial neural network

LI Xue[1], LIU Chang-fa[2], WANG Lei[2], QIU Wen-jing[1]

1. *National Marine Data and Information Service, State Oceanic Administration, Tianjin* 300171, *China;*

2. *College of Marine Environment Engineering, Dalian Ocean University, Dalian* 116023, *Liaoning Province, China*

Abstract: In order to carry out an integrated assessment of sea water quality objectively, this paper based on the concept and principle of artificial neural network, generated appropriate training samples for BP artificial neural network model through the method of producing samples to the concentration of various pollution index of sea water quality from the viewpoint of threshold, established the BP artificial neural network model of sea water quality assessment using multi-layer neural network with error back-propagation algorithm. This model was used to assess water environment and obtain sea water quality categories of offshore area in Bohai Bay through calculating. The calculations shown that pollution index in river's wet season was higher than that in dry season from 2004 to 2007, and the pollution was particularly serious in 2005 and 2006, but a little better in 2007. The assessed results of cases shown that the model was reasonable in design and higher in generalization, meanwhile, it was common, objective and practical to sea water quality assessment.

Keywords: artificial neural network, sea water quality, training sample, connection weight, assessment

The method of water quality assessment mainly contains single-index assessment and integrated assessment. In order to facilitate the protection of water environment, environmental management department applied single-index assessment method to assess environmental impact. But if the method was used to assess water quality, it will reduce water function and environmental effect. Integrated assessment of water quality is the important item of water environmental assessment. It represents the overall status of water quality with quantitative and visual characteristics, and is an important research subject of modern basic environmental science. There are many methods of integrated assessment of sea water quality. For example, composite index method, gray cluster method, gray pattern recognition method, fuzzy integrated evaluate method, fuzzy pattern recognition method, etc. [1-5]. However, these methods need to presume a model or set

Received on Aug. 10, 2011

Corresponding author: helen_li7056@sina.com

some parameters subjectively. Most of them need to design the evaluation criteria to all levels of membership functions and the index weights. The evaluation results are highly subjective, so they can not be truly applied in practice, only as reference in environmental assessment. We still use single-index assessment method to determine water quality categories [6]. Therefore, we need to study more objective method of integrated assessment of water quality.

Artificial neural network is a non-linear model technique, which was developed and applied to many disciplines rapidly since 1980s. Its advantage contains massively parallel processing, distributed storage, adaptive, fault tolerance, etc. It was widely used in many areas, for example, pattern recognition, intelligent control, knowledge process and forecast, etc. It is one of the most active frontiers, especially suitable for non-linear system [7-12]. Integrated assessment of water quality needs these features fortunately. This paper discusses the objective assessment method of water quality, which applies the BP artificial neural network model.

1 Principle of BP artificial neural network

Artificial neural network（ANN）is able to achieve a certain function on the basis of understanding human beings` brain structures. It is the theorized mathematical model of the human neural network and the information processing system based on the imitation of the structure and function of brain networks [13]. At present, there are many kinds of common neural network model, among of them, BP（back propagation）network algorithm is advanced, mature and stable in working, easy to learn as more research paradigms, especially suitable for pattern recognition and data classification [14].

BP network is a multi-layer network from the structural view, which is divided into input layer, hidden layer and output layer. It is all inter-connections between the layers, one output layer unit can not feed back to the forward layer unit, the same layer unit can not be connected(Fig. 1)[15]. BP network achieves the vision of multi-layer learning. When given the network an input mode, it send from input layer unit to hidden layer units, and after processing, it send from the hidden layer units to output layer unit, then the output layer unit generates an output mode, This is a gradual layer by layer update process, known as forward propagation. If exist error between the output response and the expected output mode, can not meet requirement, then the network transfer to back-propagation. The network send the error back to each layer through connection path and correct the connection weights. When each training mode meets requirement, then end the study.

Firstly, we should provide a set of training samples in practice. Each training sample

composes a pair of input sample and excepted output. When the network's practical output is consistency with the excepted output, then the training finish. Otherwise, it amends the weights by the method of back-propagation to integrate the network's expected output and practical output. Repeat learning until the sample total error reaches a certain precision, and record the adjusted weights for calculation [16].

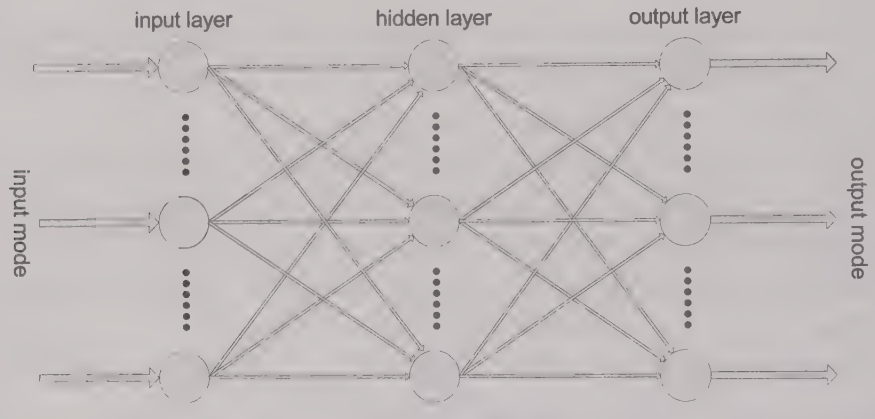

Fig. 1 Topology of BP network

2 BP network method of sea water quality assessment

2.1 Establish calculation model and training samples

2.1.1 Define input layer, hidden layer and output layer

Taking Bohai Sea for example, according to the offshore area pollution features of Bohai Bay, we select five pollution indicators: dissolved oxygen, chemical oxygen demand, active phosphate, inorganic nitrogen and petroleum for model. We use sea water quality standards (GB 3097-1997) which was implemented on July 1st 1998 as evaluation basis. It should be noted that, sea water quality standards are not divided into the Ⅱ and Ⅲ categories of activity phosphate indicator, the same as Ⅰ and Ⅱ categories of petroleum indicator. In light of two intervals are comparative large, it is susceptible to the classification results when conduct an integrated assessment. Therefore, we apply average method to divide into two intervals: 0.015 - 0.022 5 mg/L and 0.022 5 - 0.03 mg/L correspond to the Ⅱ and Ⅲ categories of active phosphate indicator respectively; ≤0.025 mg/L and 0.025 - 0.05 mg/L correspond to the Ⅰ and Ⅱ category of petroleum indicator respectively.

Input layer neural units are five, correspond to five pollution indicators respectively (Fig. 2). As sea water quality standard gives the concentrations upper (lower) limit

corresponding to various pollution indicators, when each pollution indicator value is provided in pollution indicator concentration interval, then the sea water quality belongs to the appropriate category. For example, when the pollution indicator values are provided in 5 - 6 mg/L, 2 - 3 mg/L、0.015 - 0.025 mg/L, 0.20 - 0.30 mg/L and 0.025 - 0.05 mg/L corresponding to dissolved oxygen, chemical oxygen demand, active phosphate, inorganic nitrogen and petroleum respectively, then the sea water belongs to Ⅱ category. According to this method, taking random values in the relative pollution indicators intervals, we can generate enough sea water quality samples to Ⅱ category. Similarly, we can also take random values in other intervals and generate enough sea water quality samples to other categories. Due to the reason of thesis space, Tab. 1 only shows the boundary value samples and learning outcomes.

In output layer, in order to identify sea water quality category and predict the trends, we use values to indicate the water quality categories, that is: intent output values are 1, 2, 3, 4 and 5, corresponding to five sea water quality categories respectively (correspond to Ⅰ - Ⅳ and exceeded Ⅳ category). We use one neural unit for output layer.

The number of hidden layer neural unit is calculated by the following formula theoretically [19]:

$$\text{The number of hidden layer neural unit} = \sqrt{m+n} + \alpha,$$

M is the number of input layer unit, n is the number of output layer unit, α is the constant from 1 to 10. According to this formula and try out method, we take three hidden layer units, and then generate a 5-3-1 structure BP network.

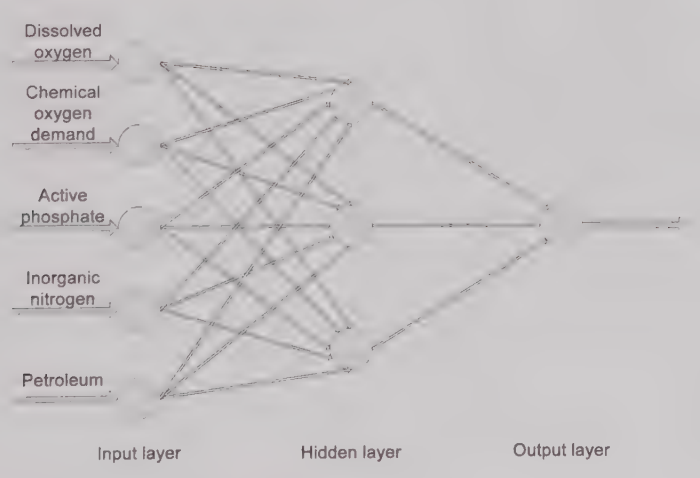

Fig. 2 Structure of BP network

2.1.2 Training samples and learning outcomes

From the categories of five pollution indicators in input layer above, we establish Ⅰ, Ⅱ, Ⅲ, Ⅳ and exceeded Ⅳ training sample. In order to accelerate the convergence of BP network, we should make the training samples non-dimensional, so that all elements in the sample should between 0 and 1, then training the network, the training samples and learning results in Tab. 1.

Tab. 1 Training sample and learning result of BP network

	Water quality category	Ⅰ category	Ⅱ category	Ⅲ category	Ⅳ category	Exceeded Ⅳ category
Training sample	Dissolved oxygen / mg/L	6	5	4	3	2
	Chemical oxygen demand / mg/L	2	3	4	5	6
	Active phosphate / mg/L	0.015	0.022 5	0.030	0.045	0.060
	Inorganic nitrogen / mg/L	0.2	0.3	0.4	0.5	0.6
	Petroleum / mg/L	0.025	0.05	0.3	0.5	0.7
Learning result	Intent output	1	2	3	4	5
	Practical output	1.001 6	1.999 2	3.000 9	3.999 1	5.001 1

2.2 Establish network parameters

Through the learning samples and training network repeatedly, we determine the learning error is 10^{-5}, learning rate 0.8, momentum term 0.2 and training times 10^5, and generate the BP network weights and threshold (Tab. 2). Thus, we establish the offshore area water quality assessment of Bohai Bay based on artificial neural network model.

Tab. 2 Connection weight and threshold between input layer and hidden layer

Weight / f_1	Hidden layer node 1	Hidden layer node 2	Hidden layer node 3
Input 1	-9.901 4	-12.404 7	-22.876 6
Input 2	2.982 8	5.374 1	14.708 0
Input 3	-10.154 0	-8.516 9	-16.872 4
Input 4	10.412 3	8.180 7	44.606 9
Input 5	-0.822 3	5.308 7	-8.836 5
Threshold (b_1)	4.628 3	4.395 5	4.766 2

Tab. 3 Connection weight and threshold between hidden layer and output layer

Hidden layer node	Hidden layer node 1	Hidden layer node 2	Hidden layer node 3
Weight / f_2	-5.975 8	-9.045 8	-2.081 3
Threshold / b_2		0.781 2	

2.3 Application

Taking the five test points (001-005, Fig. 3) in offshore area of Bohai Bay for example, the sea water quality is influenced by estuaries greatly. These five rivers are respectively Jiyun River, Beitang sewage River, Dagu sewage River, Duliujian River and North sewage River. Using BP artificial neural network model of sea water quality established above, and selecting monitoring data of five test points in dry seasons and wet seasons from the year 2004 to 2007 for the test sets, we test the established BP network, testing results in Tab. 4.

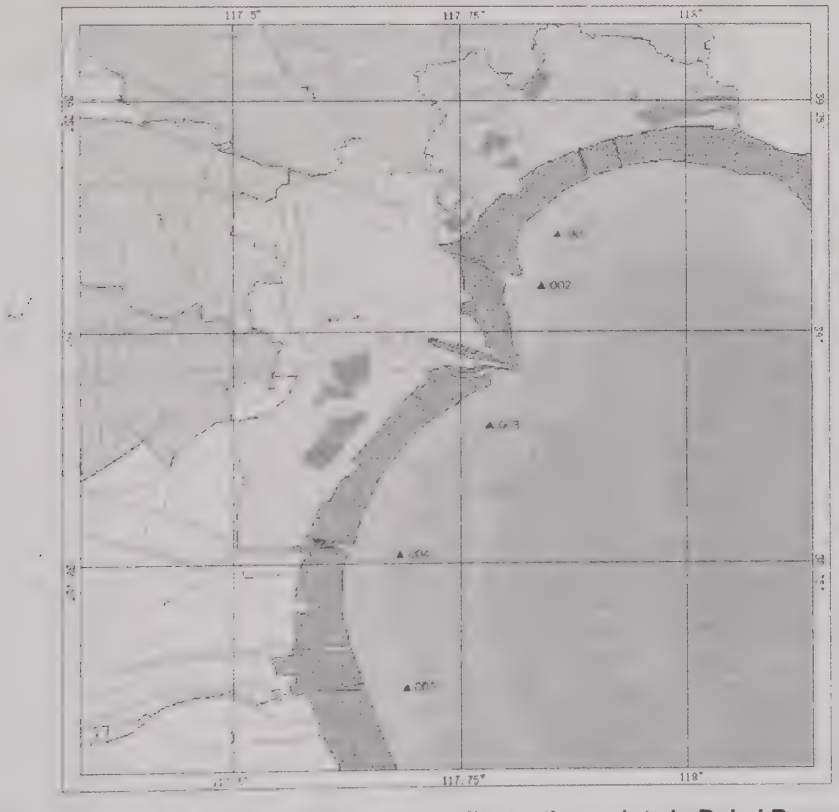

Fig. 3 Distribution of water quality testing points in Bohai Bay

Tab. 4 Sea water quality assessment model testing case of BP network

Test point	Monitoring time	Dissolved oxygen / mg/L	Chemical oxygen demand / mg/L	Active phosphate / mg/L	Inorganic nitrogen / mg/L	Petroleum / mg/L	Network output	Sea water quality category
	2004/dry	6.62	2.21	0.252 3	0.915 7	0.015 5	0.856 9	I
	2004/wet	6.49	1.89	0.007 2	0.453 5	0.026 9	3.042 7	III
	2005/dry	8.37	2.41	0.041 9	0.827 3	0.023 6	4.962 1	exceeded IV
	2005/wet	7.17	3.24	0.148 8	3.499 7	0.046 3	6.841 2	exceeded IV
	2006/dry	7.82	2.64	0.034 7	0.607 1	0.033 0	3.382 7	III
	2006/wet	7.89	2.85	0.080 9	1.459 2	0.084 4	5.558 6	exceeded IV
	2007/dry	9.09	2.22	0.003 4	0.317 8	0.036 9	0.999 5	I
001	2007/wet	5.73	1.87	0.048 0	0.968 5	0.052 6	5.520 6	exceeded IV
	2004/dry	6.78	2.12	0.131 4	0.940 8	0.038 2	4.117 7	IV
	2004/wet	6.57	1.79	0.009 1	0.334 1	0.034 9	1.549 5	II
	2005/dry	8.06	2.56	0.019 9	0.640 1	0.024 7	3.984 5	IV
	2005/wet	6.02	2.83	0.048 5	1.111 9	0.001 1	5.564 0	exceeded IV
	2006/dry	7.28	2.36	0.034 3	0.511 6	0.021 3	2.320 3	II
	2006/wet	6.24	3.17	0.145 3	1.582 9	0.063 9	5.555 1	exceeded IV
	2007/wet	8.12	1.84	0.006 9	0.433 1	0.072 5	1.306 1	I
002	2007/wet	5.45	1.66	0.046 7	0.191 4	0.047 9	0.843 8	I
	2004/dry	6.47	1.81	0.001 4	0.313 1	0.010 6	2.030 7	II
	2004/wet	7.74	1.85	0.052 2	0.565 0	0.075 2	1.731 0	II
	2005/dry	7.96	2.33	0.000 1	0.630 7	0.028 8	4.284 9	IV
	2005/wet	5.90	2.15	0.027 9	1.074 2	0.035 1	5.569 0	exceeded IV
	2006/dry	6.82	2.52	0.021 1	0.809 4	0.034 2	5.449 2	exceeded IV
	2006/wet	5.72	2.68	0.024 6	0.904 3	0.032 7	5.547 9	exceeded IV
	2007/dry	7.53	2.43	0.002 3	0.650 2	0.055 1	4.908 3	exceeded IV
003	2007/wet	6.07	1.77	0.022 7	0.536 3	0.047 4	3.522 6	exceeded IV
	2004/dry	7.86	2.21	0.000 5	0.172 9	0.040 4	0.890 1	I
	2004/wet	6.81	1.99	0.001 0	0.294 4	0.039 6	1.492 8	I
	2005/dry	7.42	2.03	0.009 7	0.414 8	0.024 2	2.118 3	II
	2005/wet	6.87	1.89	0.037 6	0.312 8	0.038 2	0.969 5	I
	2006/dry	7.33	1.92	0.001 3	0.216 7	0.044 1	0.945 6	I
	2006/wet	7.07	1.54	0.017 9	1.023 9	0.060 4	5.533 2	exceeded IV
	2007/dry	5.81	1.29	0.006 5	0.281 2	0.037 7	1.361 6	I
004	2007/wet	5.48	1.03	0.011 7	0.531 2	0.060 2	3.795 2	IV
	2004/dry	8.62	2.48	0.004 2	0.129 4	0.063 8	0.818 1	I
	2004/wet	6.83	2.29	0.018 1	0.392 8	0.029 4	1.854 4	II
	2005/dry	8.27	1.96	0.003 9	0.414 8	0.034 5	1.668 2	II
	2005/wet	6.73	2.37	0.022 4	0.248 0	0.054 3	0.906 1	I
	2006/dry	7.41	2.07	0.000 2	0.251 5	0.046 9	1.088 2	I
	2006/wet	8.92	1.91	0.010 2	0.671 8	0.038 2	3.734 5	IV
	2007/dry	9.59	1.94	0.006 2	0.437 4	0.065 8	1.178 4	I
005	2007/wet	6.67	1.34	0.007 7	0.392 0	0.037 3	2.202 5	II

From the network output of the five points' sea water category in Tab. 4, the sea water quality in offshore area of Bohai Bay is generally worse in river's wet seasons than dry seasons. Sea water quality in nearby area of North sewage River is relatively well compared with five test points, and that only in wet season of 2006 was Ⅳ category, those in category other times were Ⅰ and Ⅱ categories; The second is Duliujian River nearby area, where appeared one Ⅳ and one exceeded Ⅳ category; The worst is Dadu Sewage River nearby area, appeared four exceeding Ⅳ and two Ⅳ categories. In 2005 and 2006 water quality condition of Bohai Bay was worse, and that in the wet season of 2006 was especially serious, those in four areas exceeded Ⅳ category, except the nearby area of North Sewage River for Ⅳ category. But in 2007, each area is lightened in water quality pollution.

It shows that the assessment result of BP network is specific, accurate and realistic in testing water quality category from the confrontation between assessment result and Marine Environment Quality Bulletin 2004-2007[20]. The assessment method of BP network is highly in accuracy, and the water quality will be more quantitative. We can obtain the affiliation of each water quality samples to the corresponding category. Obviously, this method is objective and effective.

3 Conclusion

There is no need to find out the specific relationship between variables when applying artificial neural network technology in establishing integrated assessment of sea water quality model. We can only define network structure based on actual issues and obtain network weights about the issues by learning typical sample, then evaluate sea water quality. The characteristics of this model are simple in structure, easy to model, visual and objective to get the result. There exist linkage and ambiguity between water environmental pollution and water quality grade, and simultaneously the water quality change is continuous, so the result of sea water quality assessment based on BP network is more quantitative and accurate. Moreover, BP model can select any number of water quality parameters to learn, establish different assessment models. The model can obtain reliable result of any monitoring samples after successful learning, so the applicability is broad. BP artificial neural network possess bright prospects and application value in sea water assessment.

Reference

[1] Shi X X, Xia J. Grey-mode identification model for water environmental quality assessment and its

application [J]. China Environmental Science, 1997, 17(2): 127 - 130.

[2] Chen S Y, Zhao Y Q. Fuzzy pattern recognition model and water quality assessment [J]. Journal of Hydraulic Engineering, 1991, 6: 35 - 40.

[3] Liu G J, Guo S W. Gray clustering method in the assessment of water quality [J]. Water Resources and Hydropower Technology, 1988, 12: 1 - 5.

[4] Bao Y E, Huang S G. The discussion on the marine environmental quality assessment [J]. Marine Environmental Science, 1996, 15(3): 1 - 9.

[5] Xu H Z, Shang L S. Method of seawater quality assessment using grey situation decision grade [J]. Marine Environmental Science, 1994, 13(4):36 - 41.

[6] Chen L H, Ma D S. The models of artificial neural network for prehensive assessment of Yellow River water quality [J]. Journal of Northwest Minorities University (Natural Science), 2002, 23(3): 28 - 32.

[7] Yan P F, Zhang C S. Artificial neural networks and simulation evolutionary computation [M]. Beijing: Press of Tsinghua University, 2000: 1 - 37.

[8] Yan P F. Capacity learning and computational complexity of artificial neural networks [J]. Chinese Journal of Electronics, 1995, 23(1): 63 - 67.

[9] Zhao L M, Hu H Z, Wei D H, et al. Multi-layer feedforward artificial neural network [M]. Zhengzhou: Press of Yellow River water conservancy, 1999: 9 - 68.

[10] Dong C. Approximation and generalization mechanism of multilayer feedforward neural network [J]. Control and Decision, 1998, 13(sup): 413 - 417.

[11] Anderson J A. An introduction to neural networks [M]. London: MIT Press, 1995: 1 - 62.

[12] Bishop C M. Neural network for pattern recognition [M]. Oxford: Clarendon Press, 1995: 5 - 28.

[13] Cong S. Matlab toolbox for neural network theory and application [M]. Hefei: Press of University of Science and Technology of China, 1998: 1 - 29.

[14] Lou W G, Some aspects on application of BP neural network to comprehensive assessment of water environmental quality [J]. Journal of Fishery of China, 2002, 26(1): 90 - 96.

[15] Liu Z C, Liu Y C. Fuzzy logic and neural networks——theory research and exploration [M]. Beijing: Press of Beijing University of Aeronautics and Astronautics, 1996: 1 - 38.

[16] Hu S R, Yu S B, Dai K. Neural network theory [M]. Beijing: Press of National Defense University, 1993, 21(3): 312 - 317.

[17] Li Z Y. Water quality assessment method based on BP network [J]. Environmental Engineering, 1995, 13(2): 51-53.

[18] Xue J J, Yao G J. Artificial neural networks in water quality assessment [J]. Hydrology, 1997, 3: 37 - 39.

[19] Zhang L M. Artificial neural network model and its application [M]. Shanghai: Press of Fudan University, 1993, 55 - 70.

[20] Tianjin Marine environmental quality bulletin. www.coi.gov.cn.

基于 BP 人工神经网络的海水水质综合评价

李 雪[1]，刘长发[2]，王 磊[2]，邱文静[1]

（1. 国家海洋信息中心，天津 300171；2. 大连海洋大学 海洋环境工程学院，辽宁 大连 116023）

摘 要：为了能够客观地对海水水质进行综合评价，在分析人工神经网络概念和原理的基础上，从阈值角度出发，通过对各类海水水质污染指标浓度生成样本的方法，生成了适用于BP人工神经网络模型训练的样本，并应用基于误差反向传播原理的前向多层神经网络，建立了用于海水水质评价的BP人工神经网络模型。将该模型用于渤海湾近岸海域水环境评价，通过模型的计算，得到该海域的水质类别。结果表明，2004-2007年，渤海湾近岸海域污染指标总体上在河流丰水期时比枯水期时高，2005年和2006年污染较为严重，2007年有所好转。经训练的评价模型应用于实例的评价结果表明，该模型设计合理、泛化能力强，对海水水质评价具有较好的客观性、通用性和实用性。

关键词：人工神经网络；海水水质；训练样本；连接权值；评价

Investigation of fecal coliform and typical enteric virus in representative beaches of China

FAN Jing-feng [1], MING Hong-xia [2], WU Li-jun [3], LIANG Yu-bo [1], LI Xue[4]

1. *National Marine Environmental Monitoring Center, Linghe street* 42, *Dalian* 116023, *Liaoning Provine, China;*

2. *College of Environmental Science and Engineering, Key Laboratory of Pollution and Environmental Criteria Ministry of Education, Nankai University, Tianjin* 300071, *China;*

3. *Wuhan Institute of Virology, Chinese Academy of Science, Wuhan* 430071, *Hubei Province, China;*

4. *National Marine Data and Information Service, Tianjin* 300171, *China*

Abstract: Through investigating ten recreational marine beaches in China, we aimed to detect the occurrence of human enteric viruses in coastal bathing beaches and find a correlationship, if any, between the presence of enteric viruses in surface seawater and the concentrations of fecal coliforms, the conventional indicator of fecal pollution. In this study, twenty seawater samples were assayed for fecal coliforms and human pathogenic enteric viruses (hepatitis A viruses, rotaviruses, polioviruses) analysis. Enteric viruses were detected by RT-PCR, in 20 sample sites, 5%, 40%, 40% were positive for the presence of human hepatitis A viruses, rotaviruses, polioviruses, respectively. Seven of 20 sites are suffering from severe fecal contamination, based on traditional plate counts of fecal coliform outnumbering the established thresholds for recreation. Additionally, statistical analysis presented that no correlation was found between bacterial indicators and viruses in surface seawaters. The data confirmed that indicator bacteria in water are not reflective of the presence of enteric viruses in marine waters. Thus, current recreational water quality standards of both bacterial and viral indices should be reevaluated.

Keywords: fecal pollution, fecal coliform, enteric viruses, traditional indicator, public beaches

Recreational marine beach is a popular vacation spot, attracting increasing numbers of visitors to the shoreline annually. Correspondingly, with the increase of domestic sewage discharge and urban runoff into the coastal ocean, one of the major concerns worldwide about recreational water was the risks of illness from exposure to the contaminated water, which is resulting in an urgent requirement of water quality monitoring for the microbial

Received on March 24, 2010

Corresponding author: jffan@nmemc.gov.cn

indicators of fecal pollution.

Current microbiological quality standards in China and throughout most of the world for water includes only bacterial fecal indicators (FIB), such as fecal coliforms (FC) and enterococci [1]. However, whether bacterial fecal indicators are adequate to predict human pathogenic viruses, an important pathogen agent of waterborne illness, different researchers have different opinions [2, 3]. Therefore, it is necessary, in China, to investigate and confirm this issue.

Proper monitoring of human viruses in recreational water is of particular importance. Previous study indicates that the quantitative detection of coliphages and the purify of enteroviruses on cell culture are not suitable parameters for the control of the viral pollution in surface water, whereas the detection of enteroviral genomes may be useful for predicting the presence of waterborne viruses [4]. RT-PCR, the gold standard for the detection of viral gene, is a sensitive, rapid and specific method that has been successfully applied to accurately define viral burden of diseases [5].

In previous studies, enteroviruses and adenoviruses always were chosen as assembly object to study this relationship, while Hepatitis A virus (HAV) , rotaviruses (RoV) have not been selected, which are the representative of enteric viruses and closely related to fecal contaimination. RoVs are the major cause of severe gastroenteritis, and over 1 million children died of diarrhea, that is attributable to rotavirus alone. Besides, HAV is recognized as the common cause of infectious jaundice in the world. Additionally, poliovirus (PoV) has not yet been eradicated, although it is one of the objectives pursued by the WHO since 2000. Here we are the first time to detect the bacterial and viral indexes simultaneously in representative beaches in China. We selected HAV, RoV, PoV, and FC, the root cause of nosocomial infection [6], as the study objects to reflect the coastal pollution. This study focuses on determining the occurrence of enteric viruses in coastal waters, and the correlationship between FIB and the presence of enteric viruses.

1 Materials and methods

1.1 Sample sources

In August 2008, ten water samples were collected from three different monitoring stations at each of the ten representative beaches of China (Fig. 1). At each beach, samples were collected at the distance of 100 m (site 1) and 1 000 m (site 2) from the shore, respectively. We suspected that 100 m site is densely area with human activities, and samples from 1000m site locating in offshore was used as control. Amount to 20 water

samples collected from all beaches were for fecal coliform and enteric viruses analysis.

1.2 Sampling procedure

Water samples (150 mL) were filled in 200 mL sterile bottles at each sampling site to detect fecal coliforms for bacterial analysis, and 10-liter samples were collected in 20-liter sterile polypropylene containers for viral detection (according with the criterion of water) [7].

The samples were collected during low tide and transported to the laboratory at 4 °C. All bacterial analysis and viral contamination detection were performed within 24 hours of sample collection.

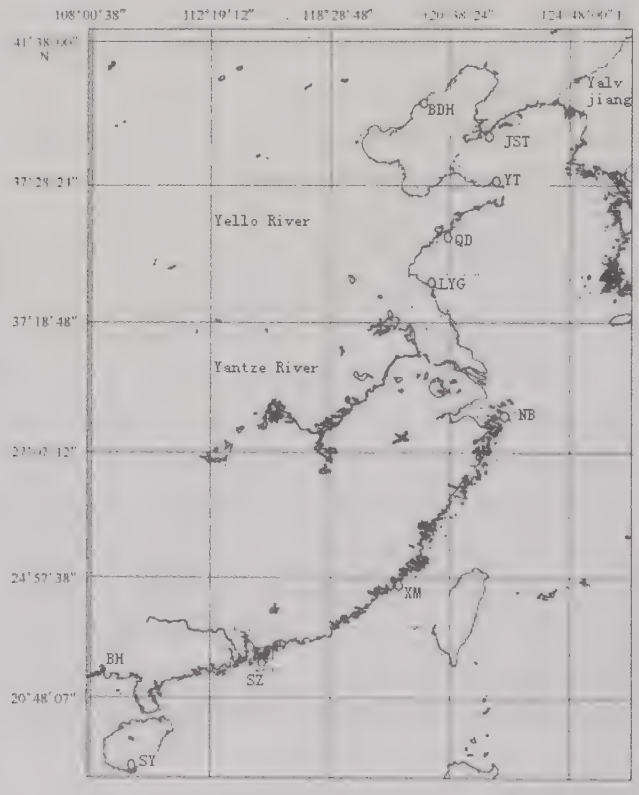

Fig. 1 Site locations of the study

1.3 Enteric viruses concentration

Viruses were concentrated by ultrafiltration and millipore virus concentration device as described previously [8]. 10-liter of seawater was sequentially filtered through a 0.8-μm diameter fiber filter and a 0.22-μm-pore-size filter to remove particulates and to prevent clogging of the spiral filter cartridge. Then filtrates were concentrated to 100-mL using the

millipore virus concentratration device (Centricon Plus-70), and then further concentrated to a final volume of about 350 μL using a Centriprep-30 ultraconcentration unit.

1.4 Virus nucleic acid extraction

All nucleic acids were extracted from 200 μL concentrated water samples by a spin column technique using Viral Nucleic Acid Extraction Kit II (Gene aid). RNA was eluted in 50 μL RNA free water. All samples were tested for the presence of HAV, RoV, and PoV nucleic acids by RT-PCR.

1.5 Detection of HAV, RoV and PoV

The positive samples of the three viruses were provided by the Center for Disease Control and Prevention of National Virus Graduate School. The primers for the detection of three different enteric viruses, HAV, RoV and PoV are shown in Tab. 1.

Tab. 1 Primer sequence of three viruses

virus	gene	primer	Sequence / 5'- 3'	The size / bp
HAV	Capsid proteins VP1 and VP3	H1	GTTTTGCTCTTTACCATGCTATG	248
		H2	GGAAATGTCTCAGGTACTTTCTTTG	
RoV	VP7	Beg9	GGCTTTAAAAGAGAGAATTTCCGTCTGG	392
		VP7-1	GATCCTGTTGGCCATCC	
PoV	5'non-coding region	Polio-R	ACGGACACCCAAAGTA	394
		Polio-F	AGCACITCTGTITCCC	

1.5.1 cDNA synthesis

Reacting conditions for three viruses were the same, RNA was reversely transcribed into cDNA for RT reaction mixture (20 uL): 5 μL of 5×AMV RT buffer, 1.3 uL each of 10 mM dNTP; 2.5 μL of each antisense primer (Tab.1) 10pM/μL, RNase inhibitor 20U, 1 μL of RT (AMV: 50 U/μL) and 2 μL of extracted RNA was added to the RT reaction mixture. The reverse transcription was performed using the following program: 37 °C for 10 min, 42 °C for 30 min and inactivated by heating to 95 °C for 5 min.

1.5.2 PCR amplification

PCR was carried out with 2.5 μL of cDNA mixed with 20 μL of PCR mixture, containing 2.5 uL of 10×PCR buffer, 2.5 μL each of 2.5 mM dNTP, 25U TaKaRa ExTaq and 25 mM each primer (Tab. 1). The product sizes of HAV, RoV and PoV were 248, 392, and 394bp, respectively. The amplication of HAV was performed as described previously by Suphachai [9]. To amplify part of the VP7 rotavirus gene segment, a single-tube method was carried out for PCR step. Primers Beg9 and VP7-1 reaction conditions were designed

according to Dubois [10]. For PoV diagnosis, sense primer Polio-F and antisense primer Polio-R were used, PCR condition was performed the same as Robert [11].

1.5.3 PCR products detection

The amplified fragments were separated by electrophoresis on a 2% agarose gel containing 2% ethidium bromide of volume and examined under UV light.

1.5.4 DNA cloning and sequencing

The corresponding positive amplicon products were purified and cloned into the pMD® 19-T Vector (TaKaRa Code: D102A, Japan), then the fragments were confirmed by sequencing.

1.6 Samples for fecal coliform (FC) analysis

FC analysis was done with unconcentrated water samples, using a most probable number (MPN) approach and fermentative method in microplates. FC were enumerated according to standardized methods [12]. FC plates were incubated for 24±2 hours at 44 °C, and each sample was prepared in triplicate.

1.7 Statistical analysis

One-way analysis of variance, Duncan's multiple range test and correlation analysis were performed as appropriate using SPSS16.0 to evaluate the relationships between the presence of enteric viruses in the seawater and fecal coliforms, as well as the distance of sampling from the seashore and pathogens.

2 Results

2.1 Detection of viral genomes in water samples

A total of twenty water samples were examined for HAV, RoV and PoV genomes by RT-PCR, the results are listed in Tab. 2. The overall percentages of positive PCR samples were 5% for HAV, 40% for RoV and PoV. We also performed sequence analysis with selected samples using PCR amplified genome fragments that were qualified for genotyping. The sequences of the selected samples were genotyped by comparison with Genbank reference sequences using the BLAST algorithm, one was typed as Hepatitis A virus strain IVA and human rotavirus G2, six as human rotavirus G1, and eight as human poliovirus 2 (Tab. 2).

Tab. 2 Detection results of three viruses in ten representative beaches and comparison to bacterial indicator

Sampling site		HAV	RoV	PoV	FC (CFU/L)
Beidaihe (BDH)	4	-	Human rotavirus G1	-	≥24 000
	7	-	Human rotavirus G1	Human poliovirus 2	50
Jinshitan (JST)	4	Hepatitis A virus strain IVA	Human rotavirus G1	Human poliovirus 2	230
	7	-	Human rotavirus G1	-	220
Yantai (YT)	4	-	-	-	1100
	7	-	-	-	<20
Qingdao (QD)	4	-	-	Human poliovirus 2	≥24 000
	7	-	-	-	≥24 000
Lianyungang (LYG)	4	-	-	Human poliovirus 2	2400
	7	-	-	-	70
Ningbo (NB)	4	-	Human rotavirus G1	-	16 000
	7	-	-	-	50
Xiamen (XM)	4	-	Human rotavirus G2	-	1300
	7	-	-	-	<20
Shenzhen (SZ)	4	-	Human rotavirus G1	Human poliovirus 2	1700
	7	-	Human rotavirus G1	-	50
Beihai (BH)	4	-	-	-	16 000
	7	-	-	-	<20
Sanya (SY)	4	-	-	Human poliovirus 2	5400
	7	-	-	Human poliovirus 2	170

"-": Negative result

2.2 Fecal coliform

Water samples were examined for FC analysis using an MPN approach. According to detection standard that the samples with less than 20 CFU/L was defined as not detected, FC was found in 18 specimens. The range of FC was from 50 to more than 24 000 CFU/L (Tab. 2), and seven out of 20 samples exceeded the Chinese state bacterial standard.

2.3 Correlation between fecal pollution indicators and human enteric viruses in seawater

When studied on the relationship among numbers of FC, and human enteric viruses HAV, RoV and PoV, none had a significant regression coefficients ($P>0.05$).

2.4 Correlation between enteric viruses, fecal contamination indicators and distance off the seashore

The statistical analysis by SPSS showed that at the selected beaches, the viral incidence in the water samples collected from 100 m off the seashore was found not to be correlated with those from 1000 meters out ($P>0.05$).

The association of the number of fecal coliforms and distance off the seashore was significant ($P<0.05$).

3 Discussions

A study by Rose demonstrated that during the summer months (June through August), in the bathing areas, the incidence of swimming-related gastroenteritis with the number of FC and viruses were positively correlated [13]. Studies also disputed whether the common bacterial assays was used to evaluate health risk frequently to alert for the presence of enteric viruses in water environment [14]. Therefore, this study was undertaken in August, 2008, to further investigate the presence of typical enteric viruses in seawater and attempt to correlate their presence in seawater with bacterial indicators of fecal pollution, preferably evaluate the pathogen pollution and public health in representative marine bathing beaches in China.

To detect the presence of enteric viruses in bathing beaches, RT-PCR was employed. After sequencing, these viruses were typed as Hepatitis A virus strain IVA, human rotavirus G1, G2, and human poliovirus 2 (Tab. 2), in which human rotavirus G1 and human poliovirus 2 gave priority to others. This data confirmed the previous two findings. One was in China, the main serum type of human rotaviruses is G1 (more than 90%), a few with G2, G3 type [15]. The other was Human poliovirus 2 pollution played a dominant role about the outbreak of enterovirues in Bohai Bay [16]. Although the detection of viral genomes in water only by RT-PCR does not provide direct information about the infectivity of the viruses, while the rate of free RNA degradation fairly rapid in seawater, so it is not likely that the RT-PCR products come from the amplication of free viral RNA [17]. In addition, Dubois [10] pointed out that the presence of viral genomes correlated with respective infectivity of those viruses in environmental samples, who also found that enteric viruses detected by PCR-based methods are typically infective. Hence, this work does provide a meaningful data for risk assessment using this method.

The Landscape Recreational Water Quality Standards for FC are a geometric mean

of 2 000 CFU/L [18], the seawater quality standards of China [19] classified the water with concentrations of FC less than 2 000 CFU/L to water quality standard class III [12], which is the lowest water class for human to contact directly. According to the above standards, only four in selected ten bathing beaches meet the recommended standard for recreation. Surprisingly, two sites in Qingdao beach are far beyond 24,000 CFU/L. If we assess the quality of bathing water only by bacterial index, this beach appears greatly polluted and may present a threat to public health. This result may be attributed to the reason that this beach has the highest number of visitors among typical coastal beaches of China [20], followed by Beidaihe beach, and Ningbo, Beihai beaches, and each bather contributed fecal coliform organisms between 10^5 and 10^6 during bathing [21]. This result coincides with our previous assume, that was in bathing beach, 100m site is intensively populated and affected by human activity, and in which the number of fecal coliforms was associated with distance off the seashore ($P<0.05$).

From Tab. 2, we can see that except Qingdao bathing beach, in other nine beaches, the number of fecal coliform in the control spot 2 all meet the bacteriological standards threshold. In contrast, the distribution of viral indicators in the water samples collected from 100 m off the seashore (spot 1) was found not to be correlated with those from 1000 meters out (spot 2). In spot 1, according to bacterial indicators, in Jinshitan bathing beach, the surface seawater met recreational water standards well, yet three types of viruses were all detected. It is becoming clear that bacterial and viral contaminations were not linked with each other, neither set of guidelines was successful for protecting the public from health hazards related to fecal contamination of bathing water. This conclusion is in agreement with findings in the previous studies [22-25]. Therefore, it is recommended that evaluation of the presence of both bacteria and viruses in seawater of marine beaches may provide additional insights into long-term water quality conditions.

4 Conclusions

The contamination of environmental waters with human enteric viruses is gaining more attention, as there was no relationships between viral indicators and fecal indicator bacteria were found. It is becoming clearer that the common bacterial assays used to evaluate health risk frequently fail to alert for the presence of enteric viruses.

In summary, our data corroborate recent evidence that bathing beach surface water is potential reservoir for enteric viral infections. This study presented a potential solution for the assessment of the validity in bathing areas, and brought forth the basal water quality of representative bathing beaches in China. These results have prompted further studies to

examine the seasonal differences and the presence of cultivatable viruses in the waters of China. Large-scale prospective investigations are needed to further characterize the health risks of bathing beaches where human exposed.

Acknowledgements

Funding for this project was provided by the National High Technology Research and Development Program ("863"Program) of China, grant no. 2006AA09Z162 and the National Key Scientific and Technological Project, grant no.908-01-ZH3.

We thank Sunny C Jiang, Yong Lin, Xueqin Gao and Hallett for constructive discussions and advices. We also acknowledge Zhaojun Duan's help for the supply of positive virus samples.

Reference

[1] Kenard R P, Valentine R S. Rapid Determination of the Presence of Enteric Bacteria in Water [J]. Appl. Environ. Microbiol., 1974, 27 (3): 484 - 487.

[2] Wyer M D, Fleisher J M, Gough J, et al. An investigation into parametric relationships between enterovirus and fecal indicator organisms in the coastal waters of England and Wales [J]. Wat. Res., 1995, 29 (8): 1 863 - 18 68.

[3] Noble R T, Fuhrman J A. Enteroviruses detected by reverse transcriptase polymerase chain reaction from the coastal waters of Santa Monica Bay, California: Low correlation to bacterial indicator levels [J]. Hydrobiol., 2001, 460: 175 - 184.

[4] Fong T T, Erin K L. Enteric viruses of human and animals in aquatic environments: health risks, detection, and potential water quality assessment tools [J]. Microbiol and Molecular biology reviews, 2005, 69 (2): 357 - 371.

[5] Aguilar J C, Pérez-Brňa M P, García M L, et al. Detection and identification of human parainfluenza viruses 1, 2, 3 and 4 in clinical samples of pediatric patients by multiplex reverse transcription-PCR [J]. J. Clin. Microbiol., 2000, 38 (3): 1 191 - 1 195.

[6] Labelle R L, Gerba C P, Goyal S M, et al. Relationships bBetween environmental factors,bacterial indicators, and the occurrence of enteric viruses in estuarine sediments [J]. Appl. Environ. Microbiol., 1980, 39 (3): 588 - 596.

[7] Laura M L, Lucena F, Jofre J. Double-layer plaque assay for quantification of enter viruses [J]. Appl. Environ. Microbiol., 2004, 70 (5): 2 801- 2 805.

[8] Jiang S C, Thurmond J M, Pichard S L, et al. Concentration of microbial populations from aquatic environments by vortex flow filtration [J]. Mar. Ecol. Prog. Ser., 1992, 80: 101 - 107.

[9] Suphachai N, Cliver D O. Capsid functions inactivated human picornaviruses and filine calicivirus.

Appl. Environ. Microbiol., 2003, 69 (1): 350 - 357.

[10] Dubois E, Le G F, Haugarreau L, et al. Molecular epidemiological survey of rotaviruses in sewage by reverse transcriptase seminested PCR and restriction fragment length polymorphism assay [J]. Appl. Environ. Microbiol., 1997, 63 (5): 1 794 - 1 800.

[11] Robert L, Atmar T G, Metcalf H N, et al. Detection of Enteric Viruses in Oysters by Using the Polymerase Chain Reaction [J]. Appl. Environ. Microbiol., 1993, 59 (2): 631 - 635.

[12] The specification for oceanographic survey - Marine biological survey (GB 17378.7-1998), State Environmental Protection Administration, 1998.

[13] Rose J B, Mullinax R L, Singh S N, et al. Occurrence of rotaviruses and enteroviruses in recreational waters of Oak Creek, Arizona [J]. Water Res., 1987, 21: 1 375 - 1 381.

[14] Marino F J, Morinigo A E, Borrego J J. Microbiological epidemiologic-study of selected marine beaches in Malaga [J]. Water Sci. Technol., 1995, 31: 5 - 9.

[15] Xu S S, Wang J W, Zhang Z H, et al. Preliminary analysis of genetic characteristics of the nonstructural protein NSP4 of rotavirus strains with different serotypes in China [J]. Chinese J. Exp. Clin. Virol., 2001, 15 (2): 132 - 134.

[16] Zhang M L, Zhao H B, Yang J, et al. Detection and quantification of enteroviruses in coastal seawaters from Bohai Bay, Tianjin, China [J]. J. Environ. Sci., 2010, 22 (1), 150 - 154.

[17] Pichard S L, Paul J H. Detection of gene expression in genetically engineered microorganisms and natural phytoplankton populations in the marine environment by mRNA Analysis [J]. Appl. Environ. Microbiol., 1991, 57 (6): 1 721 - 1 727.

[18] Water quality standard for scenery and recreation area (GB 12941-91). State Environmental Protection Administration, 1992.

[19] Seawater quality standard (GB 3097-1997) State Environmental Protection Administration, 1998

[20] Zhou L X. Forecast of seawater beach environment [J]. Marine Forecasts, 2005, 22: 161 - 166.

[21] Kamizoulis G, Saliba L. Development of coastal recreational water quality standards in the Mediterranean [J]. Environment International, 2004, 30: 841 - 854

[22] Franca B, Raffaele P. Genotyping of Rotaviruses in Environmental Water and Stool Samples in Southern Switzerland by Nucleotide Sequence Analysis of 189 Base Pairs at the 5′ End of the VP7 Gene [J]. J. Clin. Microbiol., 2000, 38 (10): 3 681 - 3 685.

[23] He J W, Jiang S C. Quantification of Enterococci and Human Adenoviruses in Environmental Samples by Real-Time PCR [J]. Appl. Environ. Microbiol., 2005, 71 (5): 2 250 - 2 255.

[24] Jiang S C, Noble R, Chu W P. Human Adenoviruses and Coliphages in Urban Runoff-Impacted Coastal Waters of Southern California [J]. Appl. Environ. Microbiol., 2001, 67 (1): 179 - 184.

[25] Pusch D, Oh D Y, Wo1f S, et al. Detection of enteric viruses and bacterial indicators in German environmental waters. Arch. Virol., 2005, 150 (5): 929 - 947.

中国重点海水浴场中粪肠球菌和主要肠道病毒的调查研究

樊景凤[1]，明红霞[2]，吴立军[3]，梁玉波[1]，李 雪[4]

（1. 国家海洋环境监测中心，辽宁 大连 116023；2. 南开大学，环境科学与工程学院，国家教育部重点实验室，天津 300071；3. 中科院武汉病毒研究所，湖北 武汉 430071；4. 国家海洋信息中心，天津 300171）

摘 要：本文调查了中国十大典型海水浴场，旨在监测人类肠道病毒在海水浴场的发生情况，并且找出表面海水中肠道病毒的存在与传统的粪便污染指示物-粪大肠菌群是否存在关系，如果存在，是什么关系。分别采用常规的平板计数法和RT-PCR技术对粪大肠菌群和人类致病性的主要肠道病毒（甲肝病毒、轮状病毒、脊髓灰质炎病毒）进行了检测。结果显示，在20个样品中人类甲肝病毒、轮状病毒、脊髓灰质炎病毒的阳性率分别为5%, 40%, 40%。有7个海水样品受到粪大肠菌群污染，并且严重超过国家规定的娱乐用水的标准。数据分析表明，在这十大海水浴场中，传统的细菌指示物与几种典型的肠道病毒之间都没有任何相关性。因此，建议当前的娱乐水质标准应该考虑将细菌和病毒学指标同时考虑在内。

关键词：粪便污染；粪大肠菌群；肠道病毒；传统指示生物；海水浴场

Organization and storage model of marine information and its application in the "China Digital Ocean"

LIU Jin[1], LI Hao-qian[1], ZHU Ji-cai[2], JIANG Xiao-yi[1], ZHANG feng[1]

1. National Marine Data and Information Service, Tianjin 300171, *China;*

2. China Nuclear Geology, Beijing 100013, *China*

Abstract: Based on the experience and achievement of the"China Digital Ocean", the classification plan for Marine data elements is made, which can be classified into five, including marine point elements, marine line elements, marine polygon elements, marine grid elements and marine dynamic elements. In this paper, the technology of features and object-oriented method, a spatial-temporal data model is proposed, which can be applied in the large information system engineering like the "Digital Ocean", and this paper discusses the application of spatial data model, marine three-dimensional raster data model and relation data model in the building of Data Warehouse in "China Digital Ocean", and concludes the merits of these models.

Keywords: digital ocean, sphere model, data warehouse, ocean elements, data organization and storage

Introduction

"Digital Ocean" is a massive and complex system supported by the newest information technology, which relies on the national information facilities and marine spatial data establishment to research the marine phenomenon [1]. It is a virtual ocean world formed by massive marine observation data with multi-resolution, multi-phase and multi-space type, and also by its analysis algorithm and model. Data model and data structure are the foundation for constructing the digital ocean information system. Most of the ocean phenomenon has a dynamic spatio-temporal feature, which is the essential difference comparing to the land information, so the traditional GIS data model is facing many embarrassments in organizing or displaying the ocean information.

Many researchers propose various types of spatio-temporal data models to organize and display the time-space phenomenon. In the Time Lab technology report, Achilleas P

Received on May 5, 2011

Corresponding author: liujin@mail.nmdis.gov.cn

and Babis T detailedly discussed 9 frequently used spatio-temporal data models and analyzed their merits and drawbacks and the relative application domain [2]. Yet, these models can not organize or display the time-space process of ocean phenomenon well, particularly when both the property and position are changeable, such as the ocean front, the vortex and the coastline, et al. LI Shan et al. proposed an "ocean line data model basing on features" and designed an ocean line storage structure with a time-space feature [3]. XUE Cun-jin et al. discussed the process objects and their logical relation according to the inner characteristics of continuous gradual changing geography substantiality. They implicitly recorded the dynamic changing mechanism of the geography substantiality by the abstract process object, and defined the function interface mode whose changing mechanism is supplied by the process object storage list. Also, they realized the process organization, storage and dynamic analysis of continuous gradual changing geography substantiality [4]. The researches of LI and XUE solved the organization and storage of the marine data with line feature and continuous gradual change feature respectively. Their work can partly fulfill the demand of ocean information system. However, the digital ocean is an integrated information system containing various types of marine data, which requires an integrated and general solution.

Aiming at project application, this paper researches the classification of marine data elements in the "Digital Ocean" system, designs a spatio-temporal data model that suits for large information system project like "Digital Ocean". Its practical application performs well.

1 Background

"China Digital Ocean" is a macro system, which recurs and predicts the real ocean based on the integrated digital platform and the virtual environment supported by the techniques of database, geographic information system, network and so on. The data this system contains are obtained from marine investigation, ocean observation (including the satellite, plane, ship, buoy, and station data) and society statistic investigation. "Digital Ocean" directly displays the real ocean phenomenon and process, predicts and simulates the future ocean scene, improves ocean development and application reliably and effectively to keep the continuable development of ocean [5].

The data sources of "Digital Ocean" information system involve: the whole data of 908 investigation project, investigation data of history projects of National Ocean Bureau, the massive marine science data and relative information conserved by subordinate ocean bureaus, marine business centers and research institutes. The data cover wide domains like ocean hydrology, meteorology (near sea surface), marine biology, marine chemistry,

marine environment quality, marine geology, marine geophysics, marine basic geography, ocean aviation and remote sensing, marine economy, ocean resource, etc. The total global ocean data volume is greater than 10 billion kb.

Compared to the other data, ocean information owns the characteristics of multi-source, multiform and multi-type. Various observation methods determine the multi-source of data, subsequently lead to accuracy differences and various formats, which cause the complex data structure. The multiform of data, namely, the ocean information are presented by various formats, like graph, image, text, etc, which induces a further complication of data processing methods. The multi-type of data means that the ocean data cover various disciplines, which brings complexity to the data management. One of the important tasks of "Digital Ocean" is to establish the data warehouse and integrate the complex various ocean data together for the further information service, what's the key point is the proper data organization & storage that can fulfill the requirements of data application.

2 Classification of the ocean data elements

Considering the multi-source and multiform of ocean data, this paper chooses a feature-based method, to categorize the complex various data and pick up their special properties for establishing the element category and the data model. A clear catalog can be formed by classifying the ocean data, which is beneficial to the construction of the database and dataset. The feature-based method is adopted to extract the common spatial character and property information, abstract them into element categories. Meanwhile, establish the relationship among the data and design the data model according to the needs of the data application, and supply the data interface, method and operation for it.

Features highly generalize and abstract the phenomenon and its display of the realistic world, which are the basic units of entity. All the objects in the realistic world are displayed by the features, which are composed of feature property and feature operation. The instantiation of the features turns out to be the object entity of the realistic world. Thus, this paper categorizes the marine data into five elements, which are marine point elements, marine line elements, marine polygon elements, marine grid elements and marine dynamic elements. The definitions and the contents of each element are as follow.

2.1 Marine point elements

The marine points can be classified into two kinds, which are feature points and measurement points. The measurement points can be similarly classified into time series points and instantaneous points, while the latter are formed by four subcategories.

Tab. 1 Classification of marine point elements

Point Elements		Definition
Feature Point		Fixed object, like immovable buoy. No measurement or time property, which is corresponding to the terrain point element.
Time Series Point		Display the fixed objects whose properties differ with time.
instantaneous Point	Instant	Involve the location (x, y, z), time (t), and the measurement property (m_1... m_n). Yet each observation is independent, such as the CTD.
	Location Series	Display the movable objects, such as ship and animal, by point series with time and location values. The unique serial number represents the different points belong to one entity.
	Sounding	The object owns only depth property in one location without any other properties.
	Survey	Only for the certain defined measurements in discrete position, like Radar Elevation.

2.1.1 Time series points

The fixed buoy, coast base and station et al. can be displayed by the Time Series Point Model due to their long time series' data collection, while the Instantaneous Point relates with a certain time. In the Time Series Point property table, X-location and Y-location define the location of the point. As the foreign key equipment list, Device ID defines the equipment information of that point. The time series parameter table keeps the parameter information. TS Type is the host key and responsible for connecting the Time Series table. Z-location can display the different profiles of the same parameter variable. The values of each variable are stored in the time series table.

Tab. 2 Parameters of time series points

Name	Type	Key	Limitation	Description
TSTypeID	CHAR(10)	*P*	*None empty*	Type label of the time series parameter.
Variable	NUMBER(20)			Name of the variable
Units	NUMBER(10)			Units
IsRegular	NUMBER (1)			Regular time interval or not
TSInterval	NUMBER(10)			Time interval
Data Type	NUMBER(10)			Data type
Origin	VARCHAR2(10)			Source of the time series data
Z-location	NUMBER(10, 3)			Elevation value

There's no definition for the time series with irregular interval. The main time intervals are 1 min, 2 mins, 30 mins, 1h, 2h, 1d and 1mon. As its name, the DataType indicates the data type, including the instantaneous data, the accumulative data, the increment, the mean, the maximum and the minimum. The Origin indicates whether the time series data are produced by a model or the real measurement data.

Tab. 3 Parameters of Time Series Point

Name	Type	Key	Limitation	Description
FeatureID	CHAR(32)	*P*	*Non empty*	Grid identification
FeatureCode	NUMBER(6)			Element code
XLocation	NUMBER(6)			The location of X
YLocation	NUMBER(6)			The location of Y
PointType	NUMBER(6)			The type of the point
DeviceID	VARCHAR2(10)			Equipment identification

2.1.2 Location series

Location Series is the subcategory of Instantaneous Point. It fits for storing the information of each point of the trace and can be used to display the information of ocean plankton. The single plankton information is stored in the Series. The Series ID represents animal, are every point of animal is described by Location Series. Property Time Value and XY coordinates represent a single point element. Property Z Value is responsible for storing the depth. As a foreign key, Survey ID connects the object class Survey Info through the relation class SurveyInfoHasPoints. Series ID is used to connect the object class Series.

2.2 Marine line elements

The profile contour, duration line, and the element line are three components of the marine line elements.

2.2.1 Profile contour

This subcategory supplies a public data type for describing the element property of the nodes along the profile contour. In ocean GIS, the profile lines frequently used are vertical profile line, section line and transport line.

2.2.2 Duration line

The initial and the end time, and the lasting time are 3 core properties of time continuous line. It can record the sample data measured on the ship, the lasting time of the trawl and the partial trace of the automatic ship. One of its subcategories is the trace line, which is used in the ship-base data model. Differing from the profile contour, the trace line is only the trace of one ship. The data along the trace may be collected, or may not. Yet the profile contour always contains data.

2.2.3 Element line

Many ocean elements, like the seafloor pipeline, the administerial boundary and the sea route, can be displayed by standard line feature. A unique symbol, the x y coordinate pair and a free style measurement property aiming for application are required.Coastline is an extended subcategory of the element line. When confirming a coastline, the vertical profile data need to be recorded. Thus, a vertical datum plane property is added to store the vertical data of the coastline.

2.3 Marine polygon elements

The two kinds of the polygon elements in marine environment are: the time-independent static element polygon and the time-continuous polygon with initial and end time and also variables.

All the marine polygon elements of the static polygon can be displayed into element polygons, such as the ocean protection district and the exclusive economic zone. The element polygon need one and the only symbol, the x y coordinate pair that form the boundary, the depth and the measurement property defined by customer. A period of changing feature of the dynamic marine polygon elements can be described by time-continuous section.

2.4 Marine grid elements

There are some sea surface features, such as SST, SSH, chlorophyll a, and waterpower measurement. Three kinds of data types can display those features, which are the regular interpolation surface, the irregular interpolation surface and the grid volume component.

2.4.1 Regular interpolation surface

This model is normally used for the remote sensing data and pictures. So far the formats that support the raster data involve ArcGIS, GRID data, GeoTiff, Band Sequential (BSQ), and Band Interleaved (BIL) data. Besides, there are many oceanography and meteorology data products organized by network Common Data Form (netCDF) or hierarchical data format (HDF).

2.4.2 Irregular interpol surface

The irregular triangle grid and many finite element models are the typical types of this kind of data, which recognize the minimum triangle piece through the pivotal node and

border. TIN is a precise and effective model for displaying the continuous surface.

2.4.3 Grid volume component

Meshes are defined to fulfill the requirements of the ocean grid model and the analytical application. It displays the data into several layer Mesh data stacks with lines and columns. The structure of the elements flexibly defines the grid elements with regular interval, and these grid points can be the discrete node data.

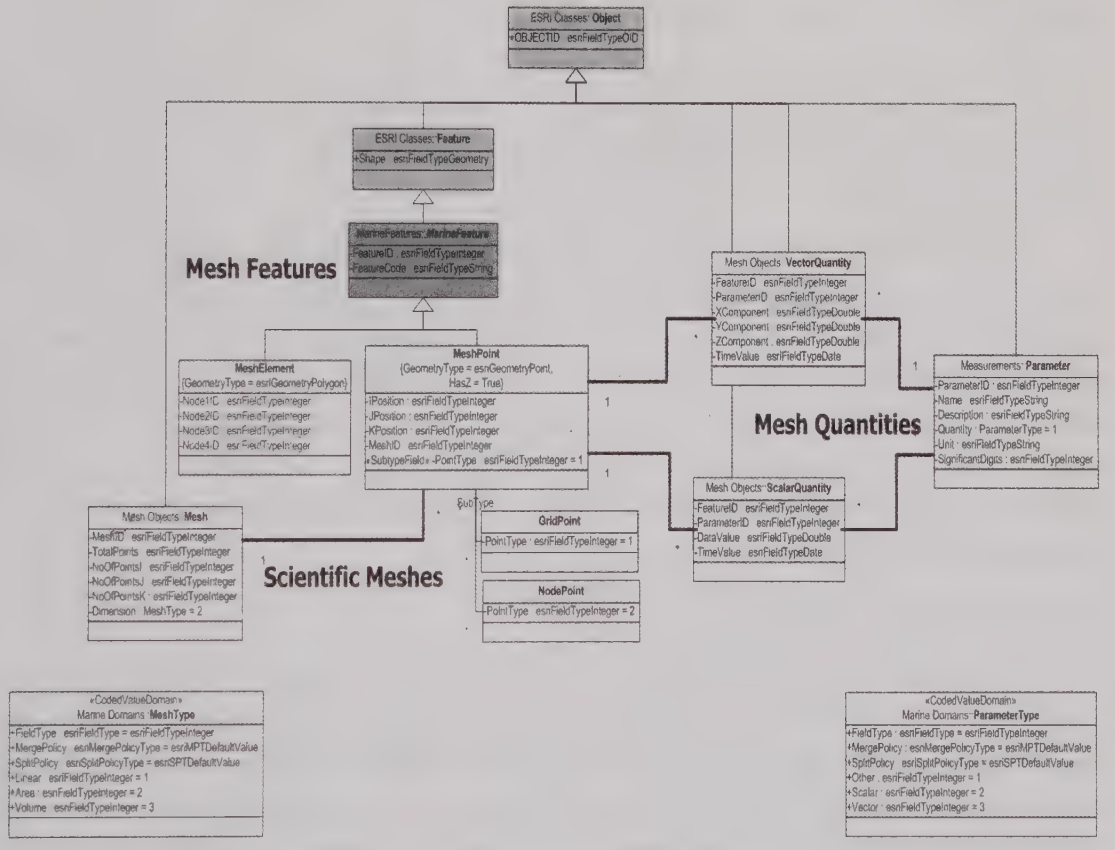

Fig. 1 Model of ocean grid elements

2.5 Ocean dynamic element

The nontraditional spatial data including, cartoon, kinescope, video and so on, aim at displaying the dynamic feature of the ocean data. The video observation data can be obtained by automatic underwater measurement equipment, aerial survey, or the video camera fixed in port, which are used to display the dynamic ocean elements and phenomenon like storm tide and current field.

3 Data model construction and application

Classify the ocean data into 5 categories according to their features, and the "object-oriented" technique is adopted in data management and storage. The object mentioned above is a concept base on the class, and the relations between feature and the object are as follows: 1) Feature is the most basic unit of data model and data structure; 2) One feature is corresponding to one object, and has one only ID. 3) Class describes the common property and type of the features, and realizes the instantiation of it. 4) The arithmetic operator of the inner class is adopted to connect the different features, so as to construct the interrelated geographical entities [3]. The foundational idea based on the feature data model is to take the feature as the basic unit and adopt the object-oriented technique to design the space, time, and time-space function, relation and operation between the features.

Most point, line and polygon data are spatial vector data, which all own spatial feature and property features, and the only difference is their spatial display style, and they can be organized and stored by the "Ocean Spatial Data Model". Although the ocean remote sensing data are raster data, its main feature is spatial feature, thus the model mentioned above can be adopted here, too. The ocean grid element, with great data volume and single property information, fits the "Ocean Grid Data Model", while the ocean dynamic elements fit the "Relation Data Model" due to the property feature information which the elements mainly contained.

3.1 Ocean spatial data model

The "Feature Dataset-Feature Class-Element" relationship is adopted for the organization of vector element data. Multi feature datasets are allowed, which are established by certain data class respectively, and multi-feature class and object class can be contained in each dataset. Each feature class involves multi geography elements, while each geography element is composed of property information, geometry information, symbol information and label information.

After setting certain grid dataset, the remote sensing image data element can be stored by Raster Mosaic method or Raster Catalog method or both. The grid datasets or grid catalogs are formed according to the name of the subjects, and can be accessed and queried through the related spatial database sheet of the ArcSDE Geodatabase.

The physical storage of the vector spatial data elements is realized by the ArcSDE Geodatabase software. Its relation sheet structure of the storage model in the

Geodatanbase is presented below:

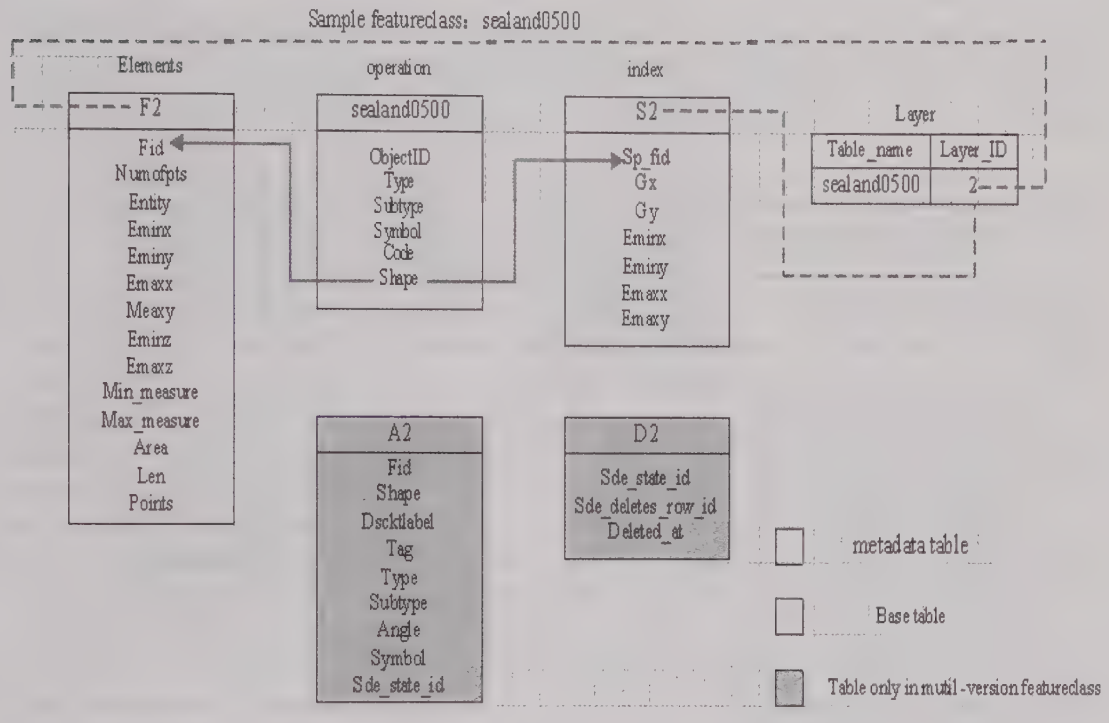

Fig. 2 ArcSDE model of vector data

Every data element vector layer has corresponding Tab. F and Tab. S. There are a series of metadata tables in the ArcSDE Geodatabase responsible for the organization of the spatial metadata and index metadata of the element layer stored in it.

The organization of the spatio-temporal dynamic data relies on the history achieving function of the Geodatabase, and below is the related storage structure.

Tab. B only stores the initial state of the object without the time information, and keeps conservation when editing and updating the data. Table H stores the changing achieving information of the object, mainly the records of property information. For the convenience of object query and historical remount, the time information is directly marked onto the property of the object, and saved in Table H. The time information in Table H includes the object's valid time (the start of the valid time Vt_start, and the end of the valid time Vt_end) and affair time (the start of the affair time GDB_from_date, and the end of the business time GDB_to_date), also supports double time operation. Table F is responsible for the storage of the spatial feature, while Table S is for the spatial index information. Table R records the changing relation among the objects, while Object ID records the element code of the new object. The label code of the father object is recorded in Father ID. The

Event ID is the serial number of the event that affects the changing of the object, which presents the combination and abruption among the objects, makes the changing process of the object clear. The changing events mainly involve the naissance, perdition, abruption and combination of the objects. Only the object formed through abruption or combination has the father object, the object that directly appears or vanishes has no father object.

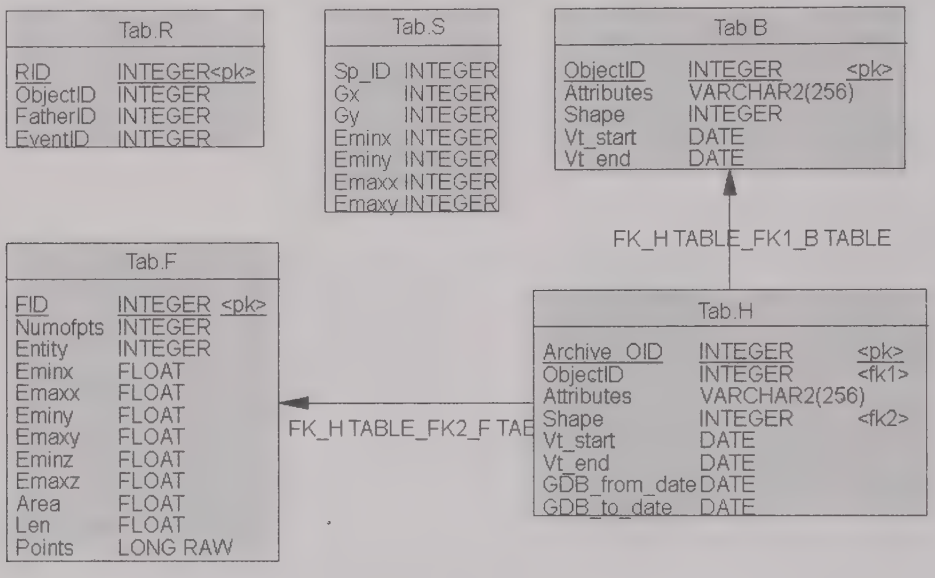

Fig. 3 Spatio-temporal data schema of Geodatabase

3.2 Ocean Solid Grid Data Model

The multi-layer grid data are the foundation of the ocean solid grid data model. It combines multi-layers into a whole object by feature class association to realize the organization and storage of the ocean solid data. Both the regular and irregular interpolation sea surfaces are single layer grid data, which can be treated as the grid volume data with only one layer, while the grid volume element can be treat as the grid volume data with multi-relating layers. Thus, this model is suitable for both the 2-D grid data and the 3-D grid volume data.

The organization and storage of the grid data are realized by designing certain feature element class and object class in the model. This paper adopts the Mesh feature element class to store the one layer or multi-layer data, which involve the vector data and the scalar data like temperature, salinity, density, sound speed, current, storm tide, single layer tide and tidal current and so on. The storage of these data needs the proper Mesh element type chosen according to the characters of the Mesh elements. For temperature, salinity, density and sound speed, we can take vertical multi-layer data at a same time as

one Mesh element, or take one layer of it as one Mesh element; while for the storm tide and tide, the field data during a time period are considered as one Mesh element. For the grid field data like current and tidal current, the data of all layers at the same time can be regarded as one Mesh element, or a single layer data at the same time as one Mesh element. Other types of element field data can be analyzed similarly.

Several relation tables need to be defined, such as grid table, grid point table, vector table, scalar table and parameters.

Tab. 4 Construction of grid table

Name	Type	Key	Limitation	Description
MeshID	CHAR(32)	*P*	*None empty*	Grid label
TotalPoints	NUMBER(6)			Total points
NoofPointsI	NUMBER(6)			Line number
NoofPointsJ	NUMBER(6)			Column number
NoofPointsK	NUMBER(6)			Layer number
Dimension	VARCHAR2(10)			Dimentionality

Tab. 5 Construction of parameters table

Name	Type	Key	Limitation	Description
ParameterID	CHAR(32)	*P*	*None empty*	Element label
Name	VARCHAR2(20)		*Must filled out*	Name
Description	VARCHAR2(40)			Element description
Quantity	VARCHAR2(20)			Quality feature
Uint	VARCHAR2(20)			Unit
SignifcantDigits	NUMBER(6)			Valid number

The relationship of the tables are as follows: the grid points relate to the Mesh table by grid label, while the vector and scalar tables relate to the grid point table by element label, and relate to the parameter table by parameter label. Besides, a metadatabase is needed to illustrate the information of various elements, including the range, name, type, grid resolution, layer depth and updating frequency, etc. The alterable grid element data require specially to be illustrated in the metadata.

In the “digital ocean” system, the environment data like seawater temperature, salinity and current, are divided into several layers by depth and stored by the solid grid data model. Consequently the information of different cross sections and vertical profiles at the same time can be visualized by depth, longitude, latitude or arbitrary direction.

3.3 Relation Data Model

Relation data model sets a certain spatial entity as the object, transforms its data information into different property features, and combines the entity object and property feature together by relating the host keys. It establishes complex data relations and organizes the various multi-source ocean data into a whole. There are two storage methods of this model. One is to store the elements directly into the relation database, which is suitable for binary or text data due to their small data volume and high demand of single-layer accessing. The organization and storage method is to form a document by layering the element data and store this document directly into the database table, namely, to dispart the multi-layer grid elements into several layers and form several documents from one. This storage method is convenient for obtaining, querying and displaying the one-layer element data with little records. Yet for multi-layer profile element data, it's not efficient. This storage method is mainly suitable for multi-layer regular binary grid data, such as temperature, salinity, density, sound speed, current, and the one-layer binary field data, like storm tide, tide, tidal current, and the modeling analysis and forecast data.

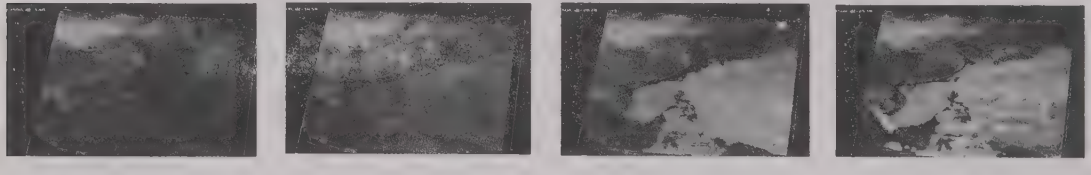

Fig. 3 Temperature information in different depths

Along arbitrary direction Along the latitude Along the longitude

Fig. 4 Temperature information in different profiles

Another method is to integrate the database sheet and the document system together, namely, store the metadata and the corresponding storage path in the database sheet, while store the relevant data entity under the directory defined by the document system. It is most efficient for data accessing and reading, which is propitious to the fast obtaining and visualization of the ocean data.

4 Conclusion

This paper classifies the features of ocean data into 5 major categories, and designs 3 data models according to an idea of "object-oriented". The 3 data models solve the organization and storage problem of the ocean spatial data, solid grid data and great volume text data, respectively. The ocean vector spatial data model integrates the common 2-D ArcGIS software to make the data storage and management easily, which can be viewed, edited and controlled (for popedom and version) by many desktop graphic software. The shortcoming of it is the low efficiency when directly accessing the vector data layer in the 3-D information system, especially the polygon layers, which need to issue the vector layers by web feature service or web map service before using in the 3-D system. The ocean grid data model is designed specially for the storage of solid grid data, which is effective in storing the great volume grid data (in TB). Thanks to the pyramid structure it adopted, the reading speed is fast enough to satisfy the demand of the 3-D information system. However, its disadvantage is the failure of directly data editing. The grid data need processing in advance before storing into the database. The relation data model is good at storing various types of property data, such as the picture, text, model and sound, etc. It's a sharp instrument for storing the "sundries" data, which plays an important role in constructing the digital ocean information system.

In conclusion, so far there is no universal model suitable for the organization and storage of all kinds of ocean element data. Each model has its own merits and drawbacks, and also the limitation in application. Thus, the choice of the organization & storage method need to base on the demand of realistic application. Some are suitable for the manner of document system, while some fit for the common relation database, also there are considerable part of them suitable for the spatial database model. New data model should be introduced to display the spatial dynamic behavior of ocean and visualize its elements. Our ocean solid grid data model is such an example. Although it still can not be realized without the Geodatabase spatial data model, the ocean data types mentioned in its model design and organization are suitable for the concrete ocean applications.

Reference

[1] HOU Wenfeng. Tentative Ideas on the Development of Digital Ocean in China [J]. Marine Science Bulletin, 1999, 12(6):1 - 10.

[2] Pavlopoulos A, Theodoul I D. Review of spatio temporal data models [R]. Time Lab Technical Report TR-98-3, 1998, 2 629 - 2 640.

[3] LI Shan, XUE Cunjin, HE Huizhong. Feature-Based Marine Line Data Model [J]. Sun Yatsen University Forum, 2006, 26(9):193 - 198.

[4] XUE Cunjin, ZHOU Chenghu, SU Fenzhen, et al. Research on Process-Oriented Temporal-Spatio Data Model [J]. Acta Geodaetica et Cartographica Sinica, 2010, 39(1):95 - 101.

[5] ZHANG Feng, SHI Suixiang, YIN Ruguang, et al. Research of Data Architecture in Digital Ocean [J], Marine Science Bulletin, 2009, 28(9):1 - 8.

[6] SU Fenzhen, DU Yunyan, PEI Xiangbin, et al., Constructing Digital Sea of China with the Datum of Coastal Line [J]. Geo-information Science, 2006, 3, 8(1):12 - 15.

[7] JIA Jun-tao, ZHAI Jing-sheng, WU Zhong-ding, et al. Constructing Digital Sea of China with the Datum of Coastal Line [J], Geo-information Science, 2007, 25(1):111 - 116.

[8] BAO Yu-bin, LU Qun, CAI Jin-ming, et al. Domain Ontology-based Multidimensional Modeling of Marine Environmental Data Warehouse [J], Marine Science Bulletin, 2009, 28(4):132 - 140.

[9] QIN Rufu, YE Na, XU Huiping, et al. Visualization of Multi-dimension Oceanographic Data in Geography Information System [J]. Journal of Tongji University (natural science), 2009, 37(2):272 - 276.

[10] HE Guangshun, LI Sihai. Constructing Spatial Information Database for Digital Ocean [J]. Marine Information, 2004, (1): 1 - 4.

海洋信息组织与存储模型研究及其在“数字海洋”中的应用

刘 金[1]，李昊倩[1]，朱吉才[2]，姜晓轶[1]，张 峰[1]

（1. 国家海洋信息中心 天津 300171；2. 中国核工业地质局 北京 100013）

摘 要：基于中国数字海洋建设的经验和成果，制定了海洋数据要素的分类方案，将海洋信息分为 5 大类：海洋点要素、海洋线要素、海洋面要素、海洋网格要素、海洋动态要素。采用基于特征的方法和面向对象的技术设计了适合数字海洋大型信息系统工程建设的时空数据模型，探讨了海洋空间数据模型、海洋立体格网数据模型、关系数据模型在数字海洋数据仓库建设中的应用，并总结了其优缺点。

关键词：数字海洋；球体模型；数据仓库；海洋要素；数据组织与存储

海 洋 通 报（英文版）

HAIYANG TONGBAO

2011 年 10 月 第 13 卷 第 2 期

目 次

中国东海北部泥质区敏感粒度组分对东亚季风演变的响应 …… 孙晓燕 等 (12)

台湾以东黑潮锋时空分布及形成机制研究 ……王 琦 等 (32)

海平面变化与未来预测——气候的过去、现在和未来…… 岳 军 等 (50)

关于定量监测悬浮泥沙浓度方法的回顾和展望……匡 良 等 (61)

基于 BP 人工神经网络的海水水质综合评价 ……李 雪 等 (71)

中国重点海水浴场中粪肠球菌和主要肠道病毒的调查研究……樊景凤 等 (82)

海洋信息组织与存储模型研究及其在“数字海洋”是的应用 …… 刘 金 等 (96)

Marine Science Bulletin

Marine Science Bulletin publishes papers on marine science and technology including physical oceanography, chemical oceanography, marine biology, marine geology, environmental oceanography, estuarine & coastal sciences, marine technology, digital ocean, coastal zone management, ocean engineering, marine economics, etc., and aims to promote international academic exchange.

Editor-in-Chief: XU Sheng (徐　胜)
Associate Editor-in-Chief: LI Dong-xu (李东旭)　XUE Hui-feng (薛惠芬)
Executive Editor: QIU Wen-jing (邱文静)　LI Xue (李　雪)　YANG Rui (杨　瑞)
LI Xiao-guang (李晓光)　DONG Yi (董　艺)　YUAN Ze-yi (袁泽轶)
English proofed by: WANG Qi (王　琦)

Semi-annually (started in 1999, sum 25)
Publication date: May 15th and Oct. 15th

Marine Science Bulletin **(Vol. 13, No. 2, Oct. 2011)**

Responsible Institution:
State Oceanic Administration of China
Sponsored by:
National Marine Data and Information Service
Edited by:
Office of Marine Science Bulletin (English edition)
Printed by:
Printery of National Marine Date and Information Service

Published by:
Office of Marine Science Bulletin (English edition)
E-mail: msb@mail.nmdis.gov.cn
Tel: (022) 24011287
Address: 93 Liuwei Rd., Hedong District, Tianjin 300171, China

---

ISSN1000-9620
CN12-1271/N

ISSN 1000-9620

Price: $ 30.00 / ￥40.00 Per year